AN ABSTRACT OF THE THESIS OF

Jin-Cherng Wang for the degree of Doctor of Philosophy in Physical Education presented on January 20, 1989

Title: The Impact Dynamics of a Tennis Ball Striking a Hard Surface

Abstract approved: Redacted for Privacy
Christian W. Zauner

Redacted for Privacy
Harry Freund

The purpose of this research was to study the impact phenomena of a tennis ball striking a hard surface. Stroboscopic photography was used to collect the ball's impact images from seven angles of incidence, ranging from -23 degrees to -70 degrees with zero, top and back initial spin respectively.

Through digitization, the image data were converted and calculated into the experimental parameters which were composed of the input/output of the translational and angular velocities, and into the system parameters which included the coefficient of restitution, coefficient of sliding friction, ball's dwell time, and ball's dwell distance. Mathematical models derived from both the differentiation and integration approach were developed to explore the impact phenomena.

A -23 degree angle of incidence for the data sets (zero-

spin, topspin, backspin) was selected to carry out the mathematical analysis using both experimental and system parameters. The results were:

1. The successive differentiation approach did not lend itself well to the investigation of tennis ball impact phenomena.

2. The successive integration approach based on the Damped Sin Pulse Model, could be used successfully to describe both the horizontal and vertical forces, velocities and positions of ball impact on a surface.

3. In the case of -23 degree incident angle, the effect of top-spin will produce a high value for the coefficient of restitution, which provides the ball a chance to rebound higher.

4. The horizontal component velocity will influence a shallow angle impact with backspin ball on a surface to have a smaller sliding friction.

5. The findings of this study will provide the instructor of tennis skills with information to fully explain the effects of utilizing the racquet to impart spin to the tennis ball.

6. This study provides guidelines for future research that is likely to affect the methodology of teaching tennis skills.

The Impact Dynamics of a Tennis Ball Striking a Hard Surface

by

Jin-Cherng Wang

A THESIS

submitted to

Oregon State University

in partial fulfillment of
the requirements for the
degree of

Doctor of Philosophy

Completed June 20, 1989

Commencement June, 1989

APPROVED:

Redacted for Privacy

Professor of Physical Education in Charge of Major

Redacted for Privacy

Professor Emeritus of Chemistry in Charge of Co-Major

Redacted for Privacy

Chair of Department of Physical Education

Redacted for Privacy

Dean of the School of Education

Redacted for Privacy

Dean of the Graduate School

Date thesis is presented January 20, 1989

Thesis prepared on computer by Jin-Cherng Wang

ACKNOWLEDGMENT

Grateful thanks is extended to Dr. Christian Zauner and Dr. Susan Hall, my present and previous major advisers, for their commitment and guidance throughout my graduate studies. I express my sincerest gratitude to Dr. Harry Freund for his untiring assistance and professional guidance in the experimentation and theoretical modelling of this dissertation.

Grateful appreciation is also extended to the members of my committee: Dr. Kathleen Heath, Dr. Carvel Wood, Dr. Terry Wood, and Dr. Howard Wilson for their support and advice for my dissertation.

Special thanks to the following companies for their generous contribution to this study: the Wilson Sporting Goods Company for providing a research grant; the JUGS Company for partial support in obtaining a ball thrower; and the Nova Sports USA for providing impact surfaces. Their generosity made this research possible.

I also want to thank Dr. Clarence Calder, Tony Vogt, Aaron Rondean, and Babak Badiee of the Mechanical Engineering Department for consultation and assistance in providing an experimental facility to obtain data for this research.

Finally, I humbly dedicate this dissertation to my wife, Chen Su-Fen Wang, and two daughters, Piggy Yuh-Ren Wang and Grace Wang, whose love and understanding made this paper possible.

TABLE OF CONTENTS

TABLE OF CONTENTS (CONTINUED)

LIST OF FIGURES

LIST OF FIGURES (CONTINUED)

LIST OF TABLES

LIST OF TABLES (CONTINUED)

The Impact Dynamics of a Tennis Ball Striking a Hard Surface

CHAPTER I

INTRODUCTION

Tennis is a very popular sport in the United States and has a large following throughout the country. According to Consumer Research Magazine (1976), there were 10 to 11 million Americans who played tennis in 1971, and this figure jumped to 35 million 5 years later. By 1980 there were 40 million American players, compared to 20 million for the rest of the world (Kennedy, 1980). Consequently, a great deal of money is spent on tennis equipment.

The more people that play tennis, the more attention is given to the improvement of both equipment and skills. In the past 10 years, many physicists, engineers and sports science researchers have been involved in tennis-related research. Many studies concerned with ball impact on rackets have examined the effects of grip tightness, string tension, string material, stringing method, racket size, and racket material (Elliott & Blanksby, 1980; Ellott,1982; Larson, 1979; Liu, 1983; Missavage et al.,1984; Putnam & Baker, 1984). Results from these types of studies have provided useful information to racket manufacturers for improving both the materials used in racket construction and

racket design.

The area of tennis skill analysis has also received attention from researchers. According to Xanthos and Crookenden (1984), there are only four basic strokes in tennis— forehand and backhand ground strokes, serve, and volley--variations on the basic strokes include spinshots, dropshots, lobs, and smashes. Obviously, the ability to analyze and to predict the behavior of a ball rebounding from the court surface bears a close relationship to tennis skill. Without this ability it is not possible to play excellent tennis, especially when there is spin on the ball. As Groppel (1984) pointed out, "Anyone who has played tournament tennis knows the value of being able to vary spins on the ball when competing," (p. 206). In his book Tennis Science for Tennis Players, Brody explores the question, "How does your opponent put that tricky spins on the ball?". It is clear that the effects of the spin serve is to complicate the game. The experienced tennis player is well aware that it is necessary to step a little bit backward to return a topspinned serve and a little bit forward to return a back-spin serve. Is this true? If it is true, how far is it necessary to step? To answer these kinds of questions, we cannot give correct information without knowing the characteristics of a tennis ball's surface impact. To date there is a scarcity of experimental literature concerning the dynamics of a tennis ball's impact on a court surface. Most

of the related studies have employed airborne input/output velocities to infer the occurrence of the ball's contact on a court surface. Daish (1972) provided a good starting point treating the bounce in terms of input/output parameters. Brody (1984) elaborated on Daish's approach, but provided little experimental data in support of the theory treatment. Both authors made two assumptions, (a) the ball skids throughout impact and (b) it rolls off the surface. The real situation might not be two such extreme conditions, and might possibly be the combination of these two conditions. Is this true? The following study was designed to provide an empirical study of this impact phenomena.

Purpose and Approach of This Study

The purpose of this study was to establish, using stroboscopic photography, a mathematical model to explore the impact dynamics of a tennis ball, a deformable membrane sphere, striking a hard surface.

Statement of the Problem

The traditional treatment of impact study has been to measure input/output airborne velocities and to elucidate impact phenomena by inference. Stroboscopic photography provides both airborne and contact positional data, which

upon digitization is amenable to mathematical analysis. Both differential and integral methods were employed to move among position, velocity, and acceleration properties of a model system. The effect of different incoming spins for the impact was also compared in this study. These results should provide useful information for quantifing court "speed", refining stroke skill, and opening a door for three dimensional modeling of rebound phenomena.

Delimitations

This study was delimited as follows:

1. The angle of ball being shot to the surface was set up at a range from -17 to -70 degrees.
2. The shortest time between strobe flashes was about 3 milliseconds. For no image overlap in the film the ball would have to move one ball diameter in this period, resulting in an upper translational velocity of approximately 17 m/s.
3. Only a shallow angle of incidence was selected for building the mathematical model to examine the ball's contact on the surface.
4. Angular velocities included three types of spins—topspin, zero-spin, and backspin. The throwing machine was capable of spins in excess of those imparted in normal tennis strokes.

5. Acrylic coated surfaces on concrete and/or asphalt were used.
6. Only new tennis balls were tested.

CHAPTER II

REVIEW OF LITERATURE

There is limited scientific literature concerning tennis ball impact, particulary concerning the analysis of ball impact during the court surface contact period. There are, however, several reports of tennis research which relate to the instrumentation and/or procedures to be used in the present study. The review of literature was divided into three sections, as follows: a) impact theory, b) research instruments, and c) tennis ball impact.

Impact Theory

The published work dealing with the impact of a ball on a hard surface has been developed via the standard linear and angular impulse-momentenum equations of rigid body Newtonian mechanics. Consideration of the nature and sequence of events taking place during the contact period, especially the consequences of severe ball deformation, are circumvented by arbitrary constraints. Most often this requires simplification of the roles of friction and restitution, or that the ball slide or roll without sliding during the contact period. Within these constraints equations have been developed to describe the relationships among input/output

velocities. Publications by Daisch (1972), Bennett (1976) and Brody (1984),(1987) have employed varying aspects of this approach.

In addition, Andrews (1983) in his investigation of the mechanics of the hop serve in handball, examined the role of ball deformation, including both linear and torsional restitution, under conditions of no slip upon impact.

Writing vector quantities in terms of scalar equations can lead to confusion in signs when differing frames of reference are employed by different authors. It is the objective of this section to develop a composite and unified treatment encompassing much of the work cited above, so that a foundation can be laid for using rigid body mechanics to assist in analyzing a range of experimental impacts. These impacts will involve significant ball deformation, with mixed skidding and rolling during contact.

Let an imperfectly elastic spherical shell ball strike a rough horizontal surface, so that the ball's center of mass velocity has a component, $\dot{x}$, parallel to the surface and a component, $\dot{y}$, perpendicular to the surface. With reference to Figure 1, the point Q is the origin of the right-handed coordinate system R:QXYZ, and is the touchdown point, P, at which the ball first contacts the surface. The x axis is chosen in the same direction as the center of mass velocity vector of the ball. The ball's angular velocity is denoted by, w_{td}, at the moment of touchdown. The spin axis is

maintained parallel to the z axis, and the magnitude and sign of w_{td} are arbitrary.

Prior to touchdown the ball is spherical in shape. Although significant distortion may occur during contact, it is assumed that once airborne, at liftoff, the ball will have regained its spherical shape. The standard linear and angular impulse-momentum equations of Newtonian rigid body mechanics can be used to describe the nature of the impact, in terms of touchdown, TD, and liftoff, LO, velocities. Between TD and LO the ball is acted upon, through the center of mass, by a gravitational force and an impact force, resolvable into components perpendicular and parallel to the surface, S.

The free body diagram in Figure 1 illustrates the most commonly observed kind of impact. The gravitational force acts in a negative direction, while the vertical component of the impact force is always positive, and throughout most of the impact much larger. The horizontal component of the impact force is attributed to friction, usually opposes forward motion, and acts at the ball periphery in contact with the surface. This impulsive torque provides an increment of negative angular velocity (topspin) to the ball.

These forces can be described analytically using Newton's Second Law.

$$F_y = m\ddot{y} = m(d\dot{y}/dt) = -mg + (F_y,\text{impact}) \quad \ldots\ldots\ldots\ldots\ldots\ldots (1)$$

Integrating between TD, when t = 0, and later in the

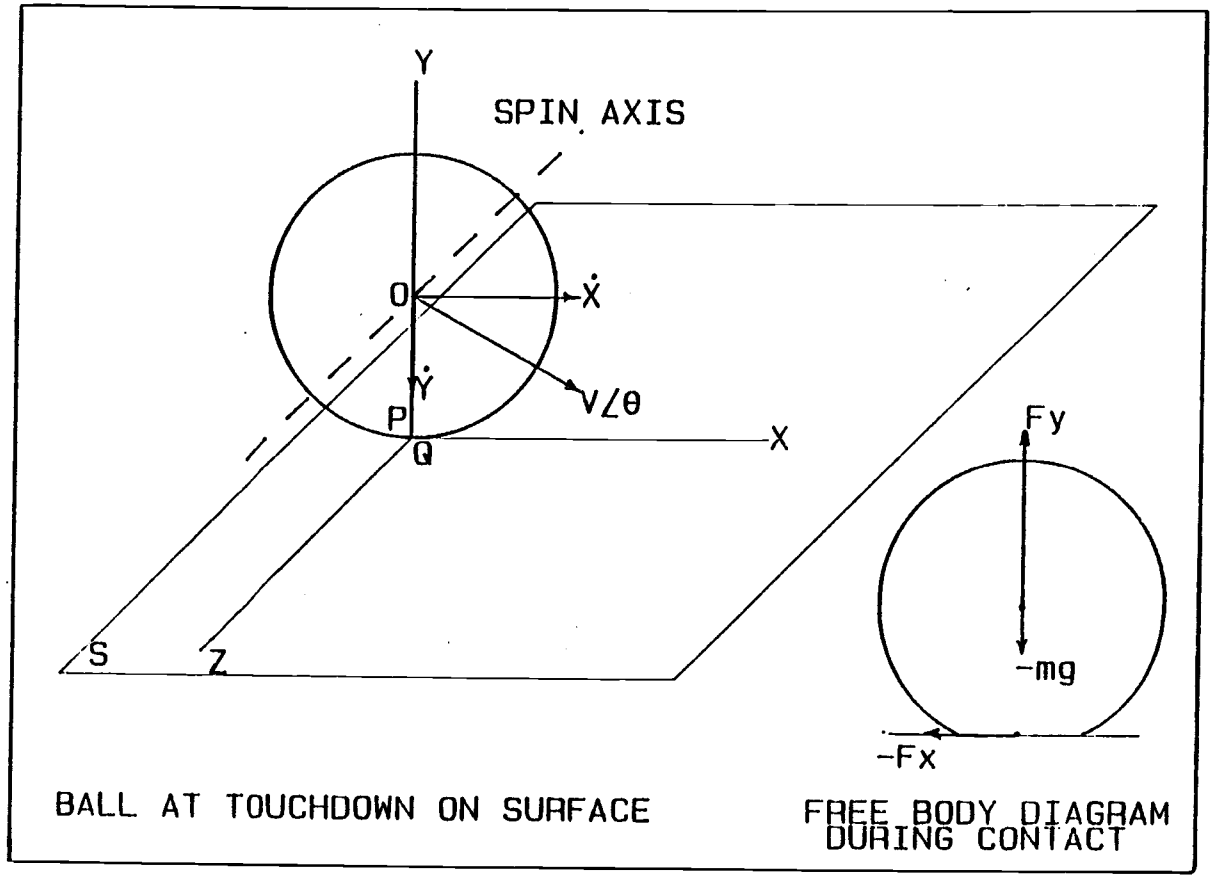

Figure 1. The diagram of ball and surface at the moment of touchdown and during contact.

contact period, at time t:

$$\dot{y} = -gt + (1/m) \int_0^t F_{y,\text{impact}}\, dt + \dot{y}_{tdt} \quad \text{.....(2)}$$

$$F_x = m\ddot{x} = m(d\dot{x}/dt) \quad \text{.....(3)}$$

$$\dot{x} = (1/m) \int_0^t F_x\, dt + \dot{x}_{td} \quad \text{.....(4)}$$

Applying Newton's Second Law to rotation yields:

$$T = (F_x)(k) = I\,\alpha = I\, dw/dt \quad \text{.....(5)}$$

Where: T = Torque tending to cause rotation about the center of mass

F_x = Frictional force

k = Radius of gyration

I = Moment of inertia about the spin axis

Solving equation (5):

$$w = (1/I) \int_0^t (F_x)(k)\, dt + w_{td} \quad \text{.....(6)}$$

The three component equations contain 7 unknowns that may vary during impact, F_x, F_y, x, y, t, k and w. In order to proceed F_x, F_y and k must be expressed as explicit functions of time, or other constraints must be placed on events occuring during contact in order to sidestep evaluation of the impulse integrals. Also a means may have to be found to cope quantitatively with the linear and torsional inelasticity of the ball.

Sliding Occurs Throughout Bounce

The most widely used approach to eliminate the impulse

integrals has been to link the component forces F_x and F_y by means of the coefficient of sliding friction, μ, assumed to be constant over a wide range of velocities. If sliding persists throughout the period of contact then:

$$F_x = -\mu F_y = -\mu (F_{y,impact} - mg) \quad \ldots\ldots\ldots\ldots\ldots\ldots (7)$$

Combining equations (1), (4) and (6) yields:

$$\mu = (\dot{x}_{td} - \dot{x} + \mu gt)/(\dot{y} - \dot{y}_{td} + gt) \quad \ldots\ldots\ldots\ldots\ldots\ldots (8)$$

If the integration is carried out over the entire time of contact Υ , then:

$$\mu = (\dot{x}_{td} - \dot{x}_{lo} + \mu g\Upsilon)/(\dot{y}_{lo} - \dot{y}_{td} + g\Upsilon) \quad \ldots\ldots\ldots\ldots\ldots (8a)$$

It is possible to rearrange the terms in equation (8a) to show that the gravitational terms can be dropped.

$$\mu = (\dot{x}_{td} - \dot{x}_{lo})/(\dot{y}_{lo} - \dot{y}_{td} + g\Upsilon) + (\mu g\Upsilon)/(\dot{y}_{lo} - \dot{y}_{td} + g\Upsilon)$$

y_{td} is always - and y_{lo} is always +, summing in the worst case to about 8.8 M/s. The term $g\Upsilon$ is typically about 0.05 M/s and can be dropped from the denominator. Further rearrangement leads to:

$$\mu(1 - g\Upsilon/(\dot{y}_{lo} - \dot{y}_{td})) = (\dot{x}_{td} - \dot{x}_{lo})/(\dot{y}_{lo} - \dot{y}_{td})$$

Similarly the gravitational term on the LHS is small with respect to 1 and the equation reduces to:

$$\mu = (\dot{x}_{td} - \dot{x}_{lo})/(\dot{y}_{lo} - \dot{y}_{td}) \quad \ldots\ldots\ldots\ldots\ldots\ldots\ldots (9)$$

As all of the terms in equation (9) are amenable to measurement the equation can be used to obtain values for the

coefficient of sliding friction.

In order to complete this analysis the coefficient of restitution e, is introduced as a system parameter to deal with elasticity and is defined as:

$$e = -\frac{\text{Relative vertical component of velocity of the colliding masses on rebound}}{\text{Relative vertical component of velocity of the colliding masses on impact}}$$

As the surface is massive and immovable, the equation simplifies to:

$$e = -(\dot{y}_{lo})/(\dot{y}_{td}) \quad \text{.....................................(10)}$$

If there is no coupling of angular and translational velocities to enhance or decrease $\dot{y}_{lo}$ then e is a measure of elasticity and is remarkably constant over a wide range of impact velocities. Substituting equation (10) into equation (9) results in the familiar form:

$$\dot{x}_{lo} = \mu(e+1)\,\dot{y}_{td} + \dot{x}_{td} \quad \text{..............................(11)}$$

Finally equation (6) can be expanded providing that the ball slides throughout contact, the moment of inertia about the spin axis is essentially that of a thin shelled sphere and that the radius of gyration is essentially the radius of the sphere, r. Substituting and rearranging terms yields:

$$w_{lo} = (3\mu(e+1)\dot{y}_{td})/2r + w_{td} \quad \text{..........................(12)}$$

Should the ball be spinning with topspin, with a peripheral velocity in excess of the center of mass component velocity,

$\dot{x}$, and opposite in sign, then the frictional force would augment the forward motion of the ball. The development of the equations would be the same, but certain signs would change.

Summary of Impact with Continuous Sliding

The Newtonian linear and angular impulse momentum equations applied to the condition of continuous skidding result in impulse integrals difficult to evaluate. The linking of F_x and F_y via a kinetic coefficient of friction, and creation of a linear coefficient of restitution linking $\dot{y}_{td}$ and $\dot{y}_{lo}$, make it possible to describe output velocities $\dot{x}_{lo}$, $\dot{y}_{lo}$ and w_{lo} as functions of input velocities $\dot{x}_{td}$, $\dot{y}_{td}$, w_{td} and system parameters e and μ. Explicit values for velocities during impact are not available.

Sliding Occurs on Initial Contact but Ceases during Period of Contact and the Ball Rolls Off the Bounce

The same linear and angular impulse momentum equations prevail as in the earlier derivation.

$$\dot{y} = -gt + (1/m) \int_0^t F_{y,\text{impact}}\, dt + \dot{y}_{td} \quad \text{.....(2)}$$

$$\dot{x} = (1/m) \int_0^t F_x\, dt + \dot{x}_{td} \quad \text{.....(4)}$$

$$w = (1/I) \int_0^t (F_x)k\, dt + w_{td} \quad \text{.....(6)}$$

Providing there is no torsional coupling tending to enhance $\dot{y}_{lo}$ the definition of the coefficient of restitution should

still be effective.

$$e = -\dot{y}_{lo}/\dot{y}_{td} \quad \text{.......................................(10)}$$

The initial frictional effect will decrease the center of mass component velocity, $\dot{x}$, below the touchdown value $\dot{x}_{td}$. The accompanying torque favors increased topspin, and the peripheral velocity, $\dot{x}_p$, of the ball at the contact area grows in magnitude, approaching $|\dot{x}|$ and opposite in sign. When the critical condition:

$$x_p = w_c\, r = -x_c \quad \text{.................................(13)}$$

is met, sliding will cease and the ball will roll, impeded only by rolling friction. As a first approximation it can be assumed that deformation is slight and that the coefficient of rolling friction is essentially zero. The velocities w_c and $\dot{x}_c$ become $\dot{x}_p/r$ and $-\dot{x}_p$. Equation (13) can be written.

$$\dot{x}_{lo} = -w_{lo}\, r \quad \text{......................................(13a)}$$

Combining equations (4), (6) and (13a) and integrating over the range 0 to Υ, yields:

$$\dot{x}_{lo} = (-2rw_{td} + 3\dot{x}_{td})/5 \quad \text{.............................(14)}$$

$$w_{lo} = (2rw_{td} - 3\dot{x}_{td})/5r \quad \text{.............................(15)}$$

The critical condition, when sliding disappears and pure rolling occurs, can be ascertained when the value for $\dot{x}_{lo}$ calculated by equation (11) is equal to the value for $\dot{x}_{lo}$ calculated by equation (14).

$$\mu(e + 1)\dot{y}_{td} + \dot{x}_{td} = (-2rw_{td} + 3\dot{x}_{td})/5 \quad \text{.....(16)}$$

Collecting variables:

$$\mu(e + 1)\dot{y}_{td} = -(2/5)(rw_{td} + \dot{x}_{td}) \quad \text{.....(16a)}$$

The coefficients of friction, μ,and restitution, e, are constants characteristic of the materials comprising the ball/surface system. The independent variables $\dot{x}_{td}$, $\dot{y}_{td}$ and w_{td} may be selected arbitrarily. Such choices would result in the following logical conditions, deriving from equation (16a).

Logical Statement	Nature of Contact
$\lvert LHS \rvert < \lvert RHS \rvert$	Ball skids throughout bounce and skids off of bounce at LO
$\lvert LHS \rvert = \lvert RHS \rvert$	Ball skids throughout bounce but ceases to skid and rolls off of bounce at LO
$\lvert LHS \rvert > \lvert RHS \rvert$	Ball skids through initial part of bounce, then ceases to skid and rolls off bounce

Research Instruments

In most of the reported ball impact studies, high speed video taping, cinematography, or stroboscopic photography were used for data collection. Of these, stroboscopic

photography is advantageous in that it can reach exposure times of a few microseconds, and can freeze multiple images on a single frame of 35 mm film. The other strength of stroboscopic photography is that the film processing can be carried out with standard equipment in any dark room in minutes. Since 1970, most tennis impact studies have involved the use of a tennis ball machine and the use of stroboscopic photography.

Sebolt (1970) studied the relationship of ball velocity and tennis performance through the use of stroboscopic photography. Two General Radio 1531-A Strobotacs were synchronized to flash 20,000 times per minute for maximum velocity tests and 15,000 times per minute for controlled velocity tests. The camera's shutter speed was set for one second exposure, and the lens aperture was set at f/1.8.

Baker and Wilson (1978) tested the effect of tennis racket stiffness and string tension on ball velocity after impact. Stroboscopic photographic equipment was also used in this study, and a Prince tennis ball machine was used to propel the tennis ball at 100±10 mph (44.7±0.44 m/s).

Elliott (1982) utilized stroboscopic photography to investigate the effect of tennis racket flexibility and string tension on rebound velocity during dynamic impact. The stroboscopes were set at 8400 flashes per minute for testing the ball velocity. The balls were thrown by a ball machine which was tested with the speed of 22.7±0.45 m/s.

Blanksby (1982) investigated the vibration and rebound velocity characteristics of conventional and oversized tennis rackets. The measurement of ball rebound velocity was achieved using stroboscope photography. The stroboscope was preset at 6000 flashes per minute and the ball was pitched from a ball machine with a speed of 21 m/s. The impact-induced vibration was recorded along the longitudinal and transverse axes of the racket by a set of amplifiers and a BWD Electronics storage oscilloscope.

Zayas (1986) determined the coefficient of drag on a tennis ball by the method of stroboscopic photography. A laser beam apparatus was added to the stroboscope to detect the velocity of the ball. The strobotacs generated 7,200 flashes per minute for this study. The experimental accuracy was tested by both the strobe method and the photogate timer method. This test showed the ball speed of 25.8±0.21 m/s by the strobe method and 25.8±15 m/s by the photogate timer method.

Tennis Ball Impact

The literature relating to tennis ball impact in regard to the coefficients of restitution and friction, incident and rebound angles, and spin effects on the ball impact is described in this section.

Coefficient of Friction

Freund (1987) found coefficients of friction for tennis balls on three pieces of acrylic coated surfaces which were termed as slow, fast, and medium. The spring-scale method was used for the test. Coefficients of friction reported were as follows: 0.68 ± 0.02 for the "slow" surface, 0.53 ± 0.02 for the "fast" surface, and 0.61 ± 0.02 for the "medium" surface. Freund also used the stroboscopic photographic method to test the dynamic coefficient of friction for the "medium" surface and obtained a value of 0.50 ± 0.04.

Chan, Seto, and Tran (1988) engaged in a project to devise a quantitative, repeatable means of measuring the coefficient of friction of balls on different tennis court surfaces. The same "fast", "medium", "slow" surfaces used in Freund's study were investigated. A set of electronic sled-motors was set up to measure the coefficients of friction. A range of 0.45 to 0.55 was identified for coefficients of friction on the different surfaces.

Brody (1984) measured the coefficients of friction of tennis ball on three different court surfaces by the spring scale method. The results were as follows: 0.25 for a Wood court, 0.49 for a Laykold (acrylic coated hard court), and 0.61 for a Supreme court (synthetic carpet).

Rebound Angle and Velocity

Lisk (1980) compared the effects of velocity, surface, and angle of incidence on the angle of rebound and the speed of rebound in tennis. The incident angles of 20, 30, 40, 50,

60, 70, and 80 degrees were selected to test the rebound effect. Three types of tennis surface——Laykol acrylic, Tartan smooth, and wood——were used, and three different incident velocities (59 ft/sec, 62 ft/sec, 86 ft/sec) were observed. The results indicated that: 1) the angle of rebound of a tennis ball is greater than its angle of incidence; 2) the angle of incidence is a better indicator for predicting the angle of rebound than is velocity of incidence or rebound surface; 3) the angle of rebound from a Laykol surface, a Tartan smooth surface, and a hardwood surface will not be different due to a surface effect; 4) deviations in the angle of rebound from the angle of incidence, though always greater, tend to increase as the angle of incidence from 20 degrees to 30 degrees and then decrease as the angle of incidence increases from 30 degrees to 80 degrees; 5) tennis balls projected with a slow incidence velocity will rebound at a greater deviation angle than those which were projected at the same angle of incidence with a faster incidence velocity.

Dowell, Smith, Miller, Hope, and Kreb (1987) studied the effect of the angle of incidence on the rebound deviation of a tennis ball. Tennis balls were projected without spin by a Prince Ball Machine onto a Laykol court at five degree angle increments between 15 and 70 degrees. The results showed that the deviation between the angle of incidence and the angle of rebound of a tennis ball contacting a smooth surface

without spin increases as the angle of incidence increases from 0 to 35 degrees. As the angle of incidence increases from 35 to 90 degree, however, the rebound deviation decreases. Vogt, Rondeau, and Badiee (1988) investigated the rebound effects of tennis ball. The tennis balls were pitched from a JUGS pitching machine at a speed around 17 m/s with topspin (-142 rad/s), zero-spin, and backspin (164 rad/s) from a incidence angle of 70 degrees and impacted on a 16" by 16" acrylic coated surface. The results indicated (a) rebound angles of 68.19 degrees for topspin, 75.64 degrees for zero-spin, and 81.65 degrees for backspin and (b) coefficients of restitutions 0.685 ± 0.019 for topspin, 0.667 ± 0.023 for zero-spin, and 0.630 ± 0.029 for backspin.

Spin Effect

Putnam and Baker (1984) tested the effect of spin imparted to a tennis ball during impact with conventionally and diagonally strung rackets. In this test, balls were projected at the rackets at an angle of approximately 45 degrees. The head of each racket was oriented vertically and clamped to eliminate any influence that deformations of the frame would have on the forces transmitted to the ball during impact. Ten multiple-image photographs were taken of a ball approaching, striking, and leaving the rackets. The results indicated that the angular impulse of the contact force applied to the ball (and hence the amount of spin) was almost identical for the two string configurations, and that the

rackets strung with a diagonal configuration did not transmit a larger amount of spin to a ball than rackets strung in a conventional pattern.

Analysis of ball contact on surface

Freund (1988) examined experimentally the events occurring before, during, and after the oblique impact of a tennis ball on a hard court playing surface. In this impact study, tennis balls were thrown by a JUGS pitching machine at a speed of 17 m/s with topspin (-138 rad/s), no-spin, and backspin (168 rad/s) from 17 degrees of incidence angle. The results indicated that: 1. lift-off angles (degree) of 20.8 ± .67 for no-spin, 23.1 ± 1.3 for top- spin, and 20.3 ± .65 for back-spin; 2. lift-off resultant velocity (m/s) of 11.7 ± .34 for no-spin, 11.9 ± .27 for topspin, and 11.3 ± .16 for backspin; 3. lift-off angular velocity (rad/s) of -239 ± 11 for no-spin, -386 ± 12 for topspin, and -106 ± 10 for backspin; 4. contact distance (mm) of 78 ± 3 for no-spin, 76 ± 3 for topspin, and 83 ± 6 for backspin; 5. contact time (ms) of 6 ± .2 for no-spin, 5.6 ± .2 for topspin, and 6.3 ± .4 for back-spin; 6. coefficients of restitution of .88 ± .05 for no-spin, .89 ± .04 for topspin, and .77 ± .02 for backspin; 7. coefficients of friction of .50 ± .05 for no-spin, .51 ± .04 for topspin, and .63 ± .04 for backspin; 8. spring constants (N/m) of 20100 ± 500 for no-spin, 23800 ± 700 for topspin, and 19300 ± 1500 for back-spin.

CHAPTER III

METHODS AND PROCEDURES

The methods and procedures used in this study are described as following: a) experimental procedures— experimental design, test equipment and apparatus, and test procedures; b) data treatment and analysis— digitizing the data, data treatment, and mathematical analysis.

Experimental Procedures

Experimental Design

Experiments were designed to use the stroboscopic photography to get ball images before, during, and after impact. Stroboscopic photography provides two-dimensional film images that are essentially projections of ball position in space. Also the repetition rate of the strobe permits relating ball position to time. The initial objective of analysis is to transform positional information to velocity and then to acceleration, which via Newton's Second Law provides estimates of the changing force acting on the ball.

By the use of film digitizing, both airborne and contact position data of ball images were obtained. Based on these data, the quantity of experimental parameters and system parameters were calculated. Finally, a mathematical

analysis was applied to investigate the impact phenomena. In order to complete each experiment, several test apparatus configurations were utilized to facilitate data collecting. Seven different incident angles ranging from -17 to 70 degrees were tested, one by one, with three types of incoming spin— top, zero, and back. Most of the experiments were conducted during the winter and spring terms 1988, working jointly with a group of senior mechanical engineering students (Vogt, Rondeau, and Badiee, 1988). To illustrate the approach advocatedin this study, the set of data for -23 degrees incident angle were used for the mathematical analysis. Analysis of data collected at the remaining angles of incidence will be completed at a future date.

Test Equipment and Apparatus

A. Ball Pitching Machine

A new 1987 model of the Jugs Curveball Pitching Machine (JUGS Co, Tualitan, OR) which could generate a wide variety of spins and translational velocities was used to launch the tennis balls.

B. Impact Surface

A 16" by 16" acrylic coated surface of average "speed" made from materials supplied by Nova Sports USA (P. O. Box 1481, Framingham, MA 01701) was used for ball impact. Procedures for making the test surfaces included:

a. A concrete slab was brushed to remove loose debris.

b. Acrylic Resurfacer, a proprietary mixture of acrylic

resin and 70 mesh silica sand, was applied with a squeegee. Gererally two voats would suffice to fill the pores.

c. Three filler coats, consisting of chrome paste (pigment + resin), abrasive and water were squeegeed on the surface, allowing several hours to overnight between applications. The following proportions were recommended by the manufacturer to produce a surface of "average" speed:

10 Gal. of Chrome Paste

100 # silica sand, 70 mesh

Mix with water to bring to a total volume of 30 gallons

d. A finish coat, consisting of equal volumes of chrome paste ,and water, were then applied by squeegee to produce the final surface. Several days were required for final curing of the surface.

e. A "faster" surface can be prepared by cutting the sand content of the filler coat in half, while a "slow" surface results from doubling the sand content.

C. Stroboscope

Two General Radio 1531A Strobotacs were used to provide light flashes of approximately 1 microsecond duration. The period between flashes of the two strobolights was synchronized by an external input from a function generator (Global Specialties, model 2001), with the time interval displayed by a counter-timer (Global Specialties, model 5001).

D. Inclinometer

A Craftsman Protractor was used to measure the angles to the horizontal plane for both the pitching machine and the rebounding surface.

E. Camera

A Nikon FE 35 mm camera driven in a single frame mode by an M1 Motor drive was used to photograph the impacts. Tri-X Pan black and white film (ASA 400) was used in these experiments.

F. Ball

The United States Tennis Association (1986) in Rule 3 sets standards for the manufacture and performance of tennis balls. R.J. LaMarche (1985) published a review of the characteristics of regular duty, extra duty, and pressureless tennis balls. Selected data are recalculated and presented in Table 1. Generally the actual physical properties of ball are in reasonably close agreement with the standards set by Rule 3. A linear regression equation for the temperature dependence of the coefficient of restitution was also obtained from LaMarche's data. The predictive equation is listed as follows: $e = 0.717 + 0.00055 * T$ and R squared = 0.988 where e is the coefficient of restitution , T is the temperature (^{o}F), and R squared is the regression coefficient. The laboratory work was conducted in a room where temperature was controlled at 68 ^{o}F. The observed maximum range, during winter and spring was 68 to 72 ^{o}F, with most of the experiments conducted at 68 ^{o}F. The maximum

effect on the coefficient of restitution was a 4 °F range would be $5.5 * 10^{-4} \approx 0.002$. Since the experimental work would provide computed values to only two significant figures, at 0.76, the variation in room temperature could be ignored.

Table 1. Comparison of commonly used ball characteristics vs U.S.T.A. Rule 3 specifications

ball identicication	average mass(kg)	e
U.S.T.A. Rule 3	0.0576 (± .0009)	0.75 (± .02)
Regular Duty		
Dunlop Champ	0.057	0.75 (± .01)
Penn Regular	0.057	0.76 (± .01)
Wilson Champ	0.0561	0.75 (± .01)
Extra Duty		
Penn	0.0581	0.76 (± .01)
Wilson Champ	0.055	0.76 (± .01)
Pressureless		
Penn	0.0581	0.76 (± .01)
Tretorn XL	0.0581	0.76 (± .01)

e: Average linear coefficient of restitution

Complications arise when assigning a value for the moment of inertia of a ball rotating about an axis coinciding with the diameter. The spherical shell is not isotropic, consisting of a rubber shell, to which a nylon felt nap is bonded. The ball's diameter must be greater than 0.0635 (M) but less than 0.0667 (M). The inner rubber spherical shell has a thickness of 0.0032 (M) and an outer diameter of 0.0600 (M). The felt cover is light, readily compressible and about

0.002 (M) thick. Practicsally all of the mass is concentrated in the rubber shell. Siegel (1968) provides formulas for calculating the moment of inertia about a diameter for either thin shelled or thick shelled spheres. For a hypothetical thin shelled sphere, described by Rule 3, the moment of inertia is (2/3)*m*r^2, where m is 0.0576 (KG) and r is the mean radius of the rubber shell, .0284 (M). The estimated value of the moment of inertia is equal to 3.10E-5 (Kg*M^2). For a thick shelled sphere, of outer radius a and inner radius b, the moment of inertia is: (2m/5)*(a^5-b^5)/(a^3-b^3). For the case where a = 0.030 (M) and b = 0.0268 (M), the moment of inertia is equal to 3.12E-4 (Kg*M^2). Thus the thin shelled model can be used for this analysis.

Test Procedures

All tests were done in a laboratory space dedicated to ball rebound testing in the Mechanical Engineering Department, at Oregon State University. Figure 2 shows the arrangement of the laboratory.

Balls marked with an equator were thrown by the thrower to impact the test surface at a speed around 17 m/s, and with angular velocities of zero, +160 (backspin), and -140 (topspin) rad/s. Three types of spins— zero-spin, topspin, and backspin— were conducted respectively. For each impact, each spin was replicated 3 times with 3 new ball, yielding 9 frames of images. To maintain consistency across tests, new set of Wilson Championship balls was used.

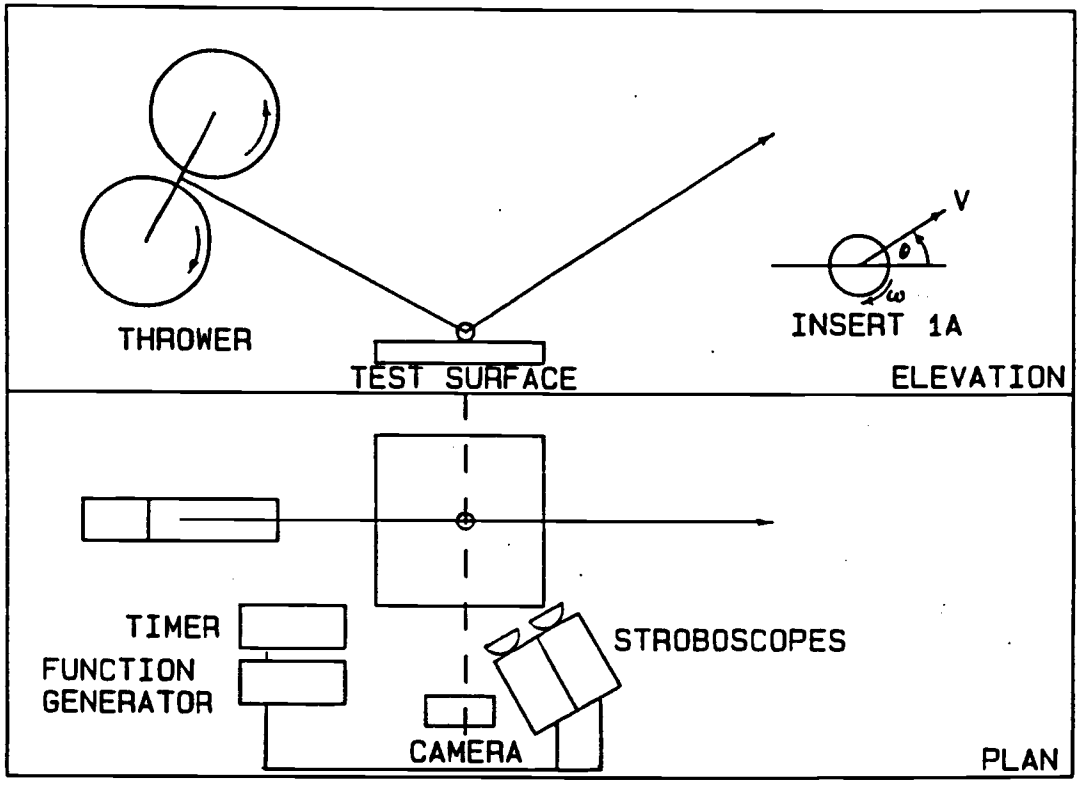

Figure 2. Schematic drawing of laboratory arrangement.

The rebounding surface was clamped on a heavy steer stand, and was placed 7.4 feet away from the center of the surface in front of thrower.

Two Strobotac strobelights (General Radio Company) were positioned at the side of the playing surface, with the lights aimed at the imapct point on the surface so that illumination provided reasonably even lighting of the tennis balls, before during, and the following impact. The period between flashes of the two strobelights was synchronized by an external input from a function generator (Global Specialties, model 2001) set up to flash 20,000 times per minute. This provided a time period about three milliseconds between sequential ball images. A counter-timer (Global Specialties, model 5001) was used to check the time period between flashes. The time interval and frame number for each shot of the ball was recorded for later use in data analysis. In order to capture the ball during the times immediately before and immediately after impact with the surface, the camera shutter speed was set at 0.5 seconds. The room temperature, the distance from the camera to the surface, and the distance from the ball thrower to the surface was recorded for each test.

After completing each test, the film used was developed in the dark room before the throwing machine and playing surface were repositioned for a different incident angle. The developed films were mounted into the slide mounts frame by frame after drying.

Data Treatment and Analysis

After finishing all experiment work, mounted slide-films were the first product of this study. Then, all the required data, the value of experimental parameters and system parameters, were calculated from the digitized data. Based on these results, there were two approaches, differentiation and integration, of mathematical analysis which were applied to explore the phenomena of impact.

Digitizing the Data

A slide projector was used to project the exposures onto a digitizing tablet (CalComp 9100 Series, 38" by 48") interfaced to an IBM-XT computer for data storage. A transparent overlap was used to facilitate the digitizing procedure. There are four points corresponding to the surface that were digitized on each frame for determining the surface axis. The center of circle on the transparent overlap and one point on the outer edge of the ball image were digitized to determine the quantity of ball diameter for converting the digitized value into the real quantity. Two cross points on the transparent overlay and the equator line marked on the ball were digitized to enable calculation of the slope of the equator, and subsequently the angular velocity of the ball. The digitized data were saved in disk files to be accessed by calculation software.

Data Treatment

After digitizing, coordinate data files were reedited for adding the strobe time period and the number of contact images into the file. A Pascal program written by the author was used to run all the necessary calculation (Appendix A). The following describes the conversion of the coordinate data into the quantitative parameters of interest before, during, and after impact.

A. Rotation of Surface Plane

Though the projector was adjusted as closely as possible to project the surface plane image parallel to the horizontal axis on the digitizing board, some small residual error still exist. Digitized data still had to be rotated mathematically to accuratrely bring the surface plane parallel to horizontal axis on the digitizer. The equations used for this rotation were as follows:

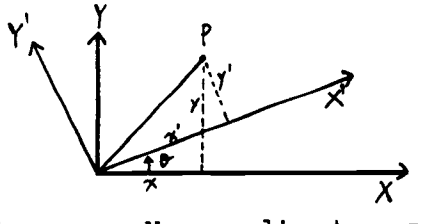

$$x = x'\cos\theta - y'\sin\theta$$

$$y = x'\sin\theta + y'\cos\theta$$

where x: X coordinate value refer to X axis.

y: Y coordinate value refer to Y axis.

x': X coordinate value refer to X' axis.

y': Y coordinate value refer to Y' axis.

B. Incoming Airborne Parameters

The schematic drawing which defines the terms for

describing the position of the ball (radius: R) images on an X, Y coordinate system were shown in Figure 3. A linear curve fit was used to extrapolate the trajectory of impact because of the short time period between images. The ball touches down upon the surface at the instant when the ball's center was 1 radius distance above the surface. Therefore, the coordinates of the ball's center at touchdown were found as:

$$Y = a_{in} \; X \; + \; b_{in}$$

$$Y_{TD} = Y_{surf} + \; R$$

$$X_{TD} = \frac{(\; Y_{TD} - b_{in} \;)}{a_{in}} .$$

where

Y: the linear function of Y and X coordinates of the path of the ball's center before impacting the surface.

a_{in}: the slope of the function Y.

b_{in}: the intercept of the function Y.

Y_{surf}: the Y coordinate of the surface plane.

Y_{TD}, X_{TD}: X Y coordinates of the ball center when the ball touches down upon the surface.

Because the time interval between two ball images was around 0.003 seconds, the velocity would change imperceptibly between the nearest image and the projected image at touchdown. Therefore, velocities would be:

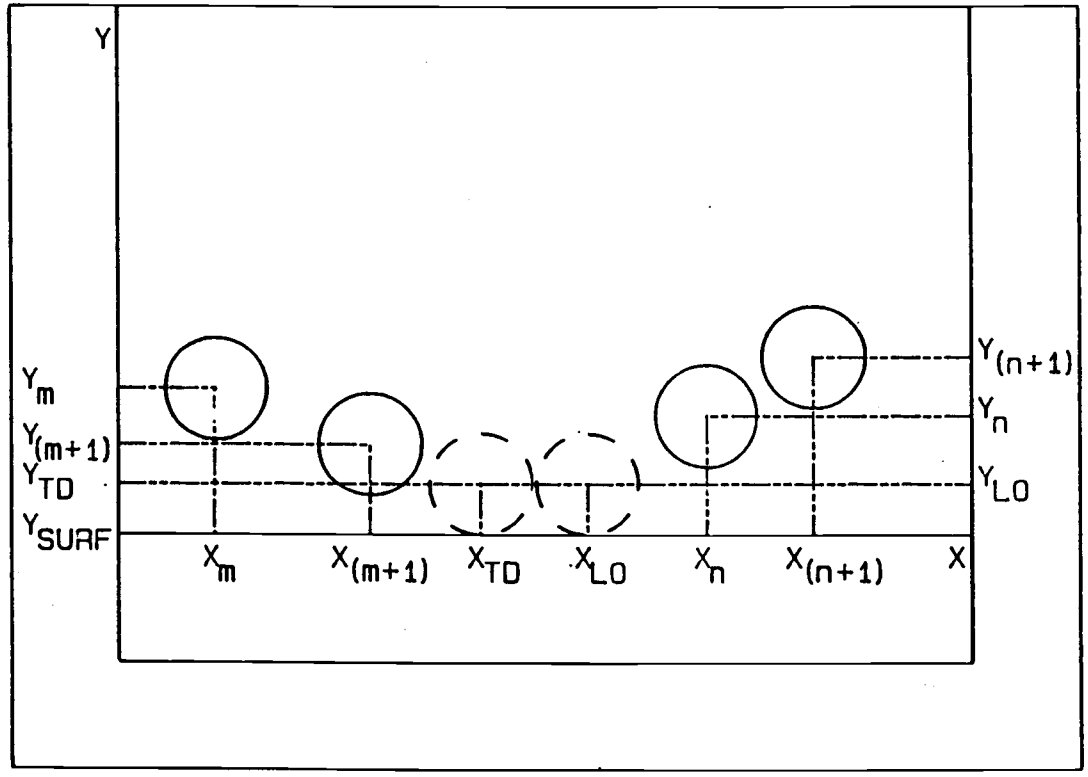

Figure 3. Schematic drawing of impact images.

$$\frac{\Delta Y_{in}}{\Delta T} = \frac{(Y_{m+1} - Y_m)}{(\text{strobe period})} = \dot{Y}_{TD}$$

$$\frac{\Delta X_{in}}{\Delta T} = \frac{(X_{m+1} - X_m)}{(\text{strobe period})} = \dot{X}_{TD}$$

$$V_{TD} = \sqrt{(X_{TD})^2 + (Y_{TD})^2}$$

$$\theta_{TD} = \text{ArcTan}(\dot{Y}_{TD} / \dot{X}_{TD})$$

$$W_{TD} = \frac{\text{ArcTan}(\text{slop}(m + 1)) - \text{ArcTan}(\text{slop}(m))}{\text{strobe period}}$$

where

ΔY_{in}, ΔX_{in}: vertical and horizontal displacement between two ball images.

ΔT: time period between two ball images.

$\dot{Y}_{TD}$, $\dot{X}_{TD}$: vertical and horizontal velocity of the ball at the instant of touchdown.

V_{TD}: resultant velocity of ball at the instant of touchdown.

θ_{TD}: incident angle of the ball.

W_{TD}: angular velocity of the ball at the instant of touchdown.

C. Rebounding Airborne Parameters

Similar to the outgoing airborne images:

$$Y = a_{out} X + b_{out}$$

$$Y_{LO} = Y_{surf} + R$$

$$X_{LO} = \frac{(Y_{LO} - b_{out})}{a_{out}}$$

$$\frac{\Delta Y_{out}}{\Delta T} = \frac{(Y_{n+1} - Y_n)}{(\text{strobe period})} = \dot{Y}_{LO}$$

$$\frac{\Delta X_{out}}{\Delta T} = \frac{(X_{n+1} - X_n)}{(\text{strobe period})} = \dot{X}_{LO}$$

$$V_{LO} = \sqrt{(X_{LO})^2 + (Y_{LO})^2}$$

$$\theta_{LO} = \text{ArcTan}(\dot{Y}_{LO} / \dot{X}_{LO})$$

$$W_{LO} = \frac{\text{ArcTan(slope(n + 1))} - \text{ArcTan(slope(n))}}{\text{strobe period}}$$

where

Y: the linear function of Y and X coordinates for the path of the ball's center after impacting the surface.

a_{out}: slope of the function Y.

b_{out}: intercept of the function Y.

Y_{LO}, X_{LO}: X Y coordinates of the ball's center when the ball lifts off from the surface.

ΔY_{out}, ΔX_{out}: vertical and horizontal displacement between two ball images.

ΔT: time period between two ball images.

$\dot{Y}_{LO}$, $\dot{X}_{LO}$: vertical and horizontal velocity of the ball at the instant of lift-off.

V_{LO}: resultant velocity of ball at the instant of lift-off.

θ_{LO}: rebound angle of the ball.

W_{LO}: angular velocity of the ball at the instant of lift-off.

D. Contact Period Parameters

The coefficient of restitution was defined by:

$$e = - \frac{\dot{Y}_{LO}}{\dot{Y}_{TD}}$$

The coefficient of friction which is a constraint continuous sliding friction between the ball and the surface, according to Brody (1984), could be computed by:

$$\mu = \frac{- (\dot{X}_{LO} - \dot{X}_{TD})}{(\dot{Y}_{LO} - \dot{Y}_{TD})}$$

The dwell distance on the surface was given by:

$$X_{LO} - X_{TD}$$

The dwell time on the surface was determined by computing the first total elapsed time between the last airbone image before touchdown and the first airbone image after lift-off:

T_{Total} = ((number of contact images - 1) + 2) * strobe period

The time between the last airborne and touchdown:

$$T_{Before} = \frac{(X_{TD} - X_{m+1})}{\dot{X}_{TD}}$$

and between liftoff and first airbone:

$$T_{After} = \frac{(X_n - X_{LO})}{\dot{X}_{LO}}$$

Therefore, the dwell time, γ, was:

$$\gamma = T_{Total} - (T_{Before} + T_{After})$$

Mathematical Analysis

By the use of digitizing, recorded on each frame were several airborne images of the ball before and after impact and one or two images of contact with the surface. Nine replicating shots generally provided 12 to 18 contact images, randomly distributed positionally and temporally in the contact area. In order to use these on a single plot, fractional distances or angles were plotted against fractional time. These plots provided a good starting point for the mathematical analysis.

A. Differential Approach

Collecting the ball images which contact the surface would give a random distibution in the strike zone. The information is plotted as a nondimensional function so that such data could be assembled into a single composite picture (Figure 4). From this information the plots of X coordinate distance vs time, Y coordinate distance vs time, and angular rotation vs time could be obtained. A successive differentiation of these plots then leads to:

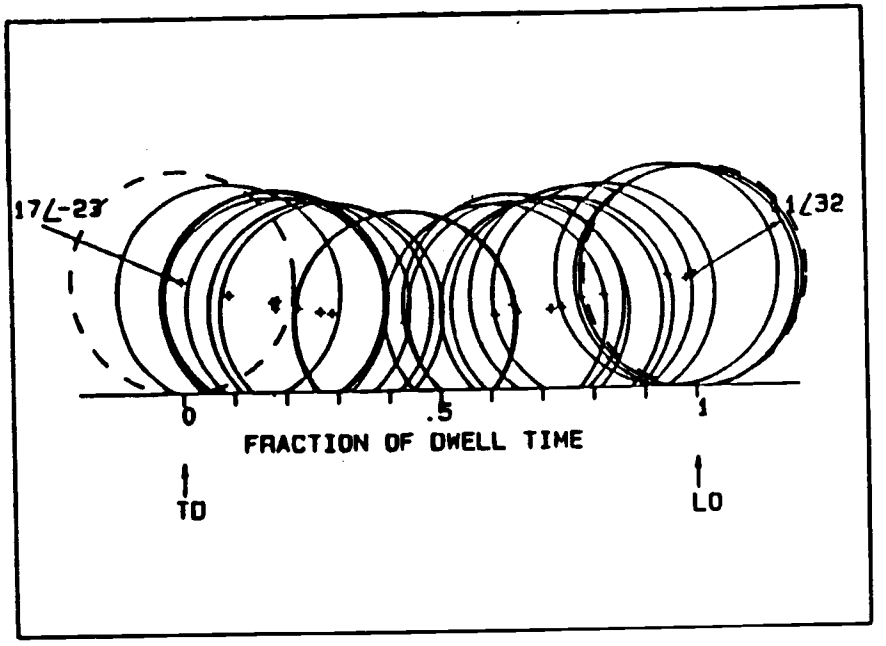

Figure 4. Computer reconstruction of impact images.

1) plots of X component, Y component translational, and angular velocities.
2) plots of X component, Y component, and angular accelerations.
3) plots of component forces and torque.

B. Integration Approach

The differential approach starts with the position then goes to the velocity and acceleration. In contrast, the integration approach starts with the force then proceeds to the velocity and position. The steps of this approach are follows:

a. The vertical component force(Fy), velocity($\dot{Y}$), and position(Y)

1. Start with Newton's second law:

$$F_y = m\,a = m\,\frac{d\dot{Y}}{dT} \quad \text{then} \quad \int F_y\,dT = m\int d\dot{Y}$$

where F_y: vertical component force which the ball acted on surface during impact.

m: mass of ball.

a: vertical component acceleration of ball.

$\dot{Y}$: vertical component velocity of ball.

T: time in contact with surface.

2. During impact, the ball behaves elastically and can be described as a mass, non-linear spring system. Therefore,

the Damped SIN Pulse Model applies to this analysis:

$$F_y = F_{max} * \varepsilon^{-fwT} * \text{SIN } wT$$

where F_{max}: maximum force during impact based on Undamped SIN Pulse Model.

f: coefficient of damping.

w: fundamental frequency of oscillation.

T: time in contact with surface.

ε: exponential function.

3. Finding the F_{max} from Undamped SIN Pulse Model:

$$F_y = F = m \frac{d\dot{Y}}{dT} = F_{max} * \text{SIN } wT$$

$$d\dot{Y} = \frac{F_{max}}{w\ m} * \text{SIN } wT\ dwT$$

Integrate the above equation from 0 to T:

$$\dot{Y} = -\frac{F_{max}}{w\ m} * \text{COS } wT + \text{constant}$$

When COS wT=0, wT=π/2; and $\dot{Y}_{\pi/2}$=constant=0.

Plugging in the vertical component velocity at touchdown (t=0) which is obtained from the digitizing data, the value of F_{max} is found as:

$$F_{max} = -\dot{Y}_{TD} * m * w$$

where $\dot{Y}_{TD}$: vertical component velocity of the ball at the instance of touchdown.

m: mass of the ball which equals 0.0576 kg.

w: fundamental frequency of oscillation which equals π divided by the total ball dwell time.

4. Integration for the vertical component velocity ($\dot{Y}$):

$$F = m \frac{d\dot{Y}}{dT} = F_{max} * \varepsilon^{-fwT} * SIN\ wT$$

$$d\dot{Y} = \frac{F_{max}}{m} * \varepsilon^{-fwT} * SIN\ wT\ dT$$

Integrate the above equation from 0 to time t:

$$\int_0^t d\dot{Y} = \frac{F_{max}}{m} * \int_0^t \varepsilon^{-fwT} * SIN\ wT\ dT$$

$$(\dot{Y} - \dot{Y}_{TD}) = \frac{F_{max}}{m} * \left[\frac{\varepsilon^{-fwT} *[(-fw*SIN\ wT)-(w*COS\ wT)]}{w^2*(f^2+1)} \right]_0^t$$

$$= \frac{F_{max}}{w\ m\ (f^2+1)} * \left[\varepsilon^{-fwT} *(-f*SIN\ wT - COS\ wT)\right]_0^t$$

$$= \frac{-F_{max}}{w\ m\ (f^2+1)} * \left[\varepsilon^{-fwt} *(f*SIN\ wt+COS\ wt) -1\right]$$

Therefore, the velocity equation is as follows:

$$\dot{Y} = \dot{Y}_{TD} - \frac{F_{max}}{w\ m\ (f^2+1)} * \left[\varepsilon^{-fwt} *(f*SIN\ wt+COS\ wt) -1\right]$$

Because of f<<1, the value of (f*SIN wT) and (f^2+1) can be ignored. The velocity equation can be simplified

as:

$$\dot{Y} = \dot{Y}_{TD} - \frac{F_{max}}{w \quad m} * \left[\varepsilon^{-fwT} * \cos wT - 1\right]$$

By plugging in the value of the ball's veritcal component velocity ($\dot{Y}_{LO}$), the damping coefficient (f) is solved.

5. Integration for the vertical position (ball deformation):

$$\dot{Y} = \dot{Y}_{TD} - \frac{F_{max}}{w \quad m} * \left[\varepsilon^{-fwT} * \cos wT - 1\right]$$

$$\frac{dY}{dT} = \dot{Y}_{TD} - \frac{F_{max}}{w \quad m} * \left[\varepsilon^{-fwT} * \cos wT - 1\right]$$

$$dY = \left[\dot{Y}_{TD} + \frac{F_{max}}{w \quad m}\right]dT - \frac{F_{max}}{w \; m} * \left[\varepsilon^{-fwT} * \cos wT\right]dT$$

Since (F_{max}=-$\dot{Y}_{TD}$*wm), the value of ($\dot{Y}_{TD}$+F_{max}/(wm)) equals zero.

$$dY = - \frac{F_{max}}{w \quad m} * \left[\varepsilon^{-fwT} * \cos wT\right]dT$$

Integrate the above equation from 0 to time t:

$$\int_0^t dY = - \frac{F_{max}}{w \quad m} * \int_0^t \left[\varepsilon^{-fwT} * \cos wT\right]dT$$

$$(Y - Y_{TD}) = \frac{-F_{max}}{w \quad m} * \left[\frac{\varepsilon^{-fwT} * [(-fw*\cos wT)+(w*\sin wT)]}{w^2*(f^2 + 1)}\right]_0^t$$

$$= \frac{-F_{max}}{w^2 m(f^2+1)} * \left[\varepsilon^{-fwT} *(-f*\text{COS } wT + \text{SIN } wT)\right]_0^t$$

$$= \frac{-F_{max}}{w^2 m(f^2+1)} * \left[\varepsilon^{-fwt} *(-f*\text{COS } wt + \text{SIN } wt) + f\right]$$

$$= \frac{F_{max}}{w^2 m(f^2+1)} * \left[\varepsilon^{-fwt} *(f*\text{COS } wt - \text{SIN } wt) - f\right]$$

Therefore, the position equation would be:

$$Y = Y_{TD} + \frac{F_{max}}{w^2 m(f^2+1)} * \left[\varepsilon^{-fwT} *(f*\text{COS } wT - \text{SIN } wT) - f\right]$$

Because of f<<1, the value of (f^2+1) and (f*COS wT) can be ignored. Finally, the equation is:

$$\boxed{Y = Y_{TD} + \frac{F_{max}}{w^2 m} * \left[\varepsilon^{-fwT} *(- \text{SIN } wT) - f\right]}$$

b. <u>The horizontal component force(friction), velocity($\dot{X}$), and position(X)</u>

In the horizontal direction, there is only frictional force acting on the ball during impact. The following steps describe the successive integration.

1. Start with Damped SIN Pulse Model:

$$F_y = m \frac{d\dot{Y}}{dT} = F_{max} * \varepsilon^{-fwT} * \text{SIN } wT$$

Since $F_x = -\mu * F_y$, the force equation can be written as:

$$\boxed{F_x = -\mu * F_y = -\mu * F_{max} * \varepsilon^{-fwT} * \text{SIN } wT}$$

where μ: coefficient of sliding friction.

2. Integration for the horizontal component velocity($\dot{X}$):

$$\text{then,} \quad m \frac{d\dot{X}}{dT} = -\mu * F_{max} * \varepsilon^{-fwT} * \text{SIN } wT$$

$$\int_0^t d\dot{X} = \frac{-\mu * F_{max}}{m} * \int_0^t \varepsilon^{-fwT} * \text{SIN } wT \, dT$$

$$(\dot{X} - \dot{X}_{TD}) = \frac{-\mu * F_{max}}{m} * \left[\frac{\varepsilon^{-fwT} * [(-fw * \text{SIN } wT) - (w * \text{COS } wT)]}{w^2 * (f^2 + 1)} \right]_0^t$$

$$\dot{X} = \dot{X}_{TD} - \frac{\mu * F_{max}}{w \, m \, (f^2+1)} * \left[\varepsilon^{-fwT} * (-f * \text{SIN } wT - \text{COS } wT) \right]_0^t$$

$$\dot{X} = \dot{X}_{TD} - \frac{\mu * F_{max}}{w \, m \, (f^2+1)} * \left[\varepsilon^{-fwt} * (-f * \text{SIN } wt - \text{COS } wt) + 1 \right]$$

$$\dot{X} = \dot{X}_{TD} + \frac{\mu * F_{max}}{w \, m \, (f^2+1)} * \left[\varepsilon^{-fwt} * (f * \text{SIN } wt + \text{COS } wt) - 1 \right]$$

Because of $f \ll 1$, the value of (f^2+1) and $(f * \text{SIN } wT)$ can be neglected. Then, the velocity equation is the following:

$$\boxed{\dot{X} = \dot{X}_{TD} + \frac{\mu * F_{max}}{w \, m} * \left[\varepsilon^{-fwt} * (\text{COS } wt) - 1 \right]}$$

By plugging in the value of the ball horizontal component velocity ($\dot{X}_{LO}$), the damping coefficient (f) is solved.

3. Integration for the horizontal position (X):

$$\dot{X} = \dot{X}_{TD} + \frac{\mu * F_{max}}{w\ m} * \left[\varepsilon^{-fwt} * (COS\ wt) - 1\right]$$

$$\frac{dX}{dT} = \dot{X}_{TD} + \frac{\mu * F_{max}}{w\ m} * \left[\varepsilon^{-fwT} * COS\ wT - 1\right]$$

$$dX = \left[\dot{X}_{TD} - \frac{\mu * F_{max}}{w\ m}\right]dT + \frac{\mu * F_{max}}{w\ m} * \left[\varepsilon^{-fwT} * COS\ wT\right]dT$$

$$\int_0^t dX = \int_0^t \left[\dot{X}_{TD} - \frac{\mu * F_{max}}{w\ m}\right]dT + \frac{\mu * F_{max}}{w\ m} * \int_0^t \left[\varepsilon^{-fwT} * COS\ wT\right]dT$$

$$X - X_{TD} = \left[\dot{X}_{TD} - \frac{\mu * F_{max}}{w\ m}\right] * t + \frac{\mu * F_{max}}{w\ m} * \left[\frac{\varepsilon^{-fwT} * (-fwCOS\ wT + wSIN\ wT)}{w^2 * (f^2 + 1)}\right]_0^t$$

$$X = X_{TD} + \left[\dot{X}_{TD} - \frac{\mu * F_{max}}{w\ m}\right] * t + \frac{\mu * F_{max}}{w^2 m (f^2 + 1)} * \left[\varepsilon^{-fwT} * (-f * COS\ wT + SIN\ wT) + f\right]$$

The horizontal position(X_{TD}) at the ball touchdown is set at zero, and the value of (f^2+1) and (-f*COS wT) are ignored as mentioned above. Therefore, the position equation is the following:

$$\boxed{X = \left[\dot{X}_{TD} - \frac{\mu * F_{max}}{w\ m}\right] * t + \frac{\mu * F_{max}}{w^2\ m} * \left[\varepsilon^{-fwT} * (SIN\ wT) + f\right]}$$

CHAPTER IV

RESULTS

The result of treatment and analysis is presented in the following sections: a) incoming airborne experimental parameters, b) rebounding airborne experimental parameters, c) system parameters, d) mathematical analysis—differentiation approach, integration approach.

Incoming Airborne Experimental Parameters

The results of incoming airborne experimental parameters, which included the angle of incidence (θ_{in}), horizontal component velocity at touchdown ($\dot{X}_{TD}$), vertical component velocity at touchdown ($\dot{Y}_{TD}$), resultant velocity at touchdown (V_{TD}), and angular velocity (w_{TD}) at touchdown for zero-spin impact are listed in Table 2. The angle of incidence ranged from -17.13 degree to -67.84 degree, and the horizontal component velocities decreased from 15.62 (m/s) to 6.57 (m/s); the vertical component velocity was getting larger and larger from -4.81 (m/s) to -16.14 (m/s) when the incident angle was increased; the incoming resultant velocities were around 17 m/s, and the incoming angular velocities were about 5 (rad/s).

The results of incoming airborne parameters for topspin

impact are listed in Table 3. These results include the angle of incidence (θ_{in}), horizontal component velocity at touchdown ($\dot{X}_{TD}$), vertical component velocity at touchdown ($\dot{Y}_{TD}$), resultant velocity at touchdown (V_{TD}), and angular velocity (w_{TD}) at touchdown. In Table 3, we can see the incident angles ranged from -18.3 degree to -70.91 degree, and the horizontal component velocities decreased from 16.13 (m/s) to 5.67 (m/s); the vertical component velocities increased from -5.33 (m/s) to -16.39 when the incident angle increased; the incoming resultant velocities were around 17.67 (m/s), and the incoming angular velocities were about -146 (rad/s).

Table 2. The results of incoming airborne experimental parameters for zero-spin impact

	θ_{in} (deg)	$\dot{X}_{TD}$ (m/s)	$\dot{Y}_{TD}$ (m/s)	V_{TD} (m/s)	w_{TD} (rad/s)
mean	-17.13	15.62	-4.81	16.36	-5.34
sd(n=10)	0.43	0.32	0.13	0.35	7.53
mean	-22.85	15.62	-6.71	17.00	2.61
sd(n=10)	0.36	0.21	0.12	0.19	1.90
mean	-34.47	14.49	-9.95	17.59	-1.10
sd(11)	1.42	0.24	0.40	0.17	7.40
mean	-41.10	13.46	-11.74	17.87	23.46
sd(n=8)	1.63	0.42	0.40	0.28	10.06
mean	-48.55	11.70	-13.25	17.70	5.60
sd(n=8)	2.66	0.60	0.59	0.19	4.72
mean	-58.94	9.16	-15.19	17.74	10.63
sd(n=10)	1.32	0.46	0.24	0.33	8.65
mean	-67.84	6.57	-16.14	17.44	1.15
sd(n=9)	2.39	0.70	0.33	0.25	12.10

Table 3. The results of incoming airborne experimental parameters for topspin impact

	θ_{in} (deg)	$\dot{X}_{TD}$ (m/s)	$\dot{Y}_{TD}$ (m/s)	V_{TD} (m/s)	w_{TD} (rad/s)
mean	-18.30	16.13	-5.33	16.99	-138.20
sd(11)	0.71	0.22	0.19	0.19	10.42
mean	-22.64	16.19	-6.75	17.54	-158.06
sd(n=8)	0.65	0.30	0.22	0.31	21.80
mean	-33.94	14.83	-9.98	17.89	-152.53
sd(n=11)	1.48	0.36	0.42	0.30	10.98
mean	-42.38	13.76	-12.55	18.64	-136.32
sd(n=8)	2.19	0.56	0.47	0.17	6.95
mean	-47.70	11.98	-13.17	17.81	-147.58
sd(n=8)	1.96	0.51	0.44	0.27	9.31
mean	-61.07	8.45	-15.29	17.48	-146.74
sd(n=8)	1.52	0.46	0.21	0.20	7.38
mean	-70.91	5.67	-16.39	17.36	-145.88
sd(n=11)	2.63	0.75	0.44	0.34	9.31

For backspin, the results of incoming airborne experimental parameters, which include the angle of incidence (θ_{in}), horizontal component velocity at touchdown ($\dot{X}_{TD}$), vertical component velocity at touchdown ($\dot{Y}_{TD}$), resultant velocity at touchdown (V_{TD}), and angular velocity (w_{TD}) at touchdown are shown in Table 4. The angle of incidence ranged from -17.42 degree to -67.62 degree , and the horizontal component velocities decreased from 16.18 (m/s) to 6.57 (m/s); the vertical component velocity increased from -5.08 (m/s) to -15.95 (m/s) associated with the increasing of incident angle; the incoming resultant

velocities were around 17 (m/s), and the incoming angular velocities were about 170 (rad/s).

Table 4. The results of incoming airborne experimental parameters for backspin impact

	θ_{in} (deg)	$\dot{X}_{TD}$ (m/s)	$\dot{Y}_{TD}$ (m/s)	V_{TD} (m/s)	w_{TD} (rad/s)
mean	-17.42	16.18	-5.08	16.96	168.32
sd(n=8)	0.65	0.19	0.18	0.18	7.21
mean	-22.44	15.95	-6.59	17.26	148.05
sd(n=12)	0.66	0.16	0.21	0.18	2.43
mean	-34.79	14.35	-9.97	17.48	157.58
sd(n=12)	1.19	0.30	0.33	0.26	7.14
mean	-40.48	13.80	-11.78	18.15	179.12
sd(n=8)	1.10	0.23	0.29	0.13	9.01
mean	-45.21	12.02	-12.11	17.07	164.57
sd(n=8)	1.89	0.45	0.41	0.23	7.09
mean	-58.76	9.12	-15.04	17.61	184.04
sd(n=8)	2.12	0.51	0.42	0.15	12.28
mean	-67.62	6.57	-15.95	17.25	165.53
sd(n=8)	1.09	0.36	0.21	0.26	8.01

Rebounding Airborne Experimental Parameters

The results of rebounding airborne parameters which include the rebounding angle (θ_{out}), horizontal component velocity at lift-off ($\dot{X}_{LO}$), vertical component velocity at lift-off($\dot{Y}_{LO}$), resultant velocity at lift-off (V_{LO}), and angular velocity at lift-off (w_{LO}) for zero-spin impact are shown in Table 5. The rebounding angle increased from 20.83 degree to 76.12 degree when the incident angle was getting

steeper. As the incident angle increased, the horizontal component velocity decreased from 11.09 (m/s) to 2.74 (m/s) and the vertical component velocity increased from 4.22 (m/s) to 11.09 (m/s). Though horizontal and vertical component velocity changed with the incident angle, the rebounding resultant velocity remained about the same around 11 (m/s). The rebounding angular velocity decreased from -239.1 (rad/s) to -96.25 (rad/s) when the incident angle was getting steeper.

Table 5. The results of rebounding airborne experimental parameters for zero-spin impact

	θ_{in} (deg)	θ_{out} (deg)	$\dot{X}_{LO}$ (m/s)	$\dot{Y}_{LO}$ (m/s)	V_{LO} (m/s)	w_{LO} (rad/s)
mean	-17.13	20.83	11.09	4.22	11.73	-239.10
sd(n=10)	0.43	0.66	0.44	0.18	0.34	11.29
mean	-22.85	32.39	8.84	5.76	10.55	-313.20
sd(n=10)	0.36	0.82	0.22	0.17	0.24	7.02
mean	-34.47	45.04	7.66	7.66	10.84	-293.31
sd(n=11)	1.42	1.88	0.32	0.28	0.23	9.54
mean	-41.10	50.33	7.25	8.73	11.36	-239.99
sd(n=8)	1.63	2.03	0.43	0.21	0.26	10.07
mean	-48.55	55.37	6.47	9.37	11.40	-213.17
sd(n=8)	2.66	2.77	0.45	0.35	0.16	16.39
mean	-58.94	70.42	3.87	10.87	11.54	-144.69
sd(n=10)	1.32	1.59	0.32	0.15	0.16	10.63
mean	-67.84	76.12	2.74	11.09	11.44	-96.25
sd(n=9)	2.39	2.39	0.47	0.19	0.15	12.46

Table 6 shows the results of rebounding airborne

parameters for topspin impact. These results include the rebounding angle (θ_{out}), horizontal component velocity at lift-off ($\dot{X}_{LO}$), vertical component velocity at lift-off ($\dot{Y}_{LO}$), resultant velocity at lift-off (V_{LO}), and angular velocity at lift-off (w_{LO}). The rebounding angle increased from 23.09 degree to 67.6 degree; the rebounding horizontal component velocities decreased from 10.98 (m/s) to 4.55 (m/s); the rebounding vertical component velocities increased from 4.67 (m/s) to 11.05 (m/s); the rebounding resultant velocities were around 12 (m/s); the rebounding angular velocities decreased from -386.1 (rad/s) to -119.09 (rad/s).

Table 6. The results of rebounding airborne experimental parameters for topspin impact

	θ_{in} (deg)	θ_{out} (deg)	$\dot{X}_{LO}$ (m/s)	$\dot{Y}_{LO}$ (m/s)	V_{LO} (m/s)	w_{LO} (rad/s)
mean	-18.30	23.09	10.98	4.67	11.94	-386.10
sd(n=11)	0.71	1.29	0.34	0.18	0.27	12.02
mean	-22.64	30.54	10.36	6.11	12.03	-398.11
sd(n=8)	0.65	0.47	0.27	0.12	0.28	7.30
mean	-33.94	40.58	9.65	8.26	12.71	-323.74
sd(n=11)	1.48	1.26	0.28	0.22	0.22	15.25
mean	-42.38	43.33	9.67	9.12	13.30	-285.46
sd(n=8)	2.19	2.12	0.37	0.41	0.25	12.07
mean	-47.70	51.88	7.75	9.88	12.56	-236.54
sd(8)	1.96	1.74	0.35	0.28	0.24	5.88
mean	-61.07	62.41	5.51	10.53	11.89	-163.87
sd(8)	1.52	2.22	0.46	0.28	0.28	10.05
mean	-70.91	67.60	4.55	11.05	11.95	-119.09
sd(n=11)	2.63	1.96	0.35	0.29	0.20	10.09

The results shown in Table 7 are the rebounding airborne parameters for back spin impact which include the rebounding angle (θ_{out}), horizontal component velocity at lift-off ($\dot{X}_{LO}$), vertical component velocity at lift-off($\dot{Y}_{LO}$), resultant velocity at touchdown (V_{LO}), and angular velocity at lift-off (w_{LO}).

Table 7. The results of rebounding airborne experimental parameters for backspin impact

	θ_{in} (deg)	θ_{out} (deg)	$\dot{X}_{LO}$ (m/s)	$\dot{Y}_{LO}$ (m/s)	V_{LO} (m/s)	w_{LO} (rad/s)
mean	-17.42	20.31	10.56	3.91	11.26	-105.50
sd(n=8)	0.65	0.66	0.18	0.10	0.15	10.02
mean	-22.44	28.25	9.82	5.27	11.14	-170.35
sd(n=12)	0.66	0.70	0.19	0.15	0.20	14.27
mean	-34.79	49.78	6.00	7.09	9.29	-261.54
sd(n=12)	1.19	1.62	0.28	0.20	0.22	12.43
mean	-40.48	58.19	5.36	8.64	10.17	-208.97
sd(n=8)	1.10	0.40	0.10	0.25	0.26	6.80
mean	-45.21	65.58	4.12	9.08	9.99	-175.12
sd(n=8)	1.98	3.03	0.47	0.31	0.19	11.78
mean	-58.76	74.78	2.81	10.29	10.68	-106.79
sd(n=8)	2.12	3.06	0.58	0.27	0.29	15.03
mean	-67.62	81.72	1.57	10.84	10.98	-71.43
sd(n=8)	1.09	3.39	0.63	0.39	0.35	13.52

The rebounding angles increased from 20.31 degrees to 81.72 degrees; the rebounding horizontal component velocities decreased from 10.56 (m/s) to 1.57 (m/s); the rebounding vertical component velocities increased from 3.91 (m/s) to 10.84 (m/s); the rebounding resultant velocities were around

10.5 (m/s); and the rebounding angular velocities decreased from -105.5 (rad/s) to - 71.43 (rad/s).

System Parameters

Table 8 shows the results of system parameters which included the coefficient of restitution (e), coefficient of sliding friction (μ), ball dwell distance (DW_{dist}), and ball dwell time (DW_{time}) for zero-spin impact.

Table 8. The results of system parameters for zero-spin impact

	θ_{in} (deg)	e	μ	DW_{dist} (cm)	DW_{time} (ms)
mean	-17.13	0.88	0.50	7.84	6.02
sd(n=10)	0.43	0.05	0.05	0.32	0.24
mean	-22.85	0.86	0.55	6.29	5.20
sd(n=10)	0.36	0.05	0.03	0.31	0.29
mean	-34.47	0.77	0.39	4.96	4.84
sd(n=11)	1.42	0.05	0.03	0.16	0.16
mean	-41.10	0.75	0.30	4.24	4.56
sd(n=8)	1.63	0.03	0.04	0.17	0.16
mean	-48.55	0.71	0.23	3.50	4.39
sd(n=8)	2.66	0.06	0.05	0.13	0.18
mean	-58.94	0.72	0.20	2.21	3.80
sd(n=10)	1.32	0.02	0.03	0.08	0.19
mean	-67.84	0.69	0.14	0.16	3.90
sd(n=9)	2.39	0.02	0.04	0.12	0.12

As the table shows, the coefficient of restitution decreased from 0.88 to 0.69 when the incident angle was

getting steeper. The sliding coefficient of friction decreased from 0.5 to 0.14 associated with the increasing of incident angle. The ball dwell distances also decreased from 7.84 (cm) to 1.61 (cm) when the incident angle increased, and the time of ball contacting the surface decreased from 6.02 (ms) to 3.9 (ms) as well as ball dwell distance.

The results in Table 9 are the system parameters for topspin impact which include the coefficient of restitution (e), coefficient of sliding friction (μ), ball dwell distance (DW_{dist}), and ball dwell time (DW_{time}).

Table 9. The results of system parameters for topspin impact

	θ_{in} (deg)	e	μ	DW_{dist} (cm)	DW_{time} (ms)
mean	-18.30	0.89	0.52	7.56	5.63
sd(n=11)	0.71	0.04	0.04	0.33	0.19
mean	-22.64	0.91	0.45	6.53	5.07
sd(n=8)	0.65	0.03	0.02	0.30	0.27
mean	-33.94	0.83	0.28	5.00	4.45
sd(n=11)	1.48	0.05	0.03	0.14	0.19
mean	-42.38	0.73	0.19	4.79	4.49
sd(n=8)	2.19	0.06	0.04	0.19	0.14
mean	-47.70	0.75	0.18	3.51	3.86
sd(n=8)	1.96	0.04	0.09	0.09	0.13
mean	-61.07	0.69	0.11	2.67	4.05
sd(n=8)	1.52	0.02	0.03	0.13	0.18
mean	-70.19	0.67	0.04	2.09	4.08
sd(n=11)	2.63	0.02	0.04	0.12	0.19

As well as the incoming zero-spin impact, the system

parameters of topspin had similar results: the coefficient of restitution decreased from 0.89 to 0.67; the sliding coefficient of friction decreased from 0.52 to 0.04; the ball dwell distance decreased from 7.56 (cm) to 2.09 (cm); the ball contact time also decreased from 5.63 (ms) to 4.08 (ms).

The results listed in Table 10 are the system parameters including the coefficient of restitution (e), coefficient of sliding friction (μ), ball dwell distance (DW_{dist}), and ball dwell time (DW_{time}) for backspin impact.

Table 10. The results of system parameters for backspin impact

	θ_{in} (deg)	e	μ	DW_{dist} (cm)	DW_{time} (ms)
mean	-17.42	0.77	0.63	8.26	6.25
sd(n=8)	0.65	0.02	0.04	0.58	0.40
mean	-22.44	0.80	0.52	6.48	5.12
sd(n=12)	0.66	0.03	0.02	0.15	0.12
mean	-34.79	0.71	0.49	4.92	5.02
sd(n=12)	1.19	0.04	0.03	0.15	0.14
mean	-40.48	0.73	0.41	3.79	4.51
sd(n=8)	1.10	0.02	0.02	0.10	0.08
mean	-45.21	0.75	0.37	3.08	4.26
sd(n=8)	1.89	0.04	0.04	0.18	1.14
mean	-58.76	0.68	0.25	1.80	3.94
sd(n=8)	2.12	0.02	0.04	0.15	0.18
mean	-67.62	0.68	0.19	1.35	4.43
sd(n=8)	1.09	0.02	0.03	0.14	0.20

In the table, the coefficient of restitution decreases obviously, ranging from 0.8 to 0.68. The sliding coefficient

of friction decreased from 0.63 to 0.19 when the incident angle was getting steeper. The ball dwell distance decreased from 8.26 (cm) to 1.35 (cm), and the ball contact time also decreased from 6.25 (ms) to 4.43 (ms).

Mathematical Analysis for Contact Period

Differentiation Approach

After the contact data was plotted as a nondimensional function, the Polynomial Least Square Regression curve fit was used for generating the predictive equation for the following functions: fraction of horizontal distance vs fraction of dwell time, fractional vertical deformation vs fraction of dwell time, and fraction of rotation vs fraction of dwell time.

The results shown in Table 11 are the polynomial predictive equations for zero-spin, topspin and backspin impact. The predicted results were compared to the actual experimental contact data shown in Figure 5, Figure 6, and Figure 7. In order to obtain the velocities and accelerations (force or torque), a successive differentiation was used for deriving the predictive equation for this purpose. Table 12 shows the predictive equations for zero-spin, topspin and backspin impact.

Table 11. The predictive equations for horizontal vertical and rotational position vs time for zero-spin, top-spin and backspin impact

spin	vs	polynomial regressional equation	R^2
zero-spin	X vs T	$X=.0065 + 1.457T - .558T^2 + .108T^3$	.99
	Y vs T	$Y= .013 - .874T + 1.108T^2 - .239T^3$	.95
	θ vs T	$\theta= .039 - .759T + 2.644T^2 - .958T^3$	.99
top-spin	X vs T	$X=-.004 + 1.386T - .395T^2 + .003T^3$	.99
	Y vs T	$Y= .010 - .919T + 1.312T^2 - .386T^3$	.92
	θ vs T	$\theta=-.003 + .310T + .914T^2 - .218T^3$	.99
back-spin	X vs T	$X=-.003 + 1.434T - .566T^2 + .128T^3$	.99
	Y vs T	$Y= .011 - .994T + 1.527T^2 - .549T^3$	.93
	θ vs T	$\theta= .312 - 17.48T + 36.34T^2 - 18.25T^3$	.99

R^2: polynomial regression coefficient
X: fraction of horizontal contact distance
Y: fractional vertical deformation
θ: fraction of rotation during contact

To check the reliability for these predictive equations, boundary conditions, beginning and end of contact time, were plugged into the equations for solving the velocities of both touchdown and lift-off. The predicted results are listed in Table 13 as well as the results obtained from experiments.

Solving the polynomial regression equations when fraction of rotation equals zero provide us an information about when and where the skidding stops and rolling begins, and the results are shown in Table 14. An overlay plot of fraction of rotation vs fraction of dwell time for zero-spin, topspin, and backspin is shown in Figure 8.

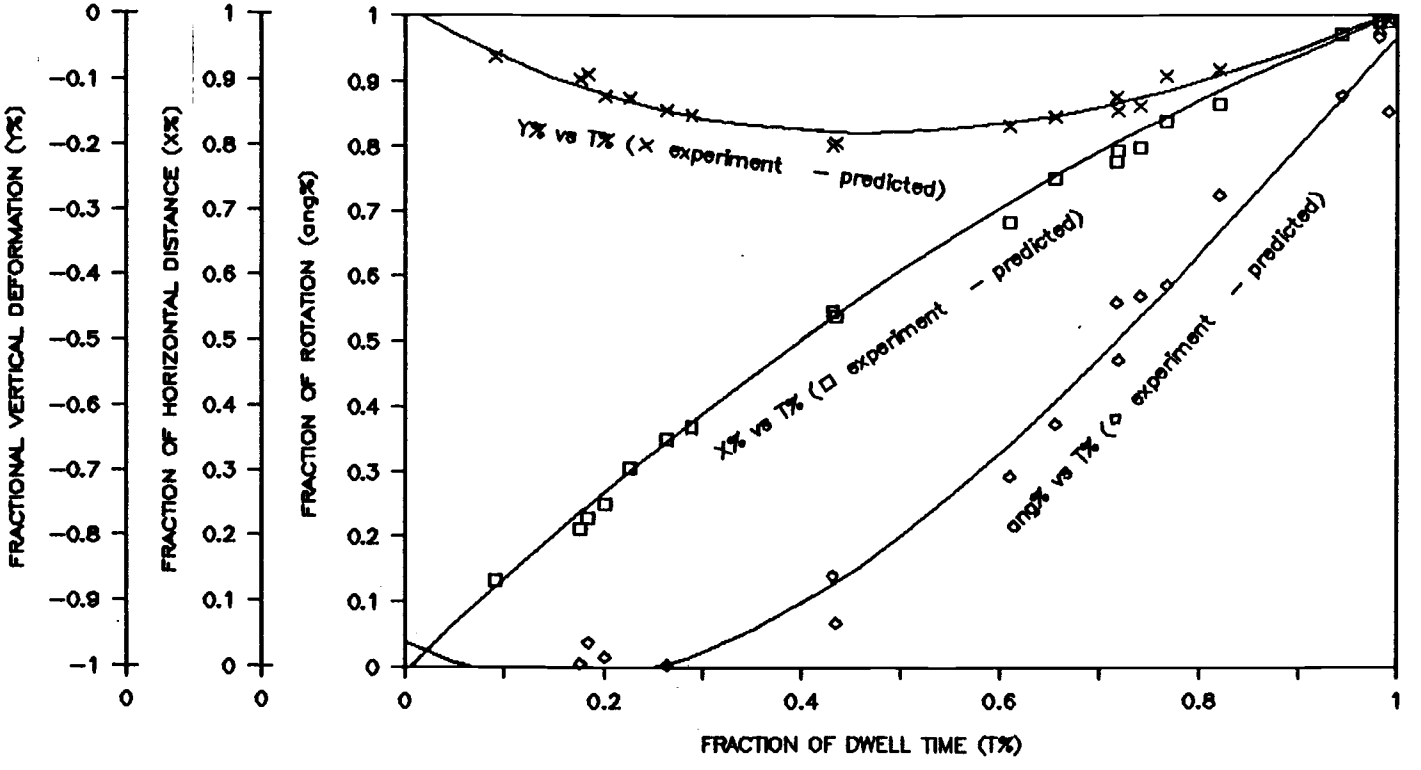

Figure 5. Plots of fraction of rotation vs fraction of dwell time, fraction of vertical distance vs fraction of dwell time, and fraction of horizontal distance vs fraction of dwell time based the polynomial regression equations for the zero-spin impact.

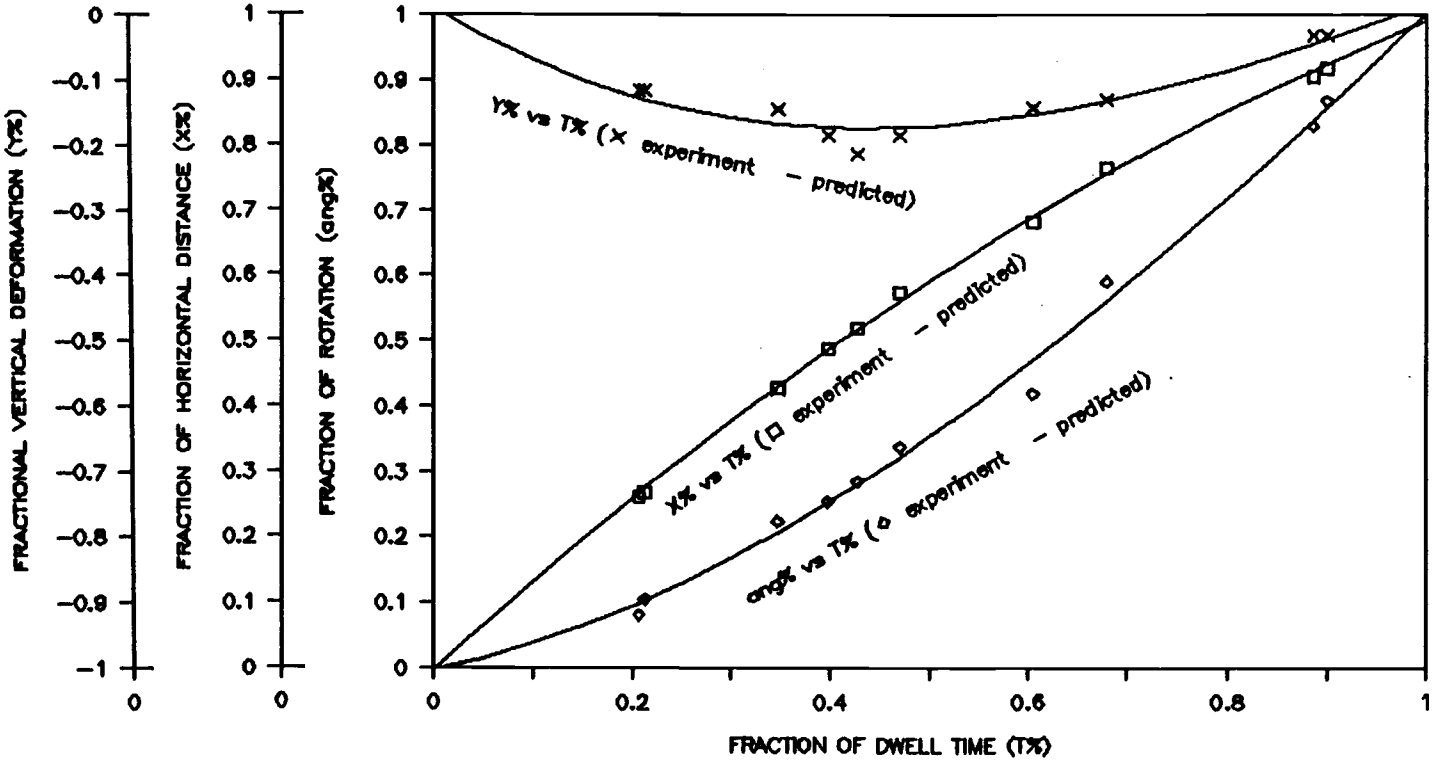

Figure 6. Plots of fraction of rotation vs fraction of dwell time, fraction of vertical distance vs fraction of dwell time, and fraction of horizontal distance vs fraction of dwell time based on the polynomial regression equations for the top-spin impact.

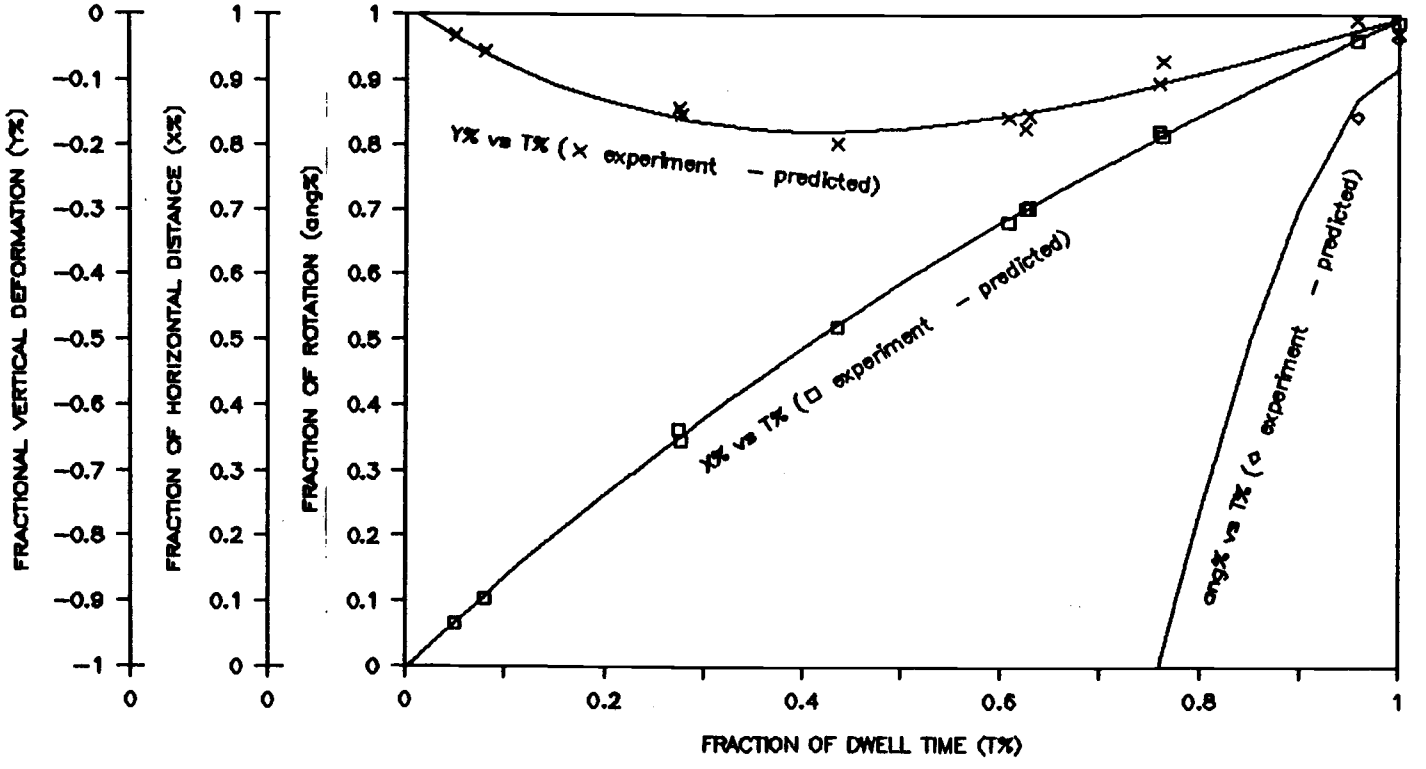

Figure 7. Plots of fraction of rotation vs fraction of dwell time, fraction of vertical distance vs fraction of dwell time, and fraction of horizontal distance vs fraction of dwell time based on the polynomial regression equations for the back-spin impact.

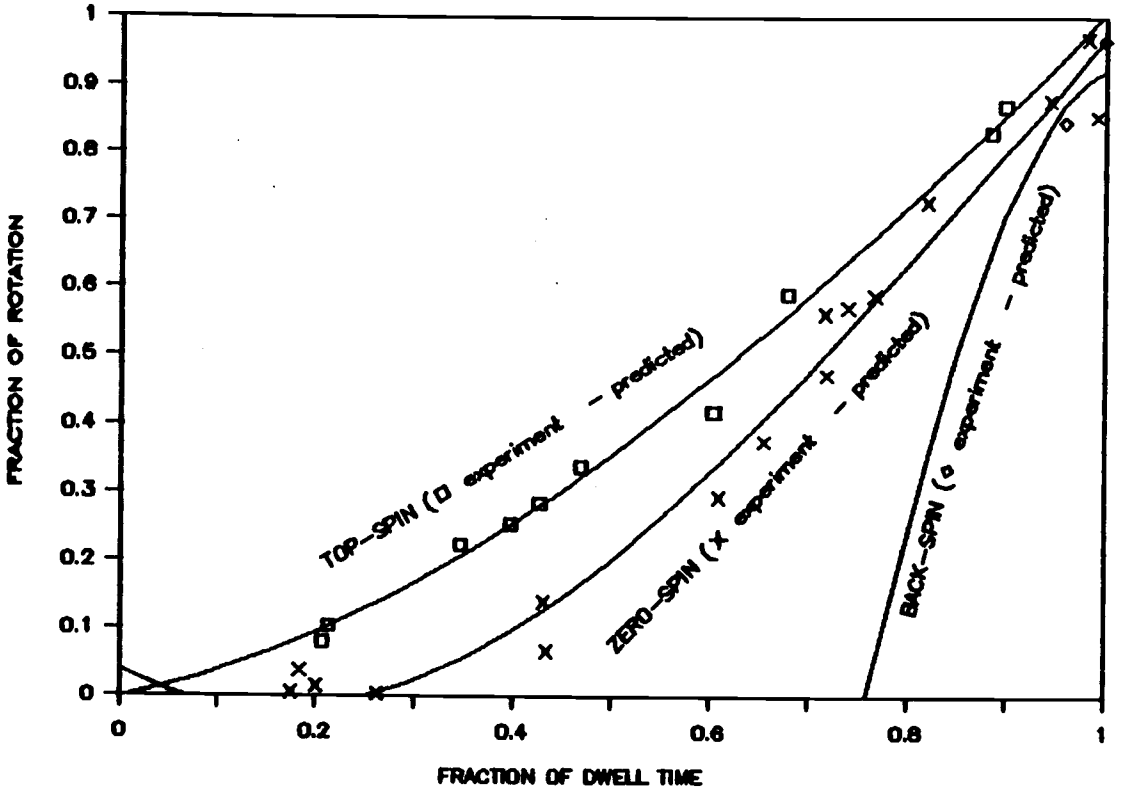

Figure 8. Plots of fraction of rotation vs fraction of dwell time for zero-spin, top-spin and back-spin.

Table 12. Predictive equations for zero-spin, topspin and backspin impact established by successive differentiation from polynomial regression equation

spin	vs	differentiation equation
zero-	X vs T	$X=.0065 + 1.457T - .558T^2 + .108T^3$
spin	$\dot{X}$ vs T	$\dot{X}=1.457 - 1.116T + .324T^2$
	F_x vs T	$F_x= m * (- 1.116 + .648T)$
	Y vs T	$Y= .013 - .874T + 1.108T^2 - .239T^3$
	$\dot{Y}$ vs T	$\dot{Y}= -.874 + 2.216T - .717T^2$
	F_y vs T	$F_y= m * (2.216 - 1.434T)$
	θ vs T	$\theta= .039 - .759T + 2.644T^2 - .958T^3$
	w vs T	$w=-.759 + 5.288T - 2.874T^2$
	Tq vs T	$Tq=2/3*m*r^2*(5.288 - 5.748T)$
top-	X vs T	$X=-.004 + 1.386T - .395T^2 + .003T^3$
spin	$\dot{X}$ vs T	$\dot{X}=1.386 - .790T + .009T^2$
	F_x vs T	$F_x= m * (-.790 + .018T)$
	Y vs T	$Y= .010 - .919T + 1.312T^2 - .386T^3$
	$\dot{Y}$ vs T	$\dot{Y}=-.919 + 2.624T - 1.164T^2$
	F_y vs T	$F_y= m * (2.624 - 2.328T)$
	θ vs T	$\theta=-.003 + .310T + .914T^2 - .218T^3$
	w vs T	$w= .310 + 1.828T - .654T^2$
	Tq vs T	$Tq=2/3*m*r^2*(1.828 - 1.308T)$
back-	X vs T	$X=-.003 + 1.434T - .566T^2 + .128T^3$
	$\dot{X}$ vs T	$\dot{X}=1.434 - 1.132T + .354T^2$
	F_x vs T	$F_x= m * (-1.132 + .708T)$
spin	Y vs T	$Y= .011 - .994T + 1.527T^2 - .549T^3$
	$\dot{Y}$ vs T	$\dot{Y}=-.994 + 3.054T + 1.647T^2$
	F_y vs T	$F_y= m * (3.054 - 3.254T)$
	θ vs T	$\theta= .312 - 17.48T + 36.34T^2 - 18.25T^3$
	w vs T	$w=17.48 + 72.68T - 54.75T^2$
	Tq vs T	$Tq=2/3*m*r^2*(72.68 - 109.50T)$

X:fraction of horizontal contact distance
$\dot{X}$:horizontal velocity based on fractional X distance
F_x:negative frictional force based on fractional X distance
Y:fractional vertical deformation
$\dot{Y}$:vertical velocity based on fractional Y deformation
F_y:vertical force based on fractional Y deformation
θ:fraction of rotation during contact
w:angular velocity based on fraction of rotation
Tq:torque based on fraction of rotation

Table 13. Predicted and experimental horizontal, vertical and angular velocities for zero-spin, topspin and backspin impact at touchdown and lift-off surface

spin		$\dot{X}_{TD}$ (m/s)	$\dot{X}_{LO}$ (m/s)	$\dot{Y}_{TD}$ (m/s)	$\dot{Y}_{LO}$ (m/s)	w_{TD} (rad/s)	w_{LO} (rad/s)
zero-spin	pdt	17.62	12.18	-5.47	3.91	-129.91	-283.10
	exp	15.62	11.09	-6.71	5.67	2.51	-313.20
top-spin	pdt	17.85	7.80	-5.90	3.48	-96.73	-463.06
	exp	16.19	10.36	-6.75	6.11	-158.06	-398.11
back-spin	pdt	18.15	8.30	-6.32	2.63	-580.39	-1175.15
	ext	15.95	9.82	-6.59	5.27	148.05	-170.35

pdt: predicted value
exp: experimental value
$\dot{X}_{TD}$, $\dot{X}_{LO}$: horizontal velocity at touchdown and lift-off
$\dot{Y}_{TD}$, $\dot{Y}_{LO}$: vertical velocity at touchdown and lift-off
w_{TD}, w_{LO}: angular velocity at touchdown and lift-off

Table 14. The time and distance in fraction when the skidding stops and rolling begins on the surface solved by the polynomial regression equation

spin	fraction of rotation	fraction of distance
zero-spin	0.26	0.35
topspin	0.01	0.01
backspin	0.76	0.82

Integration Approach

Based on Damped Sin Pulse Model, a successive integration was used, starting from force vs time, to obtain velocity and position data. Table 15 shows the predictive equations for vertical and horizontal force, velocity and contact position for zero-spin, topspin and backspin impact. With these equations, continuative data of force,

velocity, and position were generated from the beginning to the end of contact time to obtain the contact information. These results are plotted as overlap graphs in Figures 9 to Figure 14.

Table 16 shows the information about the time, vertical force, deformation, friction force, horizontal component velocity, and horizontal distance when the ball reaches its maximum deformation.

Table 15. Predictive equations via successive integration for zero-spin, topspin and backspin impact based on Damped Sin Pulse Model

spin		integration equation
zero-spin	F_y vs T	F_y=233.2*E^(-27.9*T)*SIN(604.2*T)
	$\dot{Y}$ vs T	$\dot{Y}$=-6.7-6.7*(E^(-27.9*T)*COS(604.2*T)-1)
	Y vs T	Y=.0651-.011*E^(-27.9*T)*SIN(604.2*T)
	F_x vs T	F_x=-128.2*E^(-27.9*T)*SIN(604.2*T)
	$\dot{X}$ vs T	$\dot{X}$=15.6+3.7*(E^(-27.9*T)*COS(604.2*T)-1)
	X vs T	X=11.9*T+.006*(E^(-27.9*T)*SIN(604.2*T)+.05
top-spin	F_y vs T	F_y=241.0*E^(-19.5*T)*SIN(619.6*T)
	$\dot{Y}$ vs T	$\dot{Y}$=-6.8-6.8*(E^(-19.5*T)*COS(619.6*T)-1)
	Y vs T	Y=.0651-.011*E^(-19.5*T)*SIN(619.6*T)
	F_x vs T	F_x=-109.2*E^(-19.5*T)*SIN(619.6*T)
	$\dot{X}$ vs T	$\dot{X}$=16.2+3.1*(E^(-19.5*T)*COS(619.6*T)-1)
	X vs T	X=13.1*T+.005*(E^(-19.5*T)*SIN(619.6*T)+.03
back-spin	F_y vs T	F_y=232.7*E^(-43.3*T)*SIN(613.1*T)
	$\dot{Y}$ vs T	$\dot{Y}$=-6.6-6.6*(E^(-43.3*T)*COS(613.1*T)-1)
	Y vs T	Y=.0651-.011*E^(-43.3*T)*SIN(613.1*T)
	F_x vs T	F_x=-120.5*E^(-43.3*T)*SIN(613.1*T)
	$\dot{X}$ vs T	$\dot{X}$=16.0+3.4*(E^(-43.3*T)*COS(613.1*T)-1)
	X vs T	X=12.5*T+.006*(E^(-43.3*T)*SIN(613.1*T)+.07

E : exponential function
F_y: force normal to surface
$\dot{Y}$: vertical component velocity
Y : distance from top of ball to surface
F_x: frictional force on surface
$\dot{X}$: horizontal component velocity
X : contact distance on surface

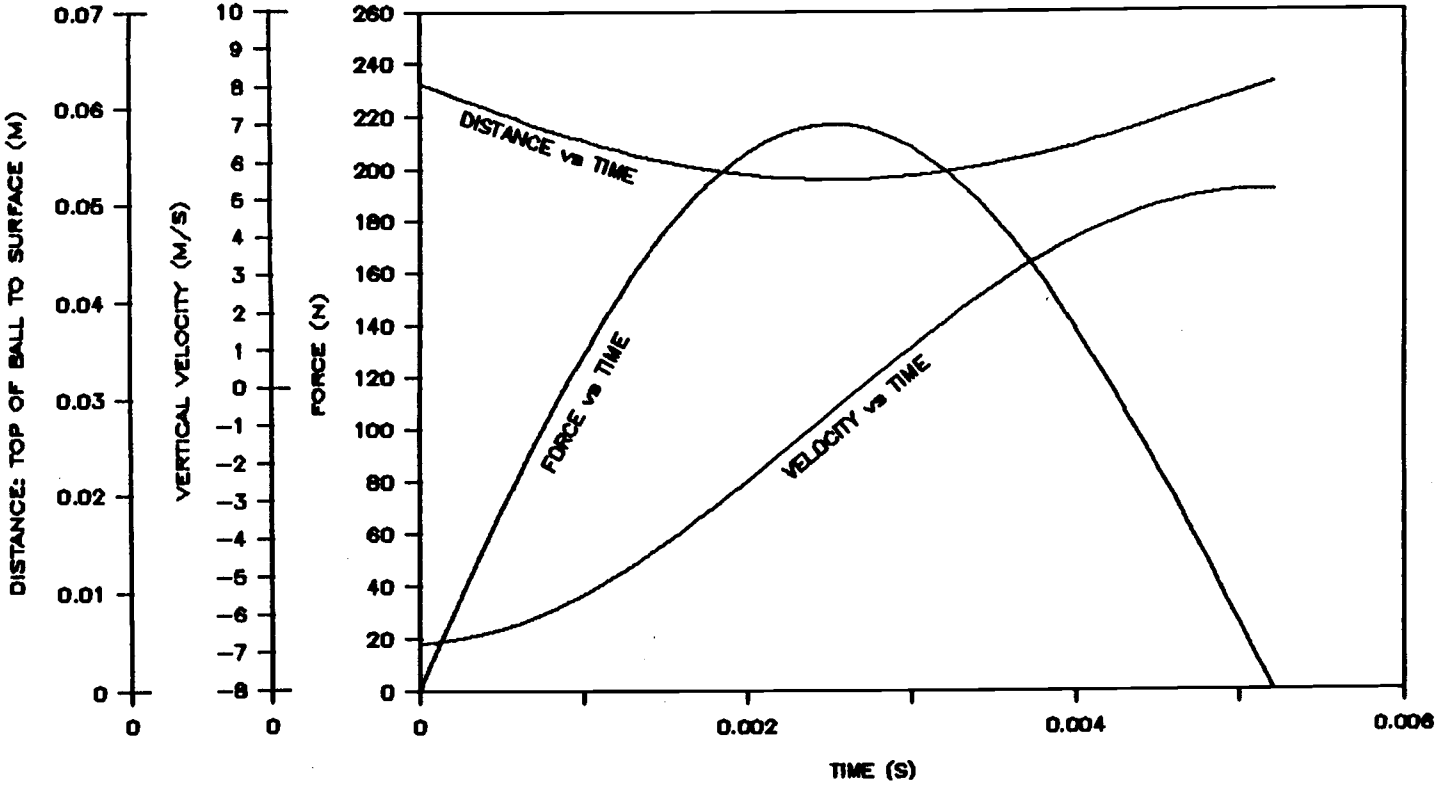

Figure 9. Plots of vertical force vs time, vertical component velocity vs time, and distance from top of ball to surface vs time for the contact period based on the integration equations for the zero-spin impact.

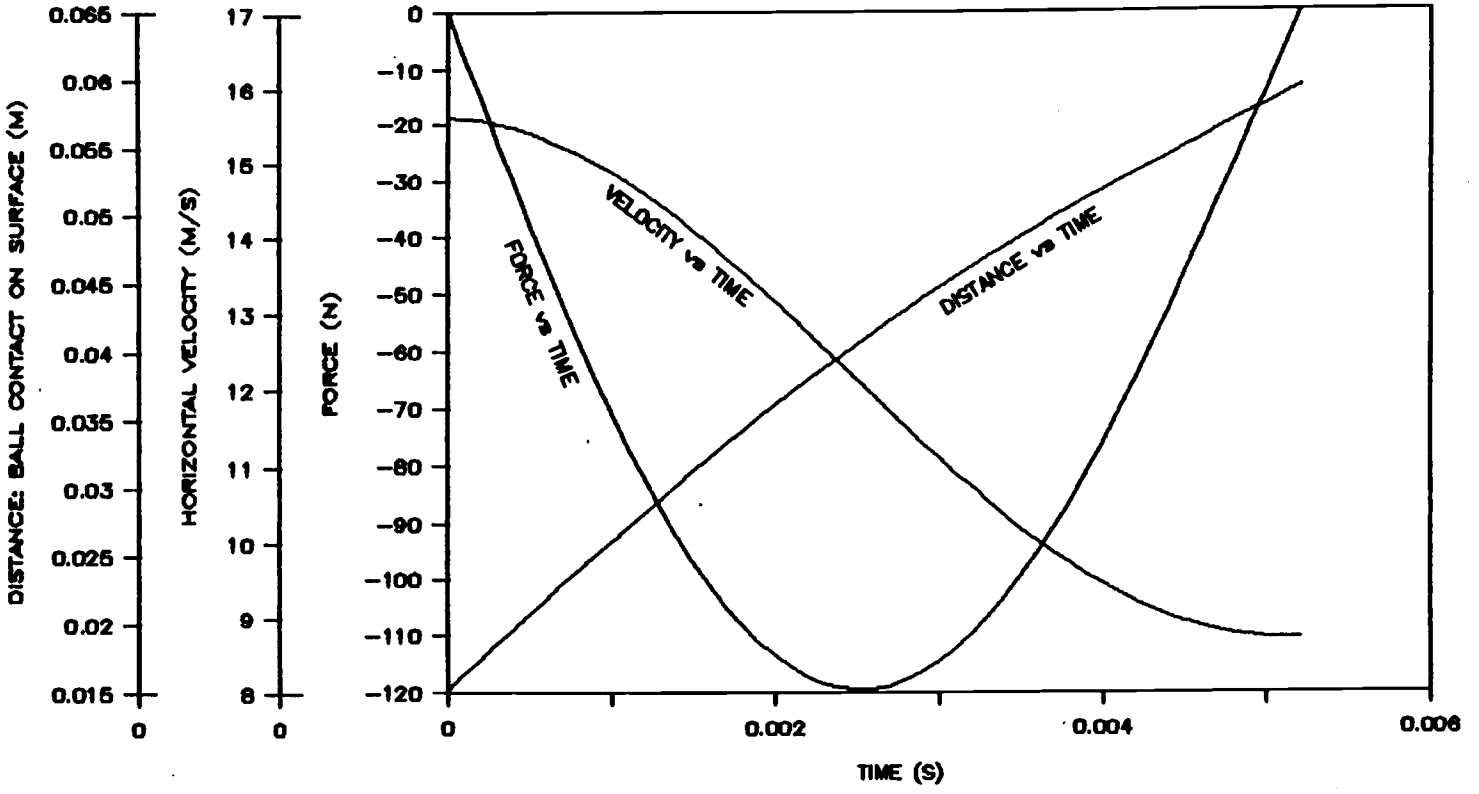

Figure 10. Plots of frictional force vs time, horizontal component velocity vs time, and ball contact distance vs time for the contact period based on the integration equations for zero-spin impact.

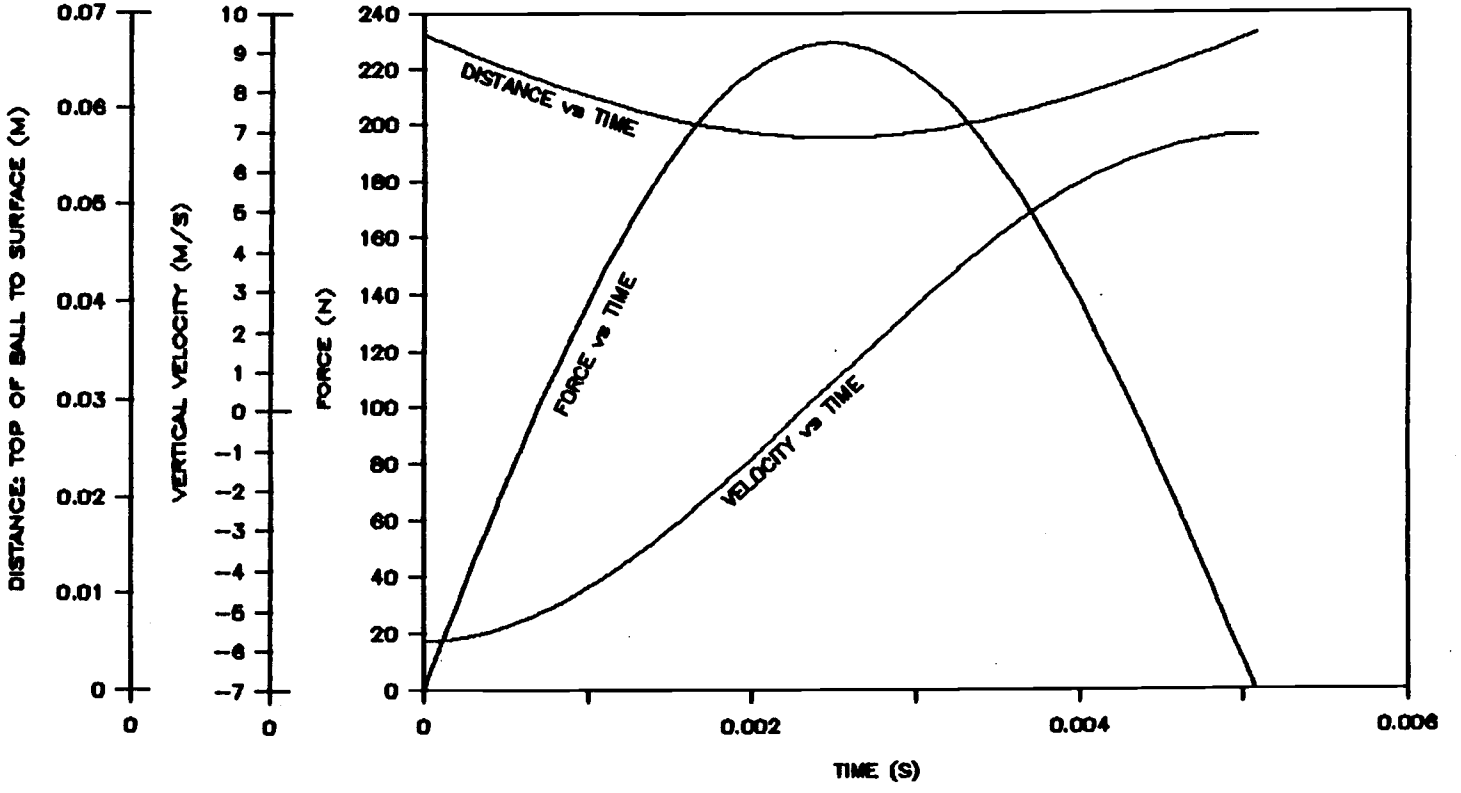

Figure 11. Plots of vertical force vs time, vertical component velocity vs time, and distance from top of ball to surface vs time for the contact period based on the integration equations for the top-spin impact.

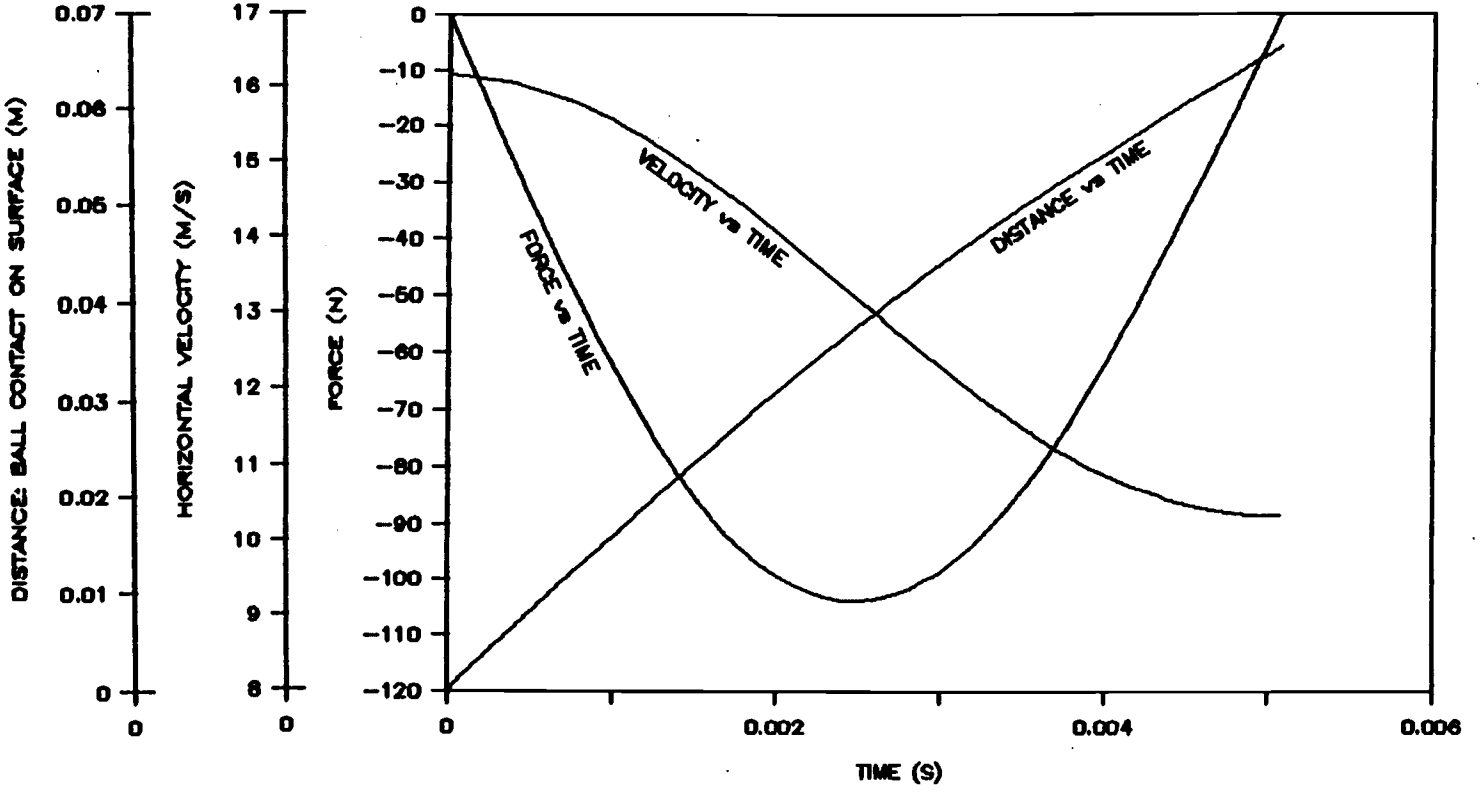

Figure 12. Plots of frictional force vs time, horizontal component velocity vs time, and ball contact distance vs time for the contact period based on the integration equations for top-spin impact.

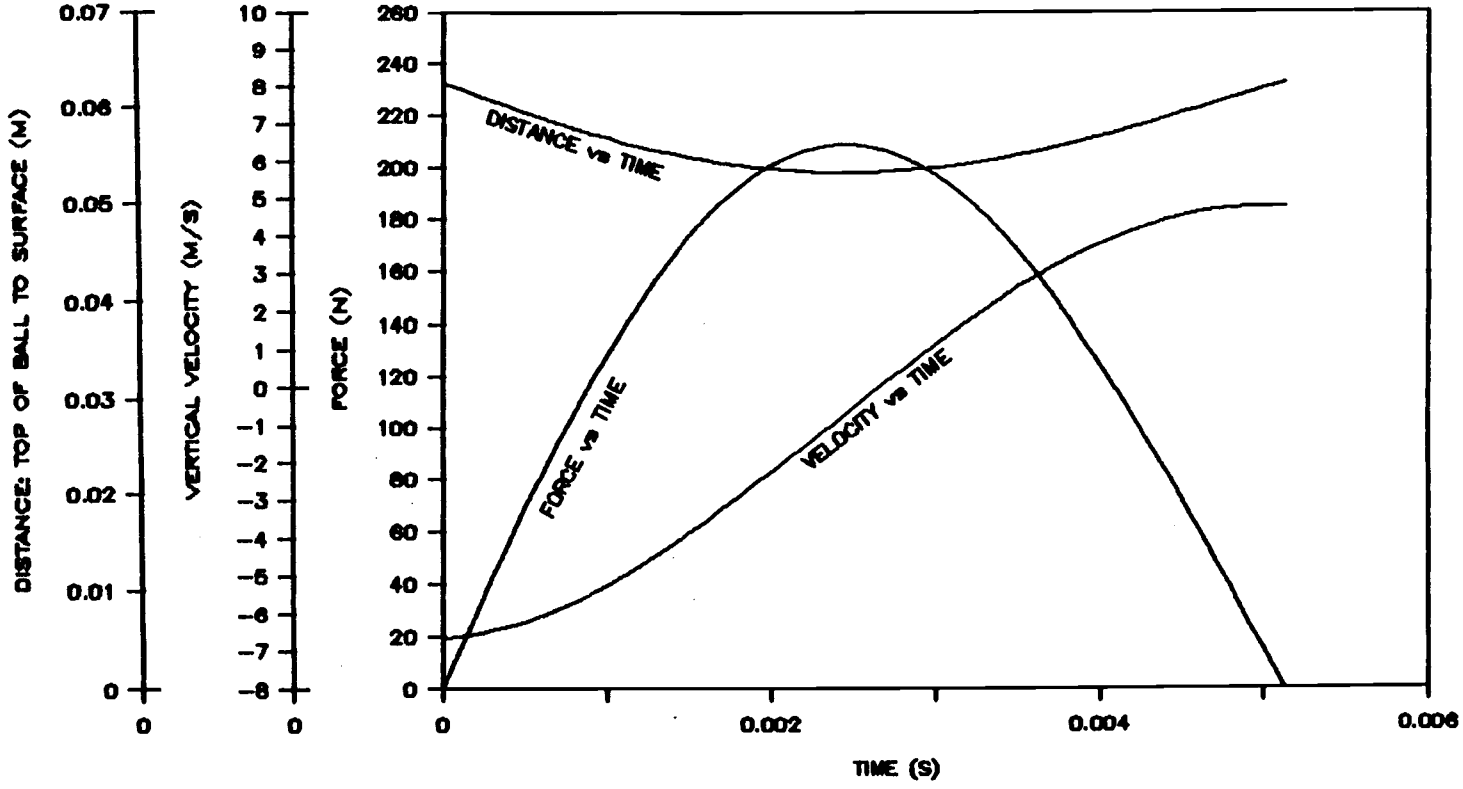

Figure 13. Plots of vertical force vs time, vertical component velocity vs time, and distance from top of ball to surface vs time for the contact period based on the integration equations for the back-spin impact.

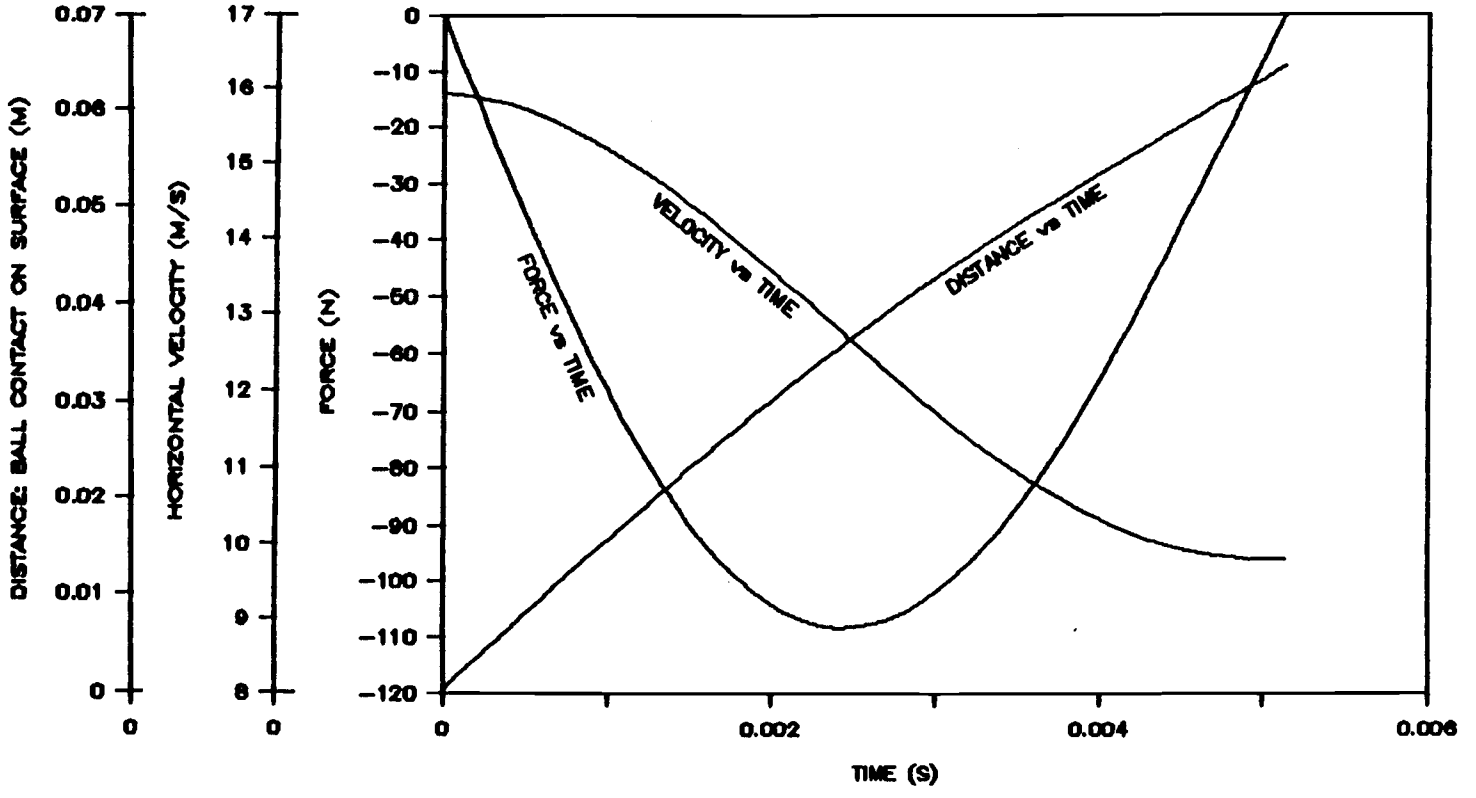

Figure 14. Plots of frictional force vs time, horizontal component velocity vs time, and ball contact distance vs time for the contact period based on the integration equations for back-spin impact.

Table 16. The values of time, vertical force, deformation, friction force, horizontal component velocity, and distance at the instance of ball's maximum deformation

spin	time%	$maxF_y$	maxDEF%	$maxF_f$	$\dot{X}$%	X%
zero	0.48	217.0N	-0.16	-119.3N	0.76	0.59
top	0.50	229.4N	-0.16	-104.0N	0.81	0.58
back	0.47	208.0N	-0.15	-108.1N	0.81	0.54

time% : fraction of the total contact time
$maxF_y$: maximum vertical force
maxDEF% : ball's maximum deformation in fraction of diameter
$maxF_f$: maximum friction force
$\dot{X}$% : fraction of horizontal component velocity
X% : fraction of the total contact distance

At the end of successive integration, the predicted data for both the vertical and the horizontal position of the ball during contact period were compared to the actual experimental contact data shown in Figure 15, Figure 16, and Figure 17. The standard error of the estimate is shown in Table 17 by the use of following equation:

$$SEE = \sqrt{\Sigma(Y - Y')^2 / (N - 1)}$$

where SEE: standard error of the estimate

Y: actual ball contact data obtained from experiments

Y': predicted value created by integration equation

N: number of contact data

Table 17. Standard error of estimate between the predicted value and the actual experimental data

spin	Standard Error of Estimate (unit: M) horizontal position	vertical position
zero-spin	0.001070	0.001180
topspin	0.001408	0.001661
backspin	0.000533	0.001688

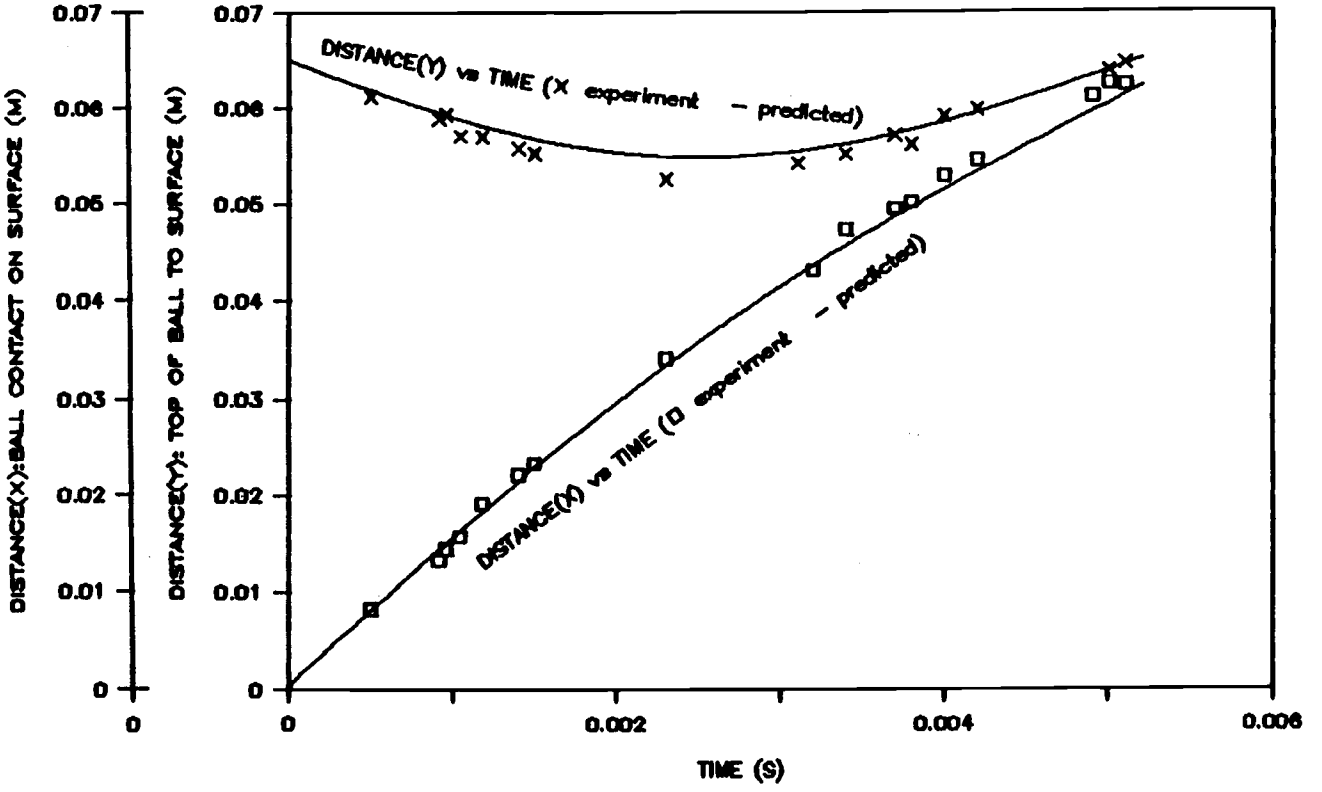

Figure 15. Plots of distance from top of ball to surface vs time and horizontal distance vs time for the contact period based on the integration equations for the zero-spin impact.

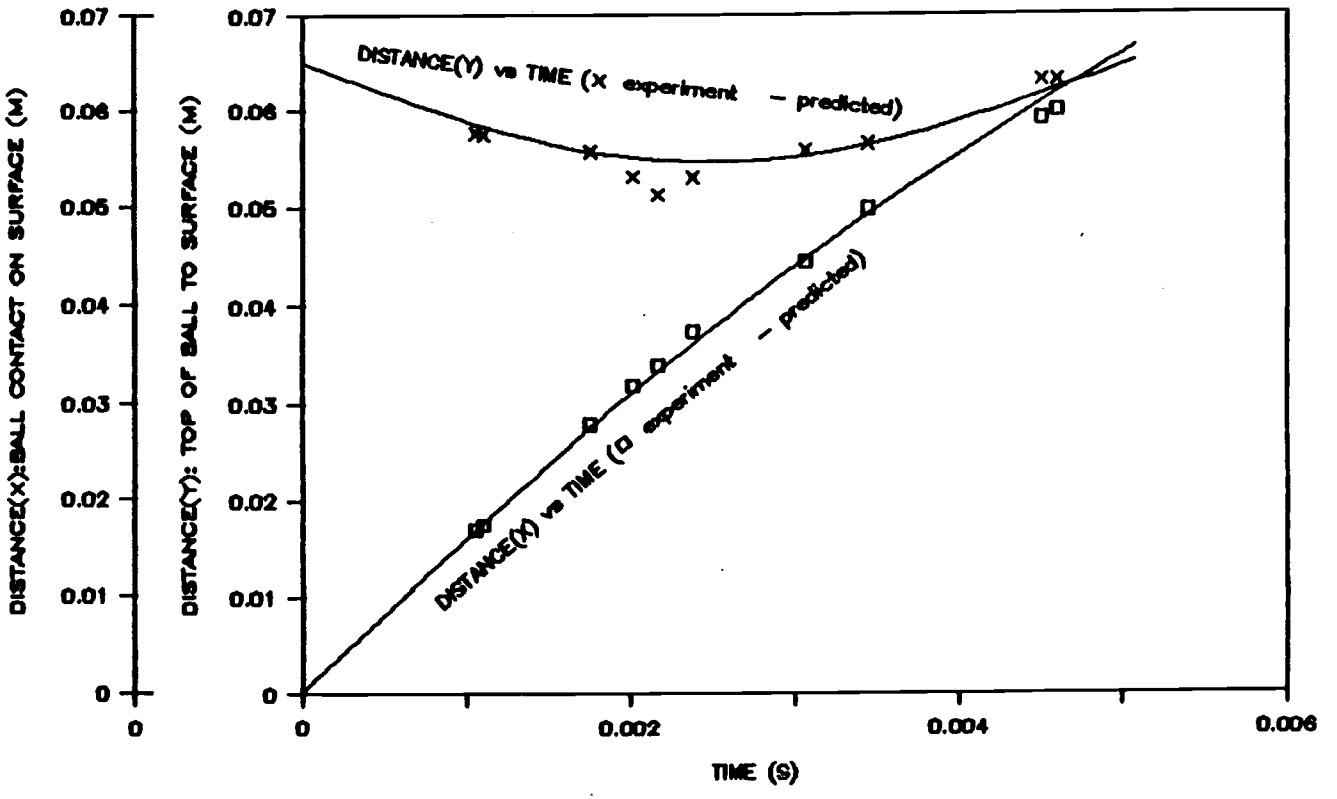

Figure 16. Plots of distance from top of ball to surface vs time and horizontal distance vs time for the contact period based on the integration equations for the top-spin impact.

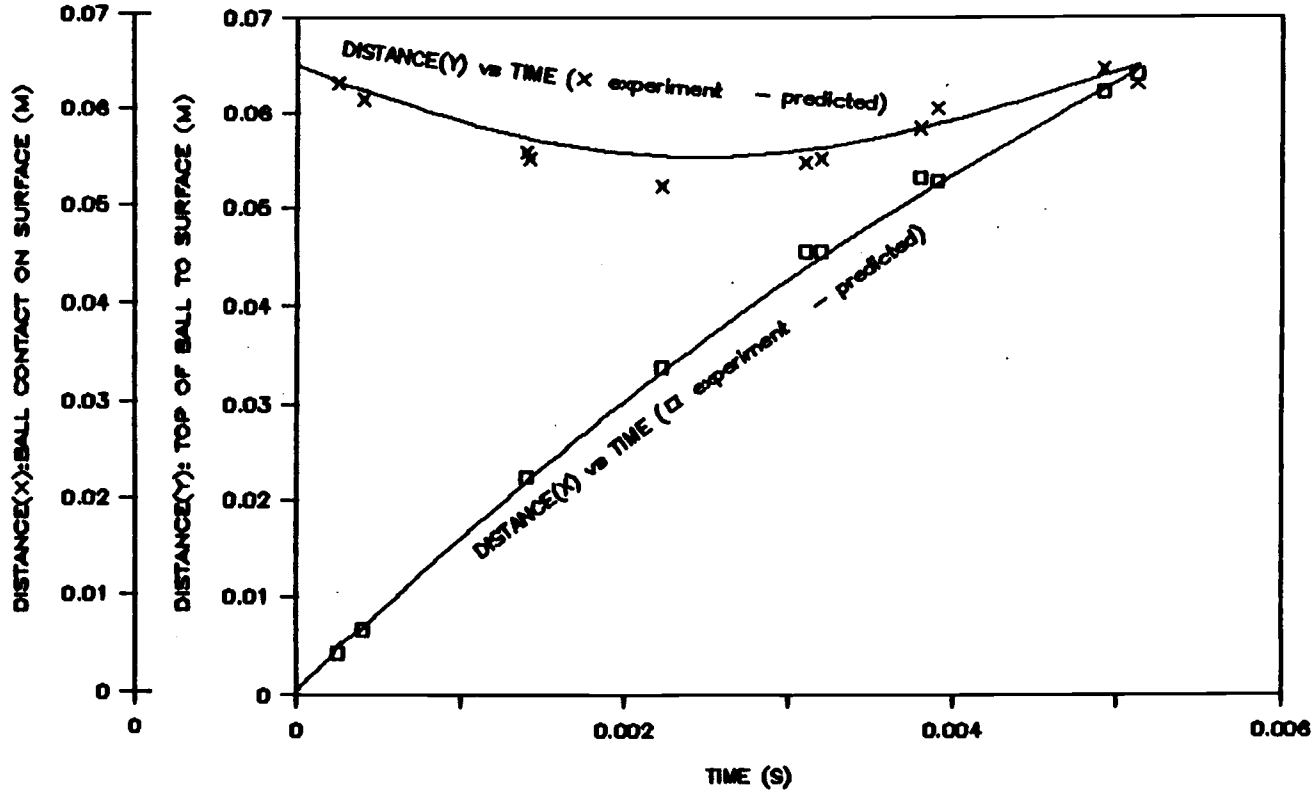

Figure 17. Plots of distance from top of ball to surface vs time and horizontal distance vs time for the contact period based on the integration equations for the back-spin impact.

CHAPTER V

DISCUSSION

This chapter includes the following sections of discussion: a) impact of an imperfectly elastic ball on a rough surface, b) evaluation of differentiation approach, c) evaluation of integration approach, d) events taking place during contact for zero-spin, topspin and backspin impact, and e) evaluation of system parameters.

Impact of an Imperfectly Elastic Ball on a Rough Surface

A Special Case: Impact Normal to Surface

Consider an imperfectly elastic hollow shell ball moving with a center of mass translational velocity V, directed normal to a rough horizontal inertial surface R. Refer to Figure 1 described earlier. The translational velocity V_{td} is negative in sign and equal to $(dy/dt)_{td}$. The ball also is spinning about a diameter parallel to the z axis, with an angular velocity w_{td}, arbitrarily assigned to be negative. Under these conditions the component velocities $(dx/dt)_{td}$ and $(dz/dt)_{td}$ will both be zero.

After impact, at the moment of liftoff, the ball will have a translational velocity V_{lo}, with a vertical component $(dy/dt)_{lo}$, where $|(dy/dt)_{lo}| < |(dy/dt)_{td}|$ and is opposite in

sign. The velocity component $(dx/dt)_{1o}$ will depend on the nature of the coupling of angular and translational velocities taking place during contact. The component velocity $(dz/dt)_{1o}$ remains equal to zero throughout the impact.

The dwell time on the surface can be divided into two periods. In the first period the ball deforms continuously as the kinetic energy due to the incident translational velocity is stored as potential energy by the elastic ball. The ball can be viewed as possessing the properties of a linear spring. The deformation consists of flattening of the contact area, with the growth of a circular footprint, while the rest of the shell retains very nearly its original spherical shape. Superimposed will be the effect of ball spin. If the ball on contact is spinning with a clockwise rotation, for the chosen reference coordinate system, the sign of the angular velocity would be negative. A frictional force exerted at the mating surface acts to impede skidding. If the surface is rough enough to prevent skidding then two possibilities exist for distribution of the angular kinetic energy. Either the ball will begin to roll in a positive direction along the x axis, and/or the ball acting as a torsional spring will store some of the angular kinetic energy as potential energy. Because the shell is a relatively stiff torsional spring, the energy distribution would be much in favor of rolling during contact. However

the incoming angular velocity will cause an asymmetry in the pressure distribution in the footprint. Topspin, in this case clockwise rotation, would drive the leading edge of the ball into the surface, causing increased compression. The trailing edge would tend to be pulled away from the surface, thereby decreasing the compression. The consequence of this asymmetry would be to shift the force exerted by the surface so that it no longer would go through the center of mass of the ball. A torque, $F*\varepsilon$, would be created around the spin diameter, opposing rolling, and would in effect be the major contributor to rolling friction. The greater the size of the footprint the greater the asymmetry and the more energy could be stored in the torsional spring. This effect is illustrated in Figure 18 showing the deformed ball at an arbitrary time during the initial increasingly compressive stage of the contact period. This analysis is consistent with research conducted on the deformation and forces involved with free rolling automobile tires (Moore, 1972; Hays, 1974).

During the second part of the dwell time on the surface relaxation of the stresses occurs as the ball regains its spherical shape on lift-off. Any oscillation at lift-off is assumed to be negligible, or that its decay is very fast compared to the dwell time on the surface. The relaxation phase of the impact begins as the translational velocity goes through zero and begins increasing in a positive sense. The

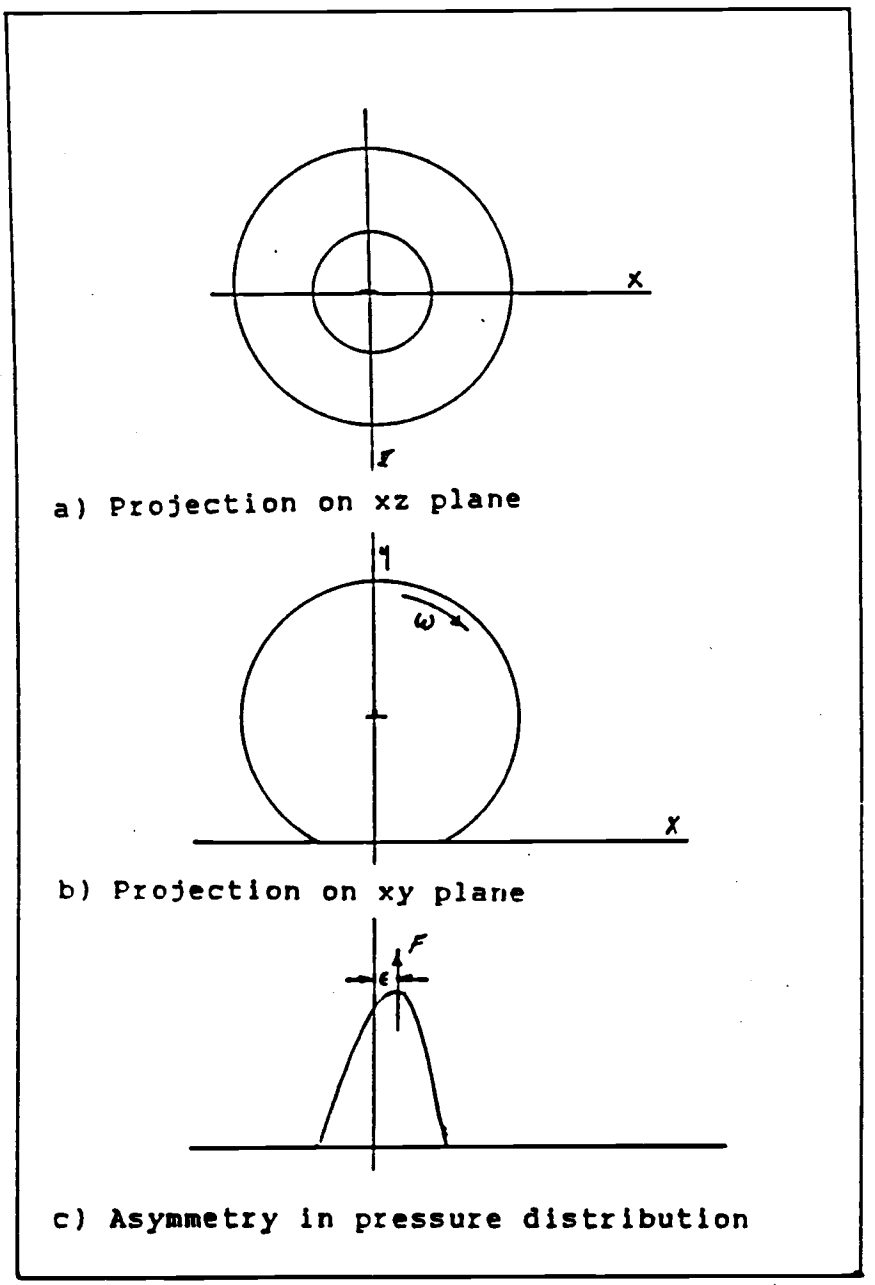

Figure 18. The diagram of ball and its footprint pressure distribution.

unwinding of the torsional spring would be in opposition to the rolling angular velocity. It could prove easier to recover the stored energy by providing it as an enhancement to the energy being recovered from the linear spring. In that case $(dy/dt)_{1o}$ would be larger than expected and unusually large coefficients of restitution would be observed.

The more usual observation, when the translational velocity vector at touchdown is normal to the horizontal surface, is for the spinning ball to skid at touchdown as the frictional torque acts to decrease the angular velocity during the growing compression phase of contact. The ball may not begin to roll immediately as the frictional torque, the product of the frictional force (parallel to the surface) multiplied by the (surface to center of mass) distance, must overcome the rolling frictional torque, generated by the asymmetry in the footprint pressure. Eventually the skidding may cease. This will occur when the peripheral velocity has decreased and the translational velocity along the x axis has increased so that no relative movement of the ball and surface occurs. The behavior then becomes that of a rough surface, and the ball would roll without skidding off the surface.

Oblique Impact

Consider a ball moving with a center of mass velocity V, striking a rough horizontal inertial surface at a glancing

angle θ. As in the previous special case the surface has a right handed orthogonal coordinate system with the origin at the point of contact. The ball is spinning about a diameter parallel to the xz surface and parallel to the z axis. As before z_{td} would be equal to zero. At the moment of touchdown V_{td} /θ can be resolved into its x and y components $(dx/dt)_{td}$ and $(dy/dt)_{td}$. Various angular velocity options must be considered. The incident spin could be zero, back spin (+) or top spin (-). In the case of top spin three possibilities exist, where the magnitude of the peripheral velocity at touchdown is equal to, greater than or less than the horizontal component of the translational velocity of the center of mass of the ball.

For incident back spin the peripheral velocity at touchdown is always in the same direction as the horizontal component of the center of mass velocity and the frictional torque will always act to decrease the magnitude of the incident angular velocity. For most conditions this effect is so great that the angular velocity changes sign and the ball leaves the surface with topspin. The greater the magnitude of backspin at touchdown the less will be the tendency to have the leading edge of the ball driven into the surface, with the resulting asymmetry in the footprint pressure pattern. Little if any coupling of angular and translational kinetic energies should occur as a result of ball deformation.

Treatment of the cases of zero spin and topspin are quite similar, the results differing only in degree. The greater the magnitude of the topspin, the harder the leading edge of the ball is driven onto the surface, resulting in enhanced compressive force on the advancing side of the footprint and a compensating stretching and decrease in force on the trailing side of the footprint. The resulting asymmetric torque will oppose the tendency to roll with topspin around an axis through the center of mass. Whether the ball skids immediately after touchdown or rolls without skidding depends on the magnitude of the topspin. When the magnitude of the peripheral velocity is exactly the same as the center of mass horizontal component of translational velocity, there would be no movement of the ball surface relative to the playing surface. The ball would therefore roll, without skidding off of the surface. The elastic compression of the ball results in the storage of potential energy, mostly with the ball acting as a dissipative essentially linear spring. Under the proper circumstances, e.g. with near zero or especially with increasing topspin, some potential energy will be stored with the ball acting as a torsional spring. During the relaxation phase of the impact some or perhaps most of the energy stored in the torsional spring will manifest itself as an enhanced vertical component of the center of mass translational energy. This will be observable in unreasonably high values for

experimentally measured coefficients of restitution obtained from topspin impacts.

Evaluation of Differentiation Approach

The approach via either successive differentiation or successive integration could be utilized to gain the maximum insight into the events occuring during contact of ball and impact surface. The stroboscopic photographs of the ball impact on the playing surface provide position data on coordinate axis for known time intervals. With this position data, the differentiation approach is capable of obtaining the information of velocity and acceleration (force) by using the successive differentiation. But the weakness of this approach is that if the original data is not very precise, random errors will be enhanced and the propogated errors soon decrease the signal to noise levels to unacceptable values.

The results of this successive differentiation are shown in Table 11, Table 12 and Figure 5 to Figure 8. Table 13 showed clear evidence by comparing the predicted touchdown and lift-off velocities. We can see that it has some amount of error between predicted value and actual experimental data. Especially for angular velocity, the predictive equation completely failed for the prediction. This is because the ball doesn't roll from the beginning to the end of contact on the surface, and the whole contact period of

impact is composed of rolling and skidding. Therefore, the accurate velocity and position data could not be obtained by differentiating this discontinuative time function. So, the differentiation approach was abandoned for describing the impact phenomena.

Evaluation of Integration Approach

As the successive differentiation has its weakness of enchancing the random errors, the successive integration, which starts from force to velocity and to position, has its merit for minimizing random errors and has less propogated errors likely to influence the signal to noise ratio.

During the impact, the ball has its spherical shape at touchdown, then reaches its maximum deformation and regains its original shape at lift-off. This kind of impact behavior could be treated as a mass spring system, and the vertical force by which the ball acts on the surface could be also described via a sinusoidal variation with time. Because of the inelasticity of the ball, the symetric Sin Pulse Model could not be applied to express the force distribution on the surface. The damped sin pulse model could be applied for this purpose via successive integration. Then, the sliding friction force could be expressed by the normal force multiplied by the coefficient of sliding friction and proceed to the successive integration steps.

After applying the integration approach, based on the Damped Sin Pulse Model, to analyse the experimental data, the results were successfully obtained for both the vertical and horizontal velocity and the position of the ball moving on the surface. From Figures 15, 16, and 17 we can see that the predicted value for both vertical and horizontal velocity and position were very close to the actual experimental data. Table 15 also provides good evidence for this approach. As the table shows, the standard error of estimate was very small, so that we can conclude that this integration approach has the predictive validity for investigating the impact of a tennis ball on a surface.

The results of successive integration didn't include the rotation which started with the torque and then proceeded to angular velocity and to the angle of rotation because of the discontinuous rolling of the ball on the surface. Figure 5 and Figure 7 show that skidding obviously happened for both zero-spin and backspin impact during some portion of the contact period; then rolling followed. Even the topspin impact, which seems to roll off of the surface contains a small amount of skidding in the contact period. So, we could not treat the angular velocity and angle by using the same integration as well as both vertical and horizontal velocity and position. However, the plots of fraction of rotation vs fraction of time, established by a polynomial regression curve fit, still provide very good information about the

effect of the ball's rolling on the surface.

Events Taking Place During Contact

As Figures 9, 11 and 13 show, the vertical force starts from zero at the beginning of impact, then reaches the maximum amount of value half way through the total contact time, and then decreases to zero again at the end of the contact period. The maximum vertical acting force for ball to the surface are listed in Table 16, and show that the top-spin impact was the largest, the zero-spin second, the back-spin smallest. The amount of vertical impact force was decided by the vertical component velocity at touchdown. As Tables 2, 3 and 4 show, the backspin impact has the smallest magnitude of vertical component velocity, zero-spin is greater, and the topspin is the greatest. Therefore, the backspin impact has a smallest value for the vertical impact force and the topspin has the largest. The time which the maximum force happened at was 48% of the total contact time for zero-spin, 50% for top-spin, and 47% for backspin. The time to reach the maximum force theoretically should be 50% of the total contact time for both skidding and rolling throughout the total contact. The topspin rolls off almost during the entire contact, so the maximum force happened at half of the total contact time. But for zero-spin and back-spin, the maximum force was reached earlier than the half

way point. This is because both zero-spin and backspin combined the skidding and rolling during contact, and the skidding part moves forward faster than the rolling does at the same period of time. The plots of position vs time in either polynomial regression plot (Figure 5 and 7) or integrational plot (Figure 10 and 14) for both zero-spin and backspin provide clear evidence that the ball moves faster in the earlier part of time than in the later part.

As the vertical force acts, the ball's deformation starts from zero, then goes to the maximum, and returns to zero again. Table 16 shows that the zero-spin and topspin have the maximum deformation, 16% of the ball's diameter, and backspin has 15% maximum deformation. This deformation is influenced by the vertical impact force directly. So the greater the vertical force acting on the surface, the greater the amount of deformation the ball has. For zero-spin and backspin, the deformation looks reasonable. The topspin has greater maximum vertical force, but the deformation is the same as zero-spin. The explaination for this is that the rolling occurred almost the entire contact period on the surface for topspin. As the ball rolls, the vertical acting force doesn't pass through the center of the ball. Then, the same amount of force applied to deform the ball will cause less deformation for a rolling ball than for a not rolling ball when the vertical acting force passes through the center of the ball. Thus, the topspin has a greater amount of

maximum vertical force than the zero-spin but has the same amount of deformation as zero-spin does.

When the ball moves on the surface, there is only the friction force acting on the ball. The sliding friction force was shown in Table 16 for three types of spin impacts. From the table we can see the sliding friction force perform similarly to the vertical force which starts from zero to the maximum limit, then back to zero finally. As usual, the harder the ball has been pressed and skidded on a rough surface, the more the sliding friction force will act on the ball. If the object is a rigid sphere, the friction force will be zero when it begins to roll. But the tennis ball is a deformable membrane sphere, it deforms and rolls at the same time when impacting on a playing surface. Though the topspin rolls almost from the beginning of contact, it still has some amount of sliding friction force acting on it. Therefore, the friction force in a tennis ball impact should include both the sliding friction force and the rolling friction force for expressing the frictional effect. When a tennis ball was impacted from a shallow incident angle with zero-spin, the sliding friction force will be very great and the rolling friction force will be very small. As the incident angle was made steeper and steeper, the sliding friction force became smaller and smaller and the rolling friction force became greater and greater. When we impart a topspin to the ball impacting on a surface, the ball's

spinning torque will cause the ball to roll along the surface so that the friction force will be smaller than a ball without any spin. It is a reverse situation for a backspin impact. The ball's peripheral velocity will act to hinder the ball from moving forward, so the friction force will be larger than that of a ball without initial spinning impact. But the results in Table 16 shows the sliding friction force for backspin to be smaller than that of zero-spin. This unusual value of sliding friction force for backspin impact is possible because of the greater amount of horizontal component velocity. As mentioned in the previous theory section, backspin, similar to topspin, has a large amount of compression at the trailing edge of the ball's footprint on the surface. According to Moore (1972), the elastomeric friction force is composed of an adhesion component and a hysteresis component force. The adhesion is caused by the surface, and the hysteresis relates to the deformation of the impact object. The hystoresis has a bell shape variation with horizontal velocity. Either smaller or larger horizontal velocity will cause the hystoresis to be a small value. In tennis ball impact, the compression of the trailing edge of the ball's footprint for backspin impact is similar to the hystoresis. When the large horizontal component velocity for a backspin reaches the critical value, the surface's roughness doesn't hinder the ball's forward movement as ususl. Because of this smaller sliding

friction force for the backspin impact, the horizontal component of velocity still has 81% of its original touchdown horizontal velocity when the ball reaches the maximum sliding friction force. Comparing this with other types of spin, zero-spin impact has 76% of its original horizontal velocity, and topspin has 81%. The other influence for this smaller friction for backspin is that the rebounding angle is the lowest one among these three types of spin impact. The rebounding angle for backspin impact is supposed to be the highest one because of decreased value of the horizontal component of velocity. This fact was written in the book by Rasch and Burke (1978) and Hay (1982). All of them believe that if the incident angle is the same, the backspin ball will rebound steeper than the zero-spin and the topspin. Therefore the backspin rebounds steeper than other types of spin only in a certain range of incident angles with certain ranges of horizontal components of velocity.

Though we could not obtain the information about the rotation of the ball on the surface, the nondimensional plots of fraction of rotation vs fraction of dwell time still provide the ball's rolling and skidding information on the surface. Figure 8 is an overlay plot of fraction of rotation vs fraction of dwell time established by the polynomial regression curve fit for all three types of spin impact. This plot gives us a brief idea about the ball which is rolling or skidding on the surface. As Table 14 shows, the

zero-spin impact skidded 26% of the total contact time, which was 35% of the total contact distance, then rolled off the surface; the topspin impact only has 1% of both the total contact time and contact distance; the backspin impact skidded 76% of the total contact time which was 82% of the total contact distance. The topspin rolls almost immediately at touchdown because the great magnitude of top-spin enhances the compression of the leading edge of the ball's footprint, which acts to decrease the peripheral velocity. So as soon as the peripheral velocity of the ball decreases upon touchdown, the horizontal translational velocity causes the ball to roll on the surface. For the zero-spin impact, the force which goes parallel to the surface takes a few moments to overcome the rolling frictional force generated by the asymmetry in the footprint pressure. Until the ball's peripheral velocity is smaller than the horizontal transltional velocity, the ball will roll on the surface. The backspin has a long period of skidding because the peripheral velocity at touchdown has the same direction as the horizontal translational velocity, and causes the larger pressure in the trailing edge of the ball's footprint, while lessening the pressure in the leading edge. Therefore, this smaller pressure in the leading edge of the ball's footprint provides the ball a chance to skid for a long period of contact for the backspin impact.

Evaluation of the System Parameters

As the results show in Table 8 to Table 10, the coefficient of restitution was 0.86 for the zero-spin impact, 0.91 for the topspin impact, and 0.80 for the backspin impact. These values, especially for the topspin, are far larger than the commonly accepted coefficient of restitution. According to the United States Tennis Association Regulation Rule 3, a ball dropped from 100 inches above a concrete base must rebound 53 to 58 inches. This yields a coefficient of restitution of 0.73 to 0.76, a regulational value accepted by most people to be a reference when a tennis ball is dropped from a height of 100 inches onto a concrete surface. This can be found in Brody's paper in 1984 which used the typical value of 0.75 for the coefficient of restitution into the derived equation inferring the tennis ball impact on a surface. As the first section of this chapter discussed, the great magnitude of topspin creates the larger pressure which is an asymmetry distribution in the leading edge of the ball's footprint on the surface, and the kinetic energy is stored as a torsional spring at the first part of contact time. Then, the kinetic energy stored by the torsional spring will enhance the energy stored by the linear deformation enabling the ball to regain its spherical shape. For this reason, the topspin impact has such a high value for the coefficient of restitution. The

zero-spin and backspin impact do not have so great a spin as topspin impact, so that torsional spring effect at the leading edge of the footprint doesn't provide the larger enhancement of kinetic energy to the linear relaxation of the ball. Hence, the zero-spin and backspin impact have the smaller coefficient of restitution than the topspin does.

In tennis competition, lots of people impart the top-spin effect on the ball to return the shot to the opponent's back-hand side. This is because the ball's rebound with top-spin jumps higher than the normal shot, and causes the opponent difficulty in returning a shot from the back-hand side. There are two factors causing the higher rebound of a topspin ball, air resistance and a high value of coefficient of restitution, caused by ball deformation. The net effect of air resistance is to cause the topspin ball to impact with a higher angle of incidence, so that it rebounds higher. The higher restitution, which was caused by the relaxational enhanced kinetic energy as mentioned above, will also influence the ball to rebound higher. In actual play, the higher rebound is caused more by the effect of air resistance than by the high value of coefficient of restitution. Once the ball's horizontal component velocity increases, the air resistance effect influencing the higher rebound will decrease, and high value of coefficient of restitution becomes the major factor to cause the higher rebound. But this is true only in both a certain range of horizontal

component velocities and in a certain range of incident angles, because the leading edge pressure of a ball's footprint on the surface acts as the hysteresis effect in the elastomeric friction. The coefficient of friction provides a measure of the ability of a surface to resist the movement of an object to move on it. Because a tennis ball can be viewed as a deformable membrane sphere, the friction effect of the surface gives on the ball includes both sliding friction and rolling friction. The coefficient of friction in this study was treated as a sliding friction because the skidding always occurs at the beginning part of contact, and may continue throughout most of the contact. The dwell time was defined as the time from the beginning of the ball's contact on the surface to the end of the contact. Table 8 to Table 10 show the ball's dwell time is 6.48 milliseconds for the zero-spin, 6.53 milliseconds for the topspin, and 6.29 milliseconds for the backspin. The ball's dwell time starts at the moment that ball begins to deform and ends at the instant that the ball regains its spherical shape and lifts off the surface. Therefore, this is related to the maximum deformation of the ball. The greater the ball's deformation, the more time the ball will take to regain it original shape. Since the zero-spin and topspin impact have almost the same amount of maximum deformation, their ball's dwell time are very close. The backspin impact has less deformation, thus the ball's dwell time is shorter than that of zero-spin and topspin.

These results seem to be reasonable.

The ball's dwell distances were shown also in Tables 8 to 10. As the table shows, the ball's dwell distance for zero-spin impact is 51.2 millimeters, and is 50.7 millimeters for the topspin, 52.0 millimeters for the backspin. The ball's dwell distance is decided by both the horizontal component velocity and the manner in which the ball is moving on the surface. The rolling or skidding condition plays a more important role than the horizontal component veloctiy does. The ball will move a greater distance skidding than rolling in the same period of time. Thus, the topspin impact rolls off in a shorter distance than the zero-spin and backspin impact do. The zero-spin skids with a smaller sliding friction force in the longer distance than the zero-spin does.

CHAPTER VI

CONCLUSIONS AND RECOMMENDATIONS

Conclusions

Research on tennis facilities and equipment is recieving increased attention by physicists, engineers and sports science reseachers. Until now, impact phenomena of a tennis ball on a hard surface was elucidated only by inferring likely performance based on input/output velocities. This thesis was designed to provide a mathematical model to explore tennis ball impact phenomena.

Stroboscopic photography was used to collect ball image position data as a function of time for a thrown tennis ball as it impacts a playing surface. Seven angles of incidence ranging from -17 degrees to -70 degrees with zero-spin, top-spin and back-spin and each was photographed. Then, image data were used to evaluate experimental parameters and system parameters via both a differentiation and integration mathematical analysis. The -23 degrees set of data were selected for the mathematical analysis because of more contact images than others.

After compilation of the data conversion and calculation, the following findings were obtained:

1. The differentiation approach could not be used because the accuracy and precision of the experimental data were not

good enough for this very sensitive approach.

2. The integration approach based on a Damped Sin Pulse Model showed a small standard error of estimate which represents a good predictive validity for the ball's horizontal and vertical position.

3. Top-spin has a high value of .91 for the coefficient of restitution reflecting a coupling of angular velocity into vertical linear velocity, the direct consequence of asymmetric foot print pressure pattern.

4. Back-spin impact has a smaller maximum sliding friction force than that of zero-spin impact.

Based on the findings and delimitations of this study, the following conclusions were established.

1. The successive differentiation approach did not lend itself well to the investigation of tennis ball impact phenomena.

2. The successive integration approach based on the Damped Sin Pulse Model, could be used successfully to describe both the horizontal and vertical forces, velocities and positions of ball impact on a surface.

3. In the case of -23 degree incident angle, the effect of top-spin will produce a high value for the coefficient of restitution, which provides the ball a chance to rebound higher.

4. The horizontal component velocity will influence a shallow angle impact with back-spin ball on a surface to have

a smaller sliding friction.

Recommendations

Based on the results and delimitations of this study, the following recommendations are advanced:

1. Application of the integration approach to the development of a mathematical model is warranted for other contact samples.
2. It is essential to more fully explore the data on angular velocity.
3. A mathematical model that permits estimation of a rolling friction should be develpoed.
4. To influence a struck tennis ball to roll on the court surface, the student player should be instructed to strike the ball at a shallow angle and to use the racquet to impart back-spin to the ball.
5. To influence the struck tennis ball to bounce high from the court surface, the student player should be instructed to impart top-spin to the ball.

REFERENCES

Andrews, J. G. (1983). A mechanical analysis of a special class of rebound phenomena. Medicine and Science in Sport and Exercise, 15, 3, 256-266.

Baker, J. W. and Wilson, B. D. (1978). The effect of tennis racket stiffness and string tension on ball velocity after impact. Research Quarterly, 49, 3, 255-259.

Bennett, W. R.. (1976). Scientific and engineering problem solving with the computer (pp. 221-223). Prentice Hall, New Jersey.

Blanksby, B. A. and Elliott, B. C. (1980). Vibration and rebound velocity characteristics of conventional and oversized tennis rackets. Research Quarterly, 51, 4, 608-615.

Brody, H. (1987). Tennis Science for Tennis Players. University of Pennsylvania Press.

Brody, H. (1984). That's how the ball bounces. The Physics Teacher, nov., 494-497.

Chan, W. and Seto, D. and Tran J. (1988). Characterization of Speed of Court Playing Surfaces by Measuring the Coefficient of Sliding Fraction (p. 12). Unpublished Senior Project of Mechanical Engineering Department of Oregon State University.

Daish, C. B. (1972). The Physics of Ball Games (pp. 168-174). The English Universities Press Ltd.

Dowell, L. and Smith J. and Miller G. and Hope A. and Kreb G. (1987). The effect of angle of incidence on rebound deviation of a tennis ball. Journal of Human Movement Studies, 13, 69-73.

Elliott, B. (1982). The influence of tennis racket flexibility and string tension of rebound velocity following a dynamic impact. Research Quarterly, 53, 277-281.

Elliott, B. (1982). Tennis: the influence of grip tightness on reaction impulse and rebound velocity. Medicine and Science in Sports and Exercise, 14, 348-352.

Freund, H. (1987). Unpublished paper for tennis ball impact test. Department of Chemistry.

Freund, H. (1988). Strosboscopic study of deformable thin-shelled spheres impacting a plane surface. PROC. VI International Congress on Experimental mechanics (pp. 1-4).

Groppel, J. L.. (1984). Improving your tennis through Biomechanics. Tennis: A Professional Guide (pp. 200-211). US Professional Tennis Association.

Hays, D. F. and Browne, A. L.. (1974). The physics of tire traction: theory and experiment (p. 70). Plenum Press.

Hays, James G. and Reid J. Gavin. (1982). The anatomical and mechanical bases of human motion (p. 174). Prentice-Hall, Inc..

Kennedy, R. (1980). The way the ball bounces. Sports Illustration, 52, 42-46.

LaMarche, R. J.. (1985). A review of the characteristics of tennis balls. Tennis, Feb., 37-39.

Larson, C. L.. (1979). The effect of selected tennis racket and string variables on ball velocity and the force of ball racket impact. Doctoral Dissertation. Indiana University.

Lisk, J. W.. (1980). Effects of velocity, surface, and angle of incidence on angle of rebound of tennis ball. Doctoral Dissertation. Texas A&M University.

Liu, Y. K. (1983). Mechanical analysis of rcket and ball during impact. Medicine and Science in Sports and Exercise, 15, 388- 392.

Missavage, R. J. and Baker, J. W. and Putnam, C. A.. (1984). Theoretical modeling of grip firmness during ball-racket impact. Research Quarterly, 55, 254-296.

Moore, D. F.. (1972). The friction and lubrication of elastomers (p. 81). Pergamon Press, New York.

Putnam, C. A. and Baker, J. W.. (1984). Spin imparted to a tennis ball during impact with conventionally and diagonally strung rackets. Research Quarterly, 55, 261-266.

Rasch, hilip J. and Burke, Roger K.. 1978). Kinesiology and applied anatomy (p. 124). Lea & Febiger.

Sebolt, D. R.. (1970). A stroboscopic study of the relationship of ball velocity and tennis performance. Research Quarterly, 41, 183-188.

Spiegel, M. R.. (1968) Schaum's outline series in mathematics. Mathematical Handbook (p. 191). McGraw Hill Book Company.

Tennis balls (1976). Consumer Research Magazine. Feb, 13-16.

Vogt, T. and Rondeau A. and Badiee B.. (1988). A study of the rebound behavior of tennis balls. Unpublished senior project of Mechanical Engineering Department of Oregon State University.

Xanthos, P. J. and Crookenden, I. (1984). The basic tennis skills. Tennis: A Professional Guide (pp. 51-78). US Professional Tennis Association.

Zayas, J. M.. (1986). Experimental determination of the coefficient of drag of a tennis ball. American Journal Physics, 54, 622-625.

APPENDICES

APPENDIX A

PASCAL PROGRAM FOR DATA CALCULATION

```
program compute(input,output);
var textin,textout:text;          { definition of variables }
    i,j,k,l,m:integer;
    sd:array[1..3,1..2] of real;
    centerX,centerY,slop:array[1..12,1..8] of real;
    TDcenterX,LOcenterX,TDcenterY,LOcenterY:array[1..12] of real;
    surfaceX,surfaceY:array[1..12,1..6] of real;
    x1,x2,x3,y1,y2,y3,z,flag,time,tan1,tan2: real;
    TDfm,dbuff,FMno,TDangle,LOangle:array[1..12] of real;
    eqX,eqY:array[1..12,1..8,1..2] of real;
    angleIN,angleOUT:array[1..12] of real;
    rfangleIN,rfangleOUT:array[1..12] of real;
    angveloIN,angveloOUT:array[1..12] of real;
    Rangveloin,Rangveloout:array[1..12] of real;
    XveloIN,YveloIN,RveloIN,anglIN:array[1..12] of real;
    XveloOUT,YveloOUT,RveloOUT,anglOUT:array[1..12] of real;
    rfXveloIN,rfYveloIN,rfRveloIN,rfanglIN:array[1..12] of real;
    rfXveloOUT,rfYveloOUT,rfRveloOUT,rfanglOUT:array[1..12] of real;
    eco,uco,DWdist,DWtm:array[1..12] of real;
    surfang,Tbefore,Tafter:array[1..12] of real;
    diameter:array[1..12,1..3] of real;
    name:array[1..6] of string[30];

{ sd:standard diviation; centerX,centerY:X & Y coordinates of ball's center; }
{ slop:slop of equator marked on ball; TDcenterX,TDcenterY:ball's center
at touchdown }
{ LOcenterX,LocenterY:bll's center at lift-off; surfaceX,surfaceY:points on
surface }
{ TDfm:number of touchdown image;FMnc:frame number;TDangle:equator
angle at touchdown }
{ LDangle:equator angle at lift-off; eqX,eqY:coordinate of equater point; }
{ angleIN,angleOUT:intident & rebound angle; angveloIN, angveloOUT:incoming &
  rebounding angular velocity) { RangveloIN,RangveloOUT:incoming angular
velovity & rebounding angular velocity when flag=1) {flag=0:the first kind of
sequency for data reading}
{ flag=1:the second kind of sequency of data reading}
{rfangIN,rfangOUT:incident angle & rebound angle when flag=1;
XveloIN,XveloOUT:horizontal velocity at touchdown & lift-off }
{ YveloIN,YveloOUT:vertical velocity at touchdown & lift-off;
RveloIN,RveloOUT:resultant velocity at touchdown & lift-off }
{ rfXveloIN,rfYveloIN,rfRveloIN,rfXveloOUT,rfYveloOUT
  rfRveloOUT: the velocities variables when flag=1}
{eco:coefficient of restitution; }
{ uco:coefficient of friction; DWdist:ball's dwell distance; DWtime:
ball's dwell time }
{ survang:angle of surface plane; Tbefore:time between last airborne
image & touchdown surface }
```

```
{ Tafter:time between ball's lift-off and first airborne image;
diameter:ball's diameter }

procedure diamet(x1,y1,x2,y2:real);    { for calculating ball's diameter }
  begin
        dbuff[1]:=2*sqrt(sqr(x1-x2)+sqr(y1-y2));
        if 1>6 then diameter[k,1-5]:=dbuff[1];
   end;

procedure touchcenter;          { for calculating ball's touchdown center }
  var a,b:real;
  begin  a:=(centerY[k,2]-centerY[k,3])/(centerX[k,2]-centerX[k,3]);
         b:=(centerY[k,2]*centerX[k,3]-centerY[k,3]*centerX[k,2])/
                     (centerX[k,2]-centerX[k,3]);
         TDcenterY[k]:=surfaceY[k,5]+diameter[k,1]/2;
         TDcenterX[k]:=(TDcenterY[k]+b)/a;
         a:=(centerY[k,4]-centerY[k,5])/(centerX[k,4]-centerX[k,5]);
         b:=(centerY[k,4]*centerX[k,5]-centerY[k,5]*centerX[k,4])/
                     (centerX[k,4]-centerX[k,5]);
         LOcenterY[k]:=surfaceY[k,6]+diameter[k,1]/2;
         LOcenterX[k]:=(LOcenterY[k]+b)/a;
  end;

  procedure anglv;              { for calculating ball's angular velocity }
  var a:integer;
  begin
      if flag=1 then begin
        a:=0;
        repeat a:=a+1;
           slop[k,a]:=(eqY[k,a,1]-eqY[k,a,2])/(eqX[k,a,1]-
                     eqX[k,a,2]);
        until a=6;

      if (slop[k,2]>1) and (slop[k,3]<-1) then
        RangveloIN[k]:=(arctan(slop[k,3])-(arctan(slop[k,2])-3.1416))/time
       else
        if (slop[k,2]<0) and (slop[k,3]>0) then
        RangveloIN[k]:=(arctan(slop[k,3])-3.1416-arctan(slop[k,2]))/time
        else
        RangveloIN[k]:=(arctan(slop[k,3])-arctan(slop[k,2]))/time;

      if (slop[k,4]>1) and (slop[k,5]<-1) then
        RangveloOUT[k]:=(arctan(slop[k,5])-(arctan(slop[k,4])-3.1416))/time
      else
        if (slop[k,4]<0) and (slop[k,5]>0) then
        RangveloOUT[k]:=(arctan(slop[k,5])-3.1416-arctan(slop[k,4]))/time
        else
        RangveloOUT[k]:=(arctan(slop[k,5])-arctan(slop[k,4]))/time;
     end
      else begin
```

```
        a:=0;
        repeat a:=a+1;
           slop[k,a]:=(eqY[k,a,1]-eqY[k,a,2])/(eqX[k,a,1]-
                      eqX[k,a,2]);
           if (TDfm[k]=1) and (a=7) then a:=8;
        until a=8;
        if (slop[k,2]>1) and (slop[k,3]<-1) then
        angveloIN[k]:=(arctan(slop[k,3])-(arctan(slop[k,2])-3.1416))/time
       else
        if (slop[k,2]<0) and (slop[k,3]>0) then
        angveloIN[k]:=(arctan(slop[k,3])-3.1416-arctan(slop[k,2]))/time
        else
        angveloIN[k]:=(arctan(slop[k,3])-arctan(slop[k,2]))/time;

      if (slop[k,4]>1) and (slop[k,5]<-1) then
        angveloOUT[k]:=(arctan(slop[k,5])-(arctan(slop[k,4])-3.1416))/time
      else
        if (slop[k,4]<0) and (slop[k,5]>0) then
        angveloOUT[k]:=(arctan(slop[k,5])-3.1416-arctan(slop[k,4]))/time
        else
        angveloOUT[k]:=(arctan(slop[k,5])-arctan(slop[k,4]))/time;
       end;
    end;
procedure velocity;                    { for calculating ball's velocities }
  begin  if flag=0 then begin
         XveloIN[k]:=(centerX[k,3]-centerX[k,2])/diameter[k,1]*
                     0.0651/time;
         YveloIN[k]:=(centerY[k,3]-centerY[k,2])/diameter[k,1]*
                     0.0651/time;
         angleIn[k]:=arctan((centerY[k,2]-centerY[k,3])/(centerX[k,2]-
                        centerX[k,3]));
         RveloIN[k]:=sqrt(sqr(XveloIN[k])+sqr(YveloIN[k]));
         XveloOUT[k]:=(centerX[k,5]-centerX[k,4])/diameter[k,1]*
                      0.0651/time;
         YveloOUT[k]:=(centerY[k,5]-centerY[k,4])/diameter[k,1]*
                      0.0651/time;
         angleOUT[k]:=arctan((centerY[k,4]-centerY[k,5])/(centerX[k,4]-
                        centerX[k,5]));
         RveloOUT[k]:=sqrt(sqr(XveloOUT[k])+sqr(YveloOUT[k])); end
        else begin
         rfXveloIN[k]:=(centerX[k,3]-centerX[k,2])/diameter[k,1]*
                     0.0651/time;
         rfYveloIN[k]:=(centerY[k,3]-centerY[k,2])/diameter[k,1]*
                     0.0651/time;
         rfangleIn[k]:=arctan((centerY[k,2]-centerY[k,3])/(centerX[k,2]-
                        centerX[k,3]));
         rfRveloIN[k]:=sqrt(sqr(rfXveloIN[k])+sqr(rfYveloIN[k]));
         rfXveloOUT[k]:=(centerX[k,5]-centerX[k,4])/diameter[k,1]*
                      0.0651/time;
         rfYveloOUT[k]:=(centerY[k,5]-centerY[k,4])/diameter[k,1]*
```

```
                    0.0651/time;
        rfangleOUT[k]:=arctan((centerY[k,4]-centerY[k,5])/(centerX[k,4]-
                        centerX[k,5]));
        rfRveloOUT[k]:=sqrt(sqr(rfXveloOUT[k])+sqr(rfYveloOUT[k])); end;
   end;

procedure clear;                    { for setting the sd array value equal 0 }
  var p,q:integer;
  begin for p:=1 to 3 do
          for q:=1 to 2 do sd[p,q]:=0;
  end;

procedure fill(x1,x2,x3:real);{ fill the required value into sd array for standard
                                                          deviation }
  begin  sd[1,1]:=sd[1,1]+x1;sd[1,2]:=sd[1,2]+sqr(x1);
         sd[2,1]:=sd[2,1]+x2;sd[2,2]:=sd[2,2]+sqr(x2);
         sd[3,1]:=sd[3,1]+x3;sd[3,2]:=sd[3,2]+sqr(x3);
   end;

procedure snd;            { for calculating standard deviation }
  var b:integer;
  procedure count(y1,y2:real);
   var mn,sdv:real;
    begin mn:=y1/k;
          sdv:=sqrt(k*y2-y1*y1)/k;
          writeln(textout,'mean',b,':',mn:8:3,'   sd:',sdv:6:3,'(%',
                 sdv/mn*100:6:4,')');
    end;
  begin for b:=1 to 3 do
        begin if sd[b,1] <>0 then count(sd[b,1],sd[b,2]);end;
        writeln(textout);
  end;

procedure restitution;      { for calculating the coefficient of restitution }
  begin  eco[k]:=-(YveloOUT[k]/YveloIN[k]);
  end;

procedure friction;          { for calculating the coefficient of friction }
  begin uco[k]:=-(XveloOUT[k]-XveloIN[k])/(YveloOUT[k]-YveloIN[k]);
  end;

procedure dwdistance;         { for calculating the ball's dwell distance }
  begin DWdist[k]:=sqrt(sqr(TDcenterX[k]-LOcenterX[k])+sqr(TDcenterY[k]-
                        LOcenterY[k]));
        DWdist[k]:=(DWdist[k]/diameter[k,1]*0.0651)*100;
  end;

procedure dwtime;                   { for calculating the ball's dwell time }
  var Ttotal:real;
  begin Ttotal:=((TDfm[k]-1)+2)*time;
```

```
        Tbefore[k]:=sqrt(sqr(TDcenterX[k]-centerX[k,3])+sqr(TDcenterY[k]-
                  centerY[k,3]))/diameter[k,1]*0.0651/RveloIN[k];
        Tafter[k]:=sqrt(sqr(centerX[k,4]-LOcenterX[k])+sqr(centerY[k,4]-
                  LOcenterY[k]))/diameter[k,1]*0.0651/RveloOUT[k];
        DWtm[k]:=(Ttotal-(Tbefore[k]+Tafter[k]))*1000;
    end;

procedure tchang;{ for finding the ball's equator angle at touchdown & lift-off }
 begin  TDangle[k]:=arctan(slop[k,3])+angveloIN[k]*Tbefore[k];
          LOangle[k]:=arctan(slop[k,4])-angveloOUT[k]*Tafter[k];
 end;

procedure rotate(var x,y:real);{ mathematically rotate image data to horizontal level }
  var xa,ya:real;
  begin xa:=x*cos(surfang[k])-y*sin(surfang[k]);
        ya:=x*sin(surfang[k])+y*cos(surfang[k]);
        x:=xa;y:=ya;
    end;

begin clrscr;                          { beginnign of the main program }
      writeln('What is the file name of input data?  ');read(name[1]);
      writeln;writeln('Give a output file name for the results---> ');
      read(name[2]);
      writeln;writeln('Input a output file name for "ball center vs fraction
                    of dwell time"---->');
      read(name[3]);writeln;
      writeln('Input a output file name for "X distance vs fraction of dwell
                    time"--->');
      read(name[4]);writeln;
      writeln('Input a output file name for "fractional Y deformation vs
                   fraction of dwell time"--->');
      read(name[5]);writeln;
      writeln('Input a output file name for "fraction of rotation vs
                    fraction of dwell time"-->');
      read(name[6]);
      clrscr; for i:=1 to 5 do writeln; writeln('-------- calculating ---------');
      assign(textin,name[1]);reset(textin);
      assign(textout,name[2]);rewrite(textout);
      readln(textin,time);l:=0;k:=0;z:=0;flag:=0;
      while not eof(textin) do
       begin k:=k+1; readln(textin,TDfm[k],FMno[k]);
                    for i:= 1 to 4 do
                     begin read(textin,surfaceX[k,i]);     { read the surface point }
                           read(textin,surfaceY[k,i]);
                           readln(textin);
                      end;
             surfaceX[k,5]:=(surfaceX[k,1]+surfaceX[k,2])/2;
             surfaceY[k,5]:=(surfaceY[k,1]+surfaceY[k,2])/2;
             surfaceX[k,6]:=(surfaceX[k,3]+surfaceX[k,4])/2;
             surfaceY[k,6]:=(surfaceY[k,3]+surfaceY[k,4])/2;
```

```
          surfang[k]:=arctan((surfaceY[k,1]-surfaceY[k,3])/
                     (surfaceX[k,1]-surfaceX[k,3]));
            rotate(surfaceX[k,5],surfaceY[k,5]);
            rotate(surfaceX[k,6],surfaceY[k,6]);
          for i:=1 to 8 do dbuff[i]:=0;
          repeat
           readln(textin);l:=l+1;
           readln(textin,centerX[k,1],centerY[k,1]); {read ball's center }
           readln(textin,x1,y1);
                                      {read diameter reference point}
           rotate(x1,y1);rotate(centerX[k,1],centerY[k,1]);
                                      { call procedure rotate }
           readln(textin,eqX[k,1,1],eqY[k,1,1]);  {read equator point 1}
           readln(textin,eqX[k,1,2],eqY[k,1,2]);  {read equator point 2}
           rotate(eqX[k,1,1],eqY[k,1,1]); rotate(eqX[k,1,2],eqY[k,1,2]);
           diamet(x1,y1,centerX[k,1],centerY[k,1]); { call procedure diamet }
           if (TDfm[k]=1) and (l=7) then l:=8;
          until l=8; l:=0;
          for j:=1 to 6 do z:=z+dbuff[j];diameter[k,1]:=z/6;
          z:=0; touchcenter; anglv; velocity;restitution; { call procedures }
          friction;dvdistance;dvtime; tchang;             { call procedures }
          flag:=1;centerX[k,3]:=centerX[k,2];centerX[k,2]:=centerX[k,1];
          centerY[k,3]:=centerY[k,2];centerY[k,2]:=centerY[k,1];
          centerX[k,4]:=centerX[k,5];centerX[k,5]:=centerX[k,6];
          centerY[k,4]:=centerY[k,5];centerY[k,5]:=centerY[k,6];
          for j:=1 to 2 do
          begin eqX[k,3,j]:=eqX[k,2,j];eqX[k,2,j]:=eqX[k,1,j];
                eqY[k,3,j]:=eqY[k,2,j];eqY[k,2,j]:=eqY[k,1,j];
                eqX[k,4,j]:=eqX[k,5,j];eqX[k,5,j]:=eqX[k,6,j];
                eqY[k,4,j]:=eqY[k,5,j];eqY[k,5,j]:=eqY[k,6,j];
          end; velocity; anglv;flag:=0;
          readln(textin); readln(textin);
 end;     close(textin);
clear;
writeln(textout,'angle in & out(deg)');            { output results }
writeln(textout,'fm #   in         out');
writeln(textout,'-------------------------');
for i:=1 to k do
 begin write(textout,FMno[i]:2:0,'A  ');
       write(textout,angleIN[i]*57.3:10:4,'  ',
          angleOUT[i]*57.3:9:4);writeln(textout);
       fill(angleIN[i]*57.3,angleOUT[i]*57.3,0);
   end;  snd;
clear;
writeln(textout,'velocities of incoming airborne period(m/s)');   { output the results }
writeln(textout,'fm #   xVin       yVin        rVin');
writeln(textout,'---------------------------------');
clear;
for i:=1 to k do
 begin write(textout,FMno[i]:2:0,'A  ');
       write(textout,XveloIN[i]:9:4,'  ',
```

```
        YveloIN[i]:9:4,'  ',RveloIN[i]:9:4);writeln(textout);
        fill(XveloIN[i],YveloIN[i],RveloIN[i]);
 end;  snd;
clear;
writeln(textout,'velocities of rebound airborne period(m/s)');     { output results }
writeln(textout,'fm #   xVout       yVout     rVout');
writeln(textout,'-----------------------------------');
for i:=1 to k do
 begin write(textout,FMno[i]:2:0,'A  ');
       write(textout,XveloOUT[i]:9:4,'  ',
          YveloOUT[i]:9:4,'  ',RveloOUT[i]:9:4);writeln(textout);
          fill(XveloOUT[i],YveloOUT[i],RveloOUT[i]);
  end;  snd;
clear;
writeln(textout,'angular velocities of in & out period(rad/s)');      { output results }
writeln(textout,'fm #    in       out');
writeln(textout,'-----------------------');
for i:=1 to k do
 begin write(textout,FMno[i]:2:0,'A  ');
       write(textout,angveloIN[i]:9:4,'  ',
          angveloOUT[i]:9:4);writeln(textout);
       fill(angveloIN[i],angveloOUT[i],0);
 end;   snd;
clear;
writeln(textout,'angle in & out(deg) using the first/last two images');  { output results }
writeln(textout,'fm #   in         out');
writeln(textout,'------------------------');
for i:=1 to k do
 begin write(textout,FMno[i]:2:0,'A  ');
       write(textout,rfangleIN[i]*57.3:10:4,'  ',
          rfangleOUT[i]*57.3:9:4);writeln(textout);
       fill(rfangleIN[i]*57.3,rfangleOUT[i]*57.3,0);
   end;  snd;
clear;
writeln(textout,'incoming velocities(m/s) using the first/last two images');
writeln(textout,'fm #   xVin       yVin        rVin');                 { output results }
writeln(textout,'-----------------------------------');
clear;
for i:=1 to k do
 begin write(textout,FMno[i]:2:0,'A  ');
       write(textout,rfXveloIN[i]:9:4,'  ',
         rfYveloIN[i]:9:4,'  ',rfRveloIN[i]:9:4);writeln(textout);
         fill(rfXveloIN[i],rfYveloIN[i],rfRveloIN[i]);
 end;  snd;
clear;
writeln(textout,'rebound velocities(m/s) using the first/last two images');
writeln(textout,'fm #   xVout       yVout     rVout');
writeln(textout,'-----------------------------------');
for i:=1 to k do
 begin write(textout,FMno[i]:2:0,'A  ');
```

```
        write(textout,rfXveloOUT[i]:9:4,'  ',
           rfYveloOUT[i]:9:4,'  ',rfRveloOUT[i]:9:4);writeln(textout);
           fill(rfXveloOUT[i],rfYveloOUT[i],rfRveloOUT[i]);
    end; snd;
  clear;
  writeln(textout,'angular velocities(rad/s) using the first/last two images');
  writeln(textout,'fm #    in       out');
  writeln(textout,'-----------------------');
  for i:=1 to k do
   begin write(textout,FMno[i]:2:0,'A  ');
        write(textout,RangveloIN[i]:9:4,'  ',
           RangveloOUT[i]:9:4);writeln(textout);
        fill(RangveloIN[i],RangveloOUT[i],0);
   end;  snd;

  clear;
  writeln(textout,'coefficient of restitution & friction');        { output results }
  writeln(textout,'fm #      e         u');
  writeln(textout,'------------------------');
  for i:=1 to k do
   begin write(textout,FMno[i]:2:0,'A  ');
        write(textout,eco[i]:9:5,'  ',uco[i]:9:5);writeln(textout);
        fill(eco[i],uco[i],0);
    end;  snd;
  clear;
  writeln(textout,'dwell distance(cm) & time(ms)');                { output results }
  writeln(textout,'fm #    DWdist     DWtime');
  writeln(textout,'----------------------------');
  for i:=1 to k do
   begin write(textout,FMno[i]:2:0,'A  ');
        write(textout,DWdist[i]:9:6,'  ',DWtm[i]:9:7);
        writeln(textout);fill(DWdist[i],DWtm[i],0);
    end;  snd; close(textout);

assign(textout,name[3]);rewrite(textout);
   l:=0; writeln(textout,'fm# fraction/time   center height');      { output results }
   for i:=1 to k do
    begin
          repeat l:=l+1;
               y1:=centerY[i,l+6]-surfaceY[i,5];
               y1:=y1/diameter[i,1]*6.51;
               x1:=(l*time-Tbefore[i])*1000/DWtm[i];
               writeln(textout,FMno[i]:2:0,'A ',x1:10:6,'   ',y1:10:6);
               if TDfm[i]=1 then l:=2;
          until l=2;
          l:=0;
     end;
     close(textout);

assign(textout,name[4]);rewrite(textout);                          { output results }
```

```
 l:=0; writeln(textout,'fm# fraction/time   fraction/X');
 for i:=1 to k do
   begin  repeat l:=l+1;
            y1:=(centerX[i,l+6]-TDcenterX[i])/(LOcenterX[i]-
                 TDcenterX[i]);
            x1:=(l*time-Tbefore[i])*1000/DWtm[i];
            writeln(textout,FMno[i]:2:0,'A ',x1:12:6,'   ',y1:12:6);
            if TDfm[i]=1 then l:=2;
          until l=2;
          l:=0;
   end;
   close(textout);

assign(textout,name[5]);rewrite(textout);                    { output results }
 l:=0;writeln(textout,'fraction/time   fraction/Y');
 for i:=1 to k do
  begin repeat l:=l+1;
          y1:=(centerY[i,l+6]+diameter[i,l+1]/2-
              (TDcenterY[i]+diameter[i,1]/2))/diameter[i,1];
          x1:=(l*time-Tbefore[i])*1000/DWtm[i];
          writeln(textout,FMno[i]:2:0,'A ',x1:12:6,'   ',y1:12:6);
          if TDfm[i]=1 then l:=2;
        until l=2;
        l:=0;
   end;
   close(textout);

assign(textout,name[6]);rewrite(textout);                     { output results }
 l:=0;writeln(textout,'fm# fraction/time   fraction/rotat.  TDi(rad)  contacti    LOi      LO-TD');
 for i:=1 to k do
  begin
           if (LOangle[i]>TDangle[i]) then
                 z:=LOangle[i]-3.1416-TDangle[i]
            else   z:=LOangle[i]-TDangle[i];
       repeat  l:=l+1;
        if (TDangle[i]>1.5708)and(slop[i,l+6]<-1) then
          y1:=(arctan(slop[i,l+6])-(TDangle[i]-3.1416))/z
        else
         if (TDangle[i]<0) and (slop[i,l+6]>0) then
         y1:=(arctan(slop[i,l+6])-3.1416-TDangle[i])/z
         else
         y1:=(arctan(slop[i,l+6])-TDangle[i])/z;
         x1:=(l*time-Tbefore[i])*1000/DWtm[i];
     writeln(textout,FMno[i]:2:0,'A ',x1:12:6,'   ',y1:12:6,'     ',TDangle[i]:7:3,'   ',
       arctan(slop[i,l+6]):7:3,'   ',LOangle[i]:7:3,'   ',z:7:3);
        if TDfm[i]=1 then l:=2;
       until l=2;
       l:=0;
   end;
   close(textout);
```

```
    clrscr; for i:=1 to 5 do writeln; writeln('-------- finished ---------');

end.
```

APPENDIX B

CONTACT DATA FOR ZERO-SPIN IMPACT

CONTACT DATA FOR -17 deg ZERO-SPIN

ΣT: FRACTION OF TIME
ΣX: FRACTION OF HORIZONTAL DISTANCE
ΣY: FRACTIONAL VERTICAL DEFORMATION
ΣR: FRACTION OF ROTATION

ΣT	ΣX	ΣY	ΣR
0	0	0	0
0.06294	0.08689	-0.0167	0.0383
0.06473	0.08331	-0.0426	-0.024
0.06569	0.08812	-0.0459	-0.0127
0.07566	0.08816	-0.0424	-0.0011
0.1114	0.13879	-0.0566	0.041
0.23249	0.2878	-0.1274	-0.0294
0.3531	0.40625	-0.1374	0.0478
0.38838	0.46244	-0.1733	0.1034
0.39112	0.46998	-0.1527	0.12
0.52983	0.60708	-0.1758	0.1578
0.53804	0.61203	-0.1649	0.261
0.56257	0.64283	-0.1561	0.2753
0.56793	0.64513	-0.1521	0.2486
0.57655	0.64613	-0.1685	0.2941
0.71927	0.77474	-0.1052	0.4885
0.82965	0.86911	-0.0576	0.6955
0.8342	0.85729	-0.0657	0.6697
0.85221	0.88258	-0.0473	0.7744
0.99673	0.9921	-0.0036	0.9858
1	1	0	1

CONTACT DATA FOR -23 deg ZERO-SPIN

ΣT: FRACTION OF TIME
ΣX: FRACTION OF HORIZONTAL DISTANCE
ΣY: FRACTIONAL VERTICAL DEFORMATION
ΣR: FRACTION OF ROTATION

ΣT	ΣX	ΣY	ΣR
0	0	0	0
0.090854	0.131737	-0.06125	-0.00339
0.176032	0.211387	-0.09565	0.004953
0.184586	0.229181	-0.08915	0.036998
0.200581	0.250124	-0.12317	0.014386
0.225782	0.305408	-0.1247	-0.00774
0.263456	0.350631	-0.14304	0.00281
0.288576	0.369025	-0.15144	-0.01041
0.431498	0.546866	-0.19923	0.139754
0.43462	0.54041	-0.19311	0.066586
0.609524	0.684129	-0.16674	0.292652
0.655904	0.751174	-0.15259	0.37398
0.717114	0.778159	-0.12202	0.560784
0.718984	0.794566	-0.14496	0.472043
0.740468	0.798457	-0.13655	0.570487
0.767174	0.840122	-0.09069	0.587754
0.820786	0.867004	-0.08073	0.725113
0.944448	0.971082	0.002565	0.878075
0.982399	0.991324	-0.01807	0.967495
0.991962	0.991037	-0.00737	0.853131
1	1	0	1

CONTACT DATA FOR -34 deg ZERO-SPIN

ZT: FRACTION OF TIME
ZX: FRACTION OF HORIZONTAL DISTANCE
ZY: FRACTIONAL VERTICAL DEFORMATION
ZR: FRACTION OF ROTATION

ZT	ZX	ZY	ZR
0	0	0	0
0.005736	0.007762	-0.01015	-0.02569
0.062897	0.096025	-0.05599	-0.00724
0.178877	0.24306	-0.12632	0.040699
0.253364	0.354855	-0.18492	0.021789
0.332254	0.444308	-0.23678	0.055232
0.415738	0.540731	-0.30226	0.08133
0.427193	0.561856	-0.27917	0.117758
0.433124	0.564302	-0.28191	0.132946
0.502261	0.652088	-0.26286	0.31064
0.571496	0.67659	-0.30840	0.332397
0.596752	0.710869	-0.22668	0.381918
0.598436	0.707942	-0.21332	0.426301
0.622127	0.725801	-0.23585	0.406718
0.754806	0.827616	-0.19179	0.685548
0.87386	0.929795	-0.13315	0.766884
0.900433	0.914446	-0.08509	0.862336
1	1	0	1

CONTACT DATA FOR -41 deg ZERO-SPIN

ZT: FRACTION OF TIME
ZX: FRACTION OF HORIZONTAL DISTANCE
ZY: FRACTIONAL VERTICAL DEFORMATION
ZR: FRACTION OF ROTATION

ZT	ZX	ZY	ZR
0	0	0	0
0.159031	0.254402	-0.13610	0.00161
0.27027	0.368364	-0.22152	-0.03283
0.27425	0.369243	-0.25025	0.031
0.320023	0.452145	-0.2505	0.031999
0.373104	0.490414	-0.32829	0.083998
0.601212	0.693542	-0.27897	0.264077
0.617591	0.698216	-0.25830	0.520844
0.715424	0.775291	-0.24343	0.648978
0.863258	0.900599	-0.13836	0.84321
0.936288	0.957522	-0.12250	0.940511
1	1	0	1

CONTACT DATA FOR -49 deg ZERO-SPIN

ZT: FRACTION OF TIME
ZX: FRACTION OF HORIZONTAL DISTANCE
ZY: FRACTIONAL VERTICAL DEFORMATION
ZR: FRACTION OF ROTATION

ZT	ZX	ZY	ZR
0	0	0	0
0.28384	0.403199	-0.25886	-0.00214
0.347344	0.462432	-0.29213	0.059489
0.373892	0.481803	-0.31080	0.080335
0.560769	0.656128	-0.29175	0.437606
0.601524	0.642896	-0.35033	0.380617
0.688153	0.792269	-0.14802	0.679414
0.713942	0.795121	-0.30757	0.615466
0.727081	0.777403	-0.20012	0.747611
1.005379	0.995032	-0.04141	1.008761
1	1	0	1

CONTACT DATA FOR -60 deg ZERO-SPIN

ZT: FRACTION OF TIME
ZX: FRACTION OF HORIZONTAL DISTANCE
ZY: FRACTIONAL VERTICAL DEFORMATION
ZR: FRACTION OF ROTATION

ZT	ZX	ZY	ZR
0	0	0	0
0.075964	0.096166	-0.06962	0.001302
0.131829	0.223172	-0.13139	0.060215
0.199961	0.399128	-0.21195	0.037819
0.301366	0.425367	-0.26425	-0.03029
0.331163	0.457668	-0.31125	0.240978
0.377641	0.547595	-0.31184	0.391389
0.5346	0.654472	-0.32868	0.58076
0.567367	0.678256	-0.25124	0.282394
0.569203	0.674431	-0.27958	0.566849
0.643806	0.741212	-0.18971	0.670915
0.955766	0.888307	-0.02221	0.92614
1	1	0	1

CONTACT DATA FOR -68 deg ZERO-SPIN

ZT: FRACTION OF TIME
ZX: FRACTION OF HORIZONTAL DISTANCE
ZY: FRACTIONAL VERTICAL DEFORMATION
ZR: FRACTION OF ROTATION

ZT	ZX	ZY	ZR
0	0	0	0
0.103847	0.197676	-0.10113	0.044593
0.117	0.253318	-0.12703	0.057296
0.314583	0.502096	-0.29599	0.222391
0.34633	0.578411	-0.28409	0.131812
0.54562	0.618834	-0.33896	0.553812
0.620255	0.649761	-0.34443	0.609734
0.646167	0.752643	-0.27916	0.588946
0.691652	0.734256	-0.16612	0.35761
0.69939	0.758967	-0.15302	0.521359
0.837751	0.852435	-0.11116	0.655182
0.897535	0.891213	-0.05939	0.834695
1	1	0	1

APPENDIX C

CONTACT DATA FOR TOP-SPIN IMPACT

CONTACT DATA FOR -18 deg TOP-SPIN

ZT: FRACTION OF TIME
ZX: FRACTION OF HORIZONTAL DISTANCE
ZY: FRACTIONAL VERTICAL DEFORMATION
ZR: FRACTION OF ROTATION

ZT	ZX	ZY	ZR
0	0	0	0
0.00248	0.01436	-0.0138	0.01104
0.17103	0.20932	-0.0861	0.04056
0.25991	0.31258	-0.1241	0.1406
0.28168	0.34208	-0.1082	0.17377
0.30304	0.37297	-0.131	0.19437
0.31584	0.37779	-0.1335	0.18716
0.32537	0.38919	-0.1683	0.21318
0.35097	0.42537	-0.1541	0.20914
0.42043	0.50846	-0.1607	0.30071
0.47527	0.54163	-0.1788	0.33084
0.50771	0.59438	-0.1856	0.3492
0.53961	0.61072	-0.1585	0.41632
0.65203	0.7199	-0.1509	0.60507
0.77094	0.81732	-0.0977	0.70082
0.77552	0.83936	-0.123	0.67054
0.81205	0.85312	-0.0626	0.75339
0.81576	0.84274	-0.063	0.77758
0.83194	0.86876	-0.0608	0.79696
0.86227	0.89334	-0.0659	0.78403
0.95256	0.96515	-0.0145	0.93353
0.97361	0.97713	-0.0123	0.9679
1	1	0	1

CONTACT DATA FOR -23 deg TOP-SPIN

ZT: FRACTION OF TIME
ZX: FRACTION OF HORIZONTAL DISTANCE
ZY: FRACTIONAL VERTICAL DEFORMATION
ZR: FRACTION OF ROTATION

ZT	ZX	ZY	ZR
0	0	0	0
0.207259	0.259841	-0.11394	0.079648
0.213626	0.267675	-0.11547	0.104085
0.346731	0.426368	-0.14363	0.222469
0.398101	0.48599	-0.18353	0.252412
0.427497	0.519063	-0.21225	0.28367
0.469117	0.573479	-0.18483	0.336264
0.603949	0.682222	-0.14077	0.417732
0.679231	0.764269	-0.13004	0.589407
0.885594	0.905445	-0.03055	0.829872
0.89916	0.918454	-0.03037	0.868333
1	1	0	1

CONTACT DATA FOR -34 deg TOP-SPIN

ZT: FRACTION OF TIME
ZX: FRACTION OF HORIZONTAL DISTANCE
ZY: FRACTIONAL VERTICAL DEFORMATION
ZR: FRACTION OF ROTATION

ZT	ZX	ZY	ZR
0	0	0	0
0.059207	0.08723	-0.04698	0.012688
0.123348	0.163469	-0.07777	0.072432
0.156616	0.211417	-0.09480	0.083066
0.347899	0.417935	-0.22898	0.250035
0.377243	0.44642	-0.25923	0.229459
0.407832	0.503995	-0.26691	0.285441
0.475425	0.588334	-0.28063	0.393809
0.496609	0.577364	-0.26849	0.412706
0.520674	0.593002	-0.25698	0.427929
0.581304	0.652874	-0.24222	0.545062
0.637339	0.696517	-0.18418	0.643247
0.680647	0.729524	-0.21579	0.612192
0.72975	0.811067	-0.11058	0.787469
0.83218	0.854853	-0.04016	0.882464
1	1	0	1

CONTACT DATA FOR -42 deg TOP-SPIN

ZT: FRACTION OF TIME
ZX: FRACTION OF HORIZONTAL DISTANCE
ZY: FRACTIONAL VERTICAL DEFORMATION
ZR: FRACTION OF ROTATION

ZT	ZX	ZY	ZR
0	0	0	0
0.081586	0.104913	-0.0787	0.002784
0.141621	0.188879	-0.09386	0.078726
0.270381	0.343947	-0.21567	0.120165
0.460491	0.5253	-0.32955	0.37728
0.495249	0.5335	-0.32411	0.409528
0.503837	0.557318	-0.3612	0.448625
0.566098	0.594741	-0.36215	0.518413
0.605576	0.665233	-0.32238	0.577743
0.782409	0.782129	-0.26829	0.767592
0.895808	0.906631	-0.02145	0.883341
1	1	0	1

CONTACT DATA FOR -48 deg TOP-SPIN

ZT: FRACTION OF TIME
ZX: FRACTION OF HORIZONTAL DISTANCE
ZY: FRACTIONAL VERTICAL DEFORMATION
ZR: FRACTION OF ROTATION

ZT	ZX	ZY	ZR
0	0	0	0
0.15961	0.223242	-0.10241	0.120023
0.192974	0.234473	-0.15780	0.082679
0.27023	0.327222	-0.22935	0.200684
0.409747	0.520926	-0.26999	0.325382
0.466605	0.527884	-0.32281	0.379253
0.537307	0.614002	-0.27415	0.479825
0.753699	0.790751	-0.12867	0.798004
0.831966	0.82686	-0.14390	0.818359
1	1	0	1

CONTACT DATA FOR -61 deg TOP-SPIN

ZT: FRACTION OF TIME
ZX: FRACTION OF HORIZONTAL DISTANCE
ZY: FRACTIONAL VERTICAL DEFORMATION
ZR: FRACTION OF ROTATION

ZT	ZX	ZY	ZR
0	0	0	0
0.040799	0.047992	-0.03223	0.035377
0.11008	0.154909	-0.12950	-0.00827
0.416428	0.454945	-0.38212	0.385266
0.44033	0.52736	-0.34080	0.423924
0.483865	0.503526	-0.37702	0.534536
0.530626	0.553927	-0.31542	0.582451
0.551789	0.577583	-0.32468	0.591576
0.705722	0.727026	-0.20591	0.772714
0.901557	0.898783	-0.04984	0.901957
0.935432	0.952255	-0.03723	0.936176
1	1	0	1

CONTACT DATA FOR -71 deg TOP-SPIN

ZT: FRACTION OF TIME
ZX: FRACTION OF HORIZONTAL DISTANCE
ZY: FRACTIONAL VERTICAL DEFORMATION
ZR: FRACTION OF ROTATION

ZT	ZX	ZY	ZR
0	0	0	0
0.096157	0.09047	-0.09741	0.122456
0.104657	0.12146	-0.11145	0.118794
0.154896	0.186287	-0.17519	0.153119
0.202015	0.240014	-0.21156	0.188658
0.242411	0.273121	-0.25554	0.219389
0.347929	0.398298	-0.34836	0.427292
0.37423	0.40694	-0.36873	0.309138
0.499273	0.432121	-0.45025	0.622324
0.585729	0.573218	-0.34784	0.516825
0.722851	0.791845	-0.16141	0.779772
0.787267	0.776522	-0.22511	0.83176
0.896924	0.858813	-0.10332	0.916223
0.92248	0.86923	-0.05525	0.94427
0.929662	0.930517	-0.00062	0.992213
1	1	0	1

APPENDIX D

CONTACT DATA FOR BACK-SPIN IMPACT

CONTACT DATA FOR -17 deg BACK-SPIN

IT: FRACTION OF TIME
IX: FRACTION OF HORIZONTAL DISTANCE
IY: FRACTIONAL VERTICAL DEFORMATION
IR: FRACTION OF ROTATION

IT	IX	IY	IR
0	0	0	0
0.11935	0.13053	0.0518	-1.489
0.14372	0.15792	0.072	-0.9879
0.21983	0.26493	0.0941	-3.509
0.35718	0.4269	0.1512	-2.28
0.43572	0.51874	0.1695	-3.1875
0.43573	0.5007	0.1671	-2.33
0.44891	0.54234	0.1682	-2.88
0.4493	0.51	0.1694	-2.25
0.56425	0.64213	0.1795	-2.4647
0.574	0.63127	0.1596	-4.02
0.64042	0.70801	0.1606	-2.008
0.83639	0.87208	0.0818	-1.55
0.88728	0.89885	0.0438	-1.3798
0.88161	0.89522	0.0545	-1.734
0.93072	0.94365	0.03424	-1.39
0.95053	0.9358	0.03888	-1.095
0.98471	0.9915	0.0127	-1.106
1	1	0	1

CONTACT DATA FOR -22 deg BACK-SPIN

IT: FRACTION OF TIME
IX: FRACTION OF HORIZONTAL DISTANCE
IY: FRACTIONAL VERTICAL DEFORMATION
IR: FRACTION OF ROTATION

IT	IX	IY	IR
0	0	0	0
0.04956	0.064627	-0.03050	-0.24054
0.079411	0.102803	-0.05588	-0.43914
0.273127	0.36219	-0.14093	-1.65599
0.275962	0.344832	-0.15036	-3.38487
0.434096	0.52104	-0.19730	-1.57607
0.606743	0.682238	-0.15642	-0.54496
0.623528	0.703315	-0.17219	-0.90719
0.627151	0.704204	-0.15206	-0.73028
0.758204	0.822211	-0.10232	-0.08666
0.761567	0.815332	-0.06956	-0.45855
0.959098	0.960528	-0.00697	0.844997
0.999638	0.988385	-0.02966	0.964736
1	1	0	1

CONTACT DATA FOR -35 deg BACK-SPIN

ZT: FRACTION OF TIME
ZX: FRACTION OF HORIZONTAL DISTANCE
ZY: FRACTIONAL VERTICAL DEFORMATION
ZR: FRACTION OF ROTATION

ZT	ZX	ZY	ZR
0	0	0	0
0.068328	0.038613	-0.0542	-0.22962
0.086577	0.130835	-0.06464	-0.27182
0.105432	0.152279	-0.07609	-0.18893
0.123891	0.172279	-0.09320	-0.25331
0.192558	0.264554	-0.15082	-0.51120
0.304009	0.450628	-0.21161	-0.43134
0.310903	0.472401	-0.25789	-0.47779
0.330783	0.457457	-0.25720	-0.34279
0.373928	0.494533	-0.27718	-0.71442
0.41879	0.578119	-0.26377	-0.32522
0.445939	0.573346	-0.27040	-0.58805
0.493184	0.678264	-0.27241	-0.17649
0.624781	0.748085	-0.28131	-0.06916
0.654975	0.783017	-0.25354	-0.11340
0.668612	0.774261	-0.21376	0.000793
0.698875	0.804051	-0.17242	0.20361
0.738711	0.826509	-0.22250	0.368879
0.869838	0.918132	-0.15545	0.48484
0.875544	0.920078	-0.08305	0.663223
0.886968	0.911266	-0.11181	0.635941
0.954039	0.938699	-0.12253	0.963501
0.998925	0.980044	-0.0116	1.060981
1	1	0	1

CONTACT DATA FOR -40 deg BACK-SPIN

ZT: FRACTION OF TIME
ZX: FRACTION OF HORIZONTAL DISTANCE
ZY: FRACTIONAL VERTICAL DEFORMATION
ZR: FRACTION OF ROTATION

ZT	ZX	ZY	ZR
0	0	0	0
0.091668	0.154304	-0.04858	-0.56645
0.131057	0.190299	-0.11029	-0.17178
0.348603	0.533055	-0.27958	-0.30059
0.362905	0.574681	-0.27161	-0.47959
0.507312	0.714056	-0.30532	-0.07069
0.549025	0.691929	-0.31708	-0.10594
0.595593	0.738545	-0.28651	0.107151
0.620807	0.771182	-0.24852	0.215823
0.816441	0.889486	-0.16288	0.599812
0.848484	0.894604	-0.14035	0.604392
1	1	0	1

CONTACT DATA FOR -45 deg BACK-SPIN

ZT: FRACTION OF TIME
ZX: FRACTION OF HORIZONTAL DISTANCE
ZY: FRACTIONAL VERTICAL DEFORMATION
ZR: FRACTION OF ROTATION

ZT	ZX	ZY	ZR
0	0	0	0
0.337767	0.556916	-0.27364	-0.39310
0.340171	0.551285	-0.30005	-0.34971
0.369526	0.61906	-0.28470	-0.17425
0.466806	0.70722	-0.31337	-0.00231
0.499168	0.69704	-0.28720	0.098003
0.565819	0.68465	-0.35891	-0.01703
0.668804	0.799132	-0.17499	0.448937
0.864563	0.445977	-0.21630	-0.28990
1	1	0	1

CONTACT DATA FOR -59 deg BACK-SPIN

ZT: FRACTION OF TIME
ZX: FRACTION OF HORIZONTAL DISTANCE
ZY: FRACTIONAL VERTICAL DEFORMATION
ZR: FRACTION OF ROTATION

ZT	ZX	ZY	ZR
0	0	0	0
0.013399	0.026575	-0.02160	0.048057
0.124781	0.213026	-0.11157	-0.41572
0.228446	0.40099	-0.23127	-0.92606
0.326628	0.594677	-0.28129	-0.62896
0.583303	0.740229	-0.27219	0.201615
0.61293	0.775229	-0.25567	0.364879
0.633952	0.798155	-0.22576	0.236804
0.649362	0.711354	-0.31789	0.460767
0.796263	0.869213	-0.08121	0.643506
1	1	0	1

CONTACT DATA FOR -68 deg BACK-SPIN

ZT: FRACTION OF TIME
ZX: FRACTION OF HORIZONTAL DISTANCE
ZY: FRACTIONAL VERTICAL DEFORMATION
ZR: FRACTION OF ROTATION

ZT	ZX	ZY	ZR
0	0	0	0
0.027816	0.17606	-0.04756	0.381113
0.05456	0.042621	-0.07175	-0.29571
0.067221	0.153281	-0.06664	-2.50379
0.382215	0.625488	-0.38653	-6.08758
0.430776	0.671064	-0.43553	-1.69627
0.507354	0.708933	-0.36648	-0.29952
0.527335	0.955273	-0.38454	-1.67742
0.64653	0.697303	-0.25134	0.20126
0.792713	0.822404	-0.14474	-0.33795
0.80229	0.922433	-0.10748	-1.10007
0.821731	0.749179	-0.09664	0.21268
1	1	0	1